

## **FIGURES 1-52**

**Figure 1.** **a)** A molten glass rod is subjected to a tensile force,  $F$ , which causes the rod to flow into a fiber. **b)** Tensile testing of a metal specimen. "Conventional" alloys neck down during tensile testing. After necking the gauge length of a tensile specimen diminishes and deformation occurs in the neck, resulting in high loads and relatively rapid fracture of the specimen. Superplastic alloys resist necking; a diffuse neck forms that spreads out along the gauge length of the specimen. Diffuse necks allow very large relative length changes ( $> 1000\%$ ), or *strains* to occur. **c)** A two-dimensional illustration of three potential microstructural responses (shown exaggerated) of a single phase superplastic material to an applied load: no grain growth; *deformation-enhanced grain growth*, and *homogeneous* or "*static*" *grain growth*. Deformation-enhanced grain growth is inhomogeneous: it only occurs in the gauge length of the test specimen. If the microstructure is unstable at the forming temperature, then grain growth will occur homogeneously throughout the tensile specimen. In this case, necking can develop, along with grain plasticity, which is shown here. See Hamilton (1989) for a full treatment. **d)** The strain rate sensitivity is illustrated for a typical superplastic alloy. For low strain rates diffusional creep is obtained. As the strain rate increases Regions I, II, and III are entered, and eventually the strain rate can be increased at a constant flow stress. See Arieli and Mukherjee (1982) for additional details.

Figure 1 (Continued).

# Necking

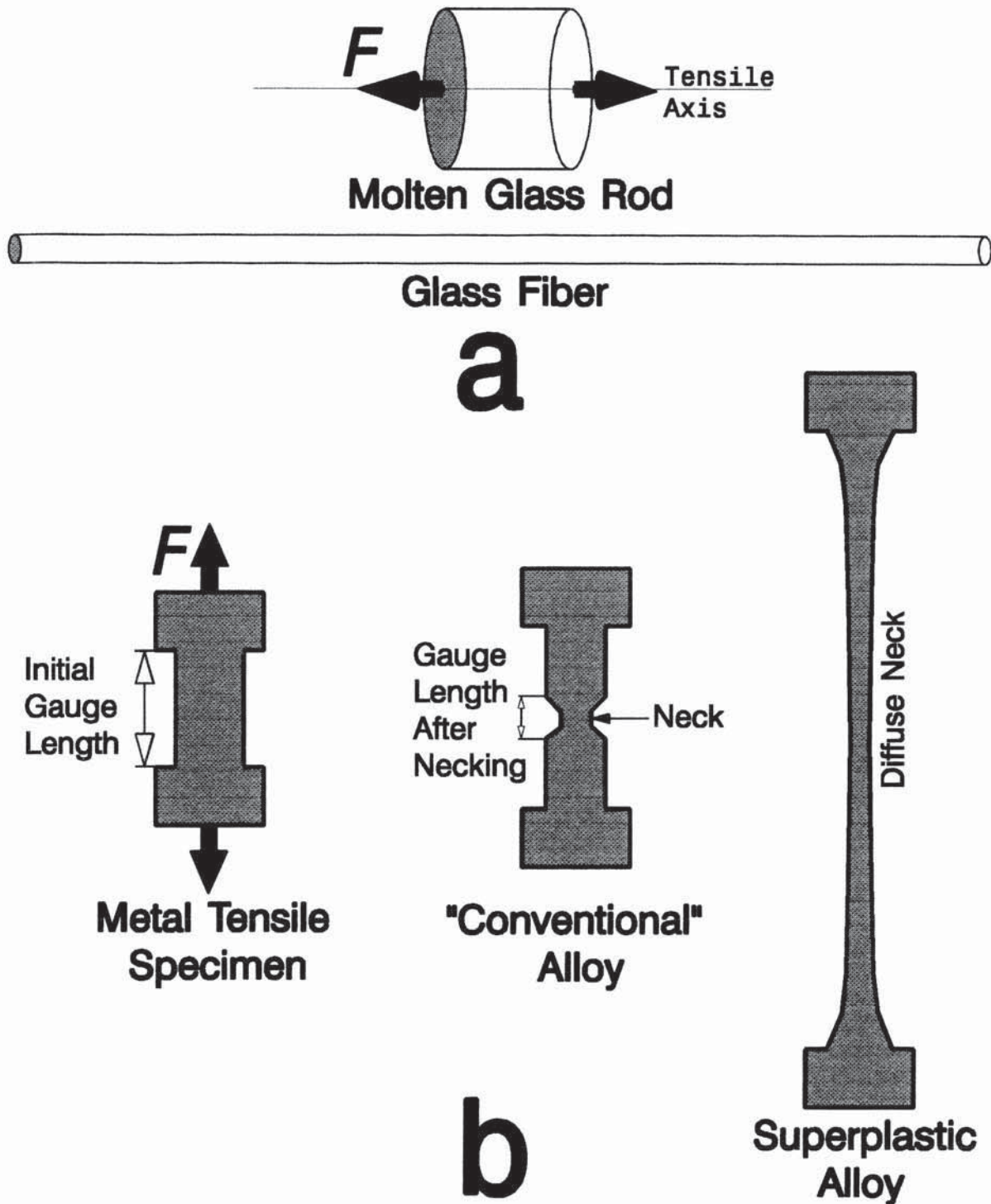
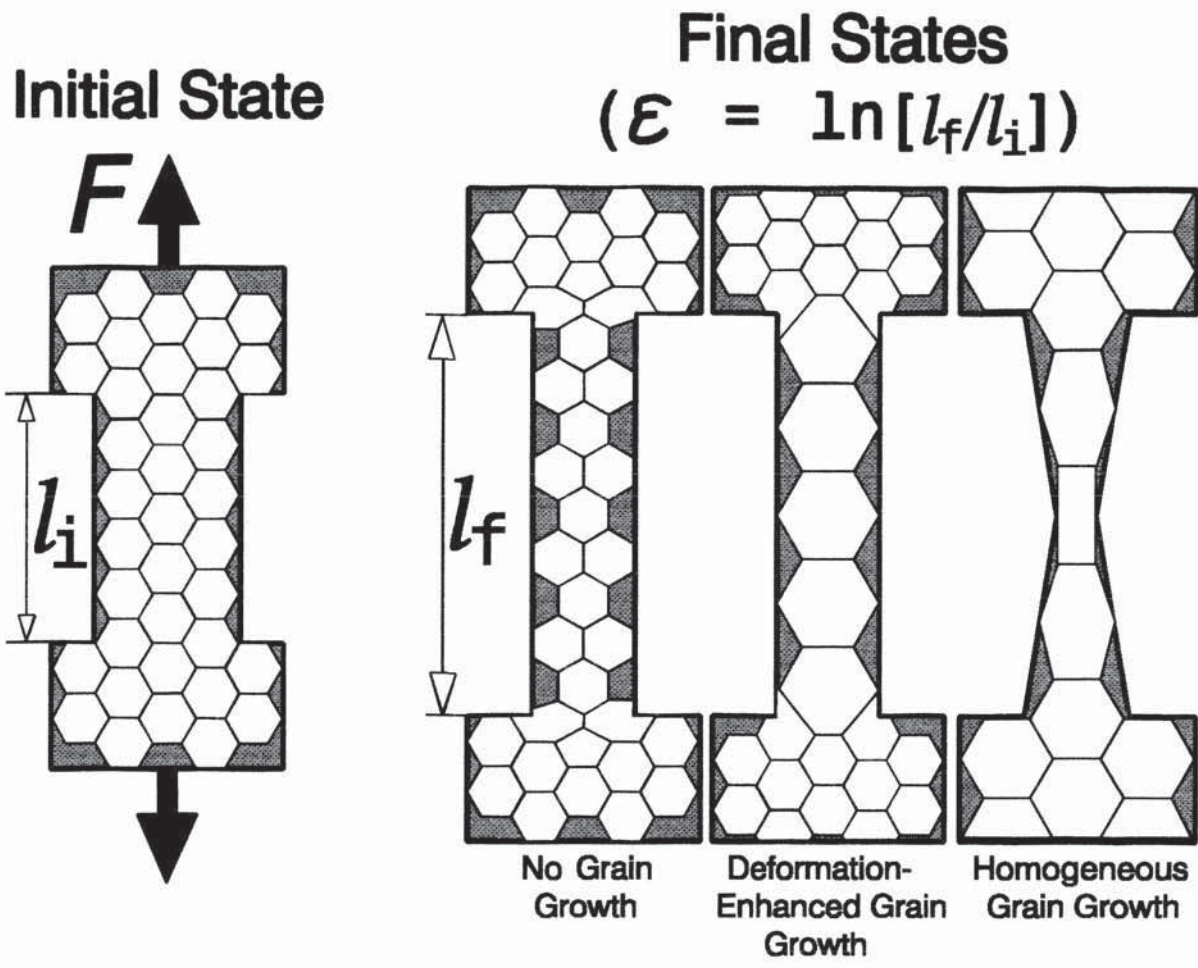


Figure 1 (Continued).

# Microstructural Responses to Deformation



C

Figure 1 (Continued).

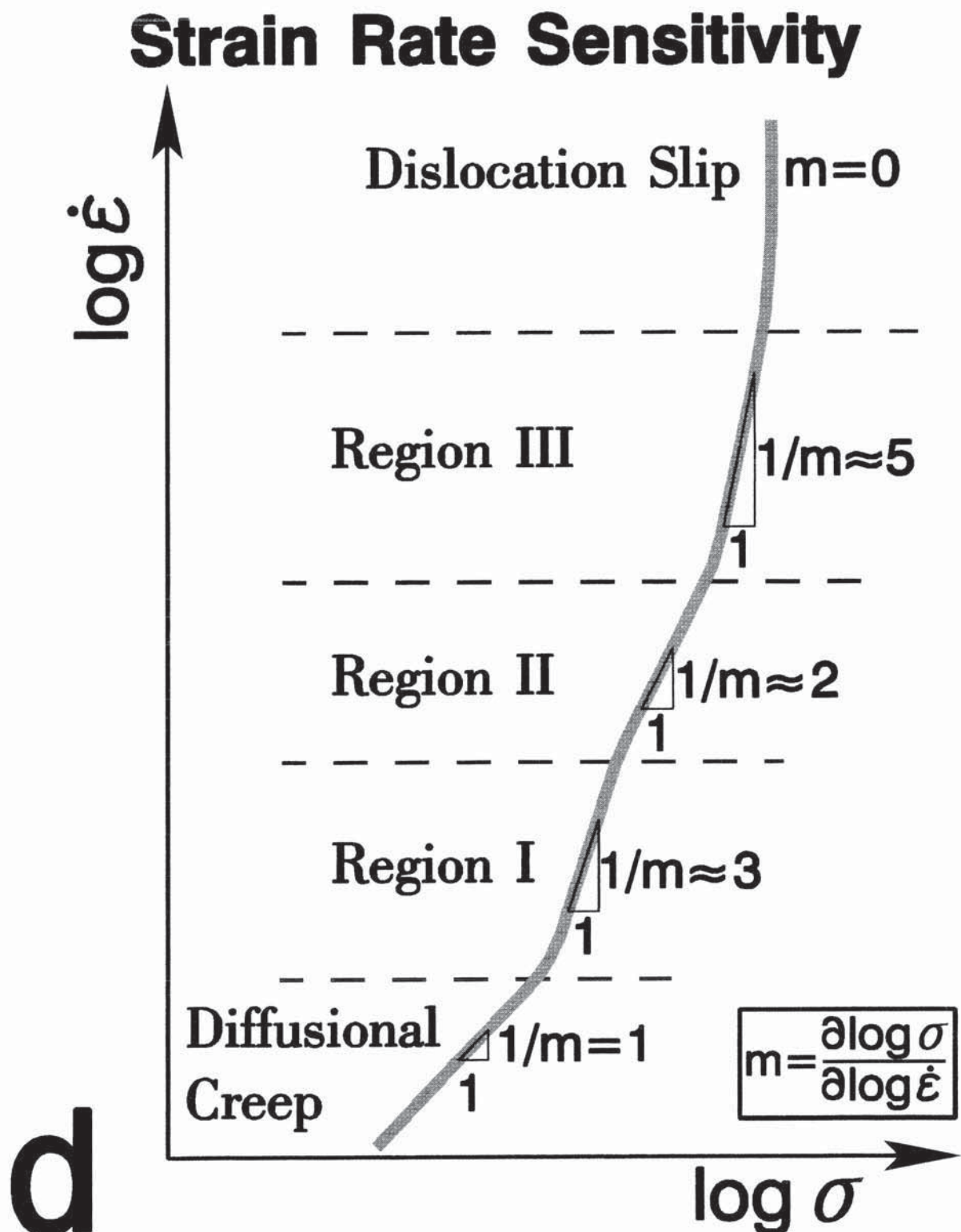


**Figure 2.** Grain boundary model (Christian 1965). In two dimensions surface tension demands that all edges meet at angles of  $120^\circ$ ; a uniform hexagonal array fills space, satisfies surface tension equilibrium, and minimizes the edge length per unit area. An analogous polyhedron for a three dimensional space does not exist. In three dimensions surface tension equilibrium requires that surfaces meet at angles of  $120^\circ$  along lines which meet in groups of four at angles of  $\cos^{-1}(-1/3) = 109^\circ 28'$ . If the hexagonal faces in a regular tetrakaidecahedra are doubly curved, then this polyhedron fills space and, edges and faces satisfy surface tension equilibrium. **a)** A *regular*, or *orthic tetrakaidecahedra* (truncated octahedra). **b)** A stack of regular tetrakaidecahedra fills space and models a polycrystalline material if hexagonal faces are doubly curved. Each tetrakaidecahedra contains a single crystal. The *crystal* is an atomic array constructed by repeating the pattern of a single motif. The interfaces between the crystals, shown as tetrakaidecahedra here, are *grain boundaries*. **c)** Surface tension requirements for a stack of tetrakaidecahedra to have minimum surface area: Only junctions between three grains are stable; here they are grains 1, 2 and 3. Boundaries, or faces meet in groups of three; here faces i, ii and iii are such a group, as are faces iii, iv and v, and iv, v and i. Faces meet at dihedral angles of  $120^\circ$  along lines which meet each other in groups of four at  $109^\circ 28'$  angles. Examples of such lines are shown thick here. **d)** After Desch (1919), a tetrakaidecahedra of minimum surface area results when regular tetrakaidecahedra satisfy the surface tension equilibrium described by 'c'. Minimum surface area requires that all hexagonal faces have the curvature shown here: hexagons are divided into six regions, bounded by straight lines, in between these lines the face leaves the x-y plane towards either the  $+z$  or  $-z$  axis, with radii of curvature,  $\varrho$ , as indicated.

**Figure 2** (Continued).

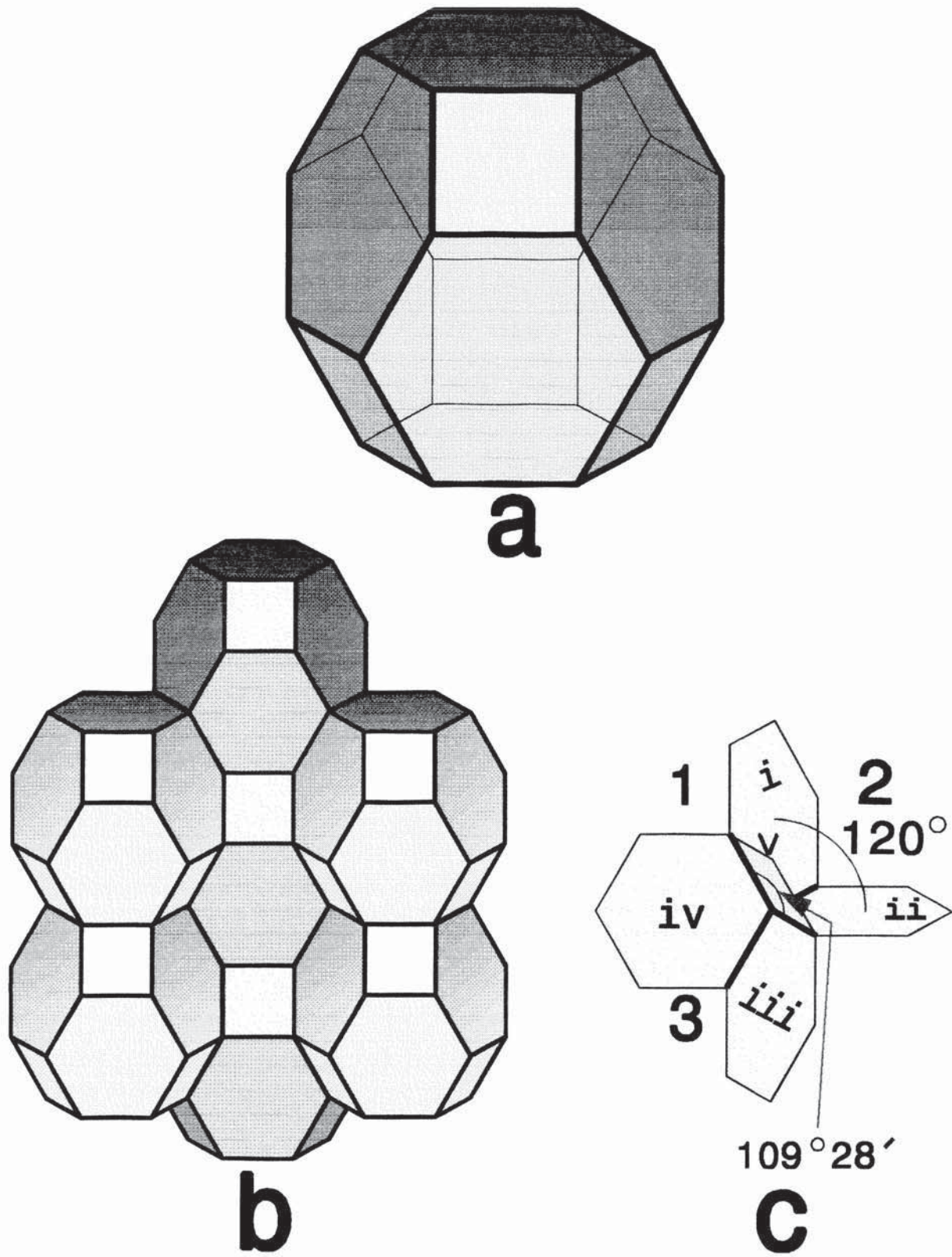
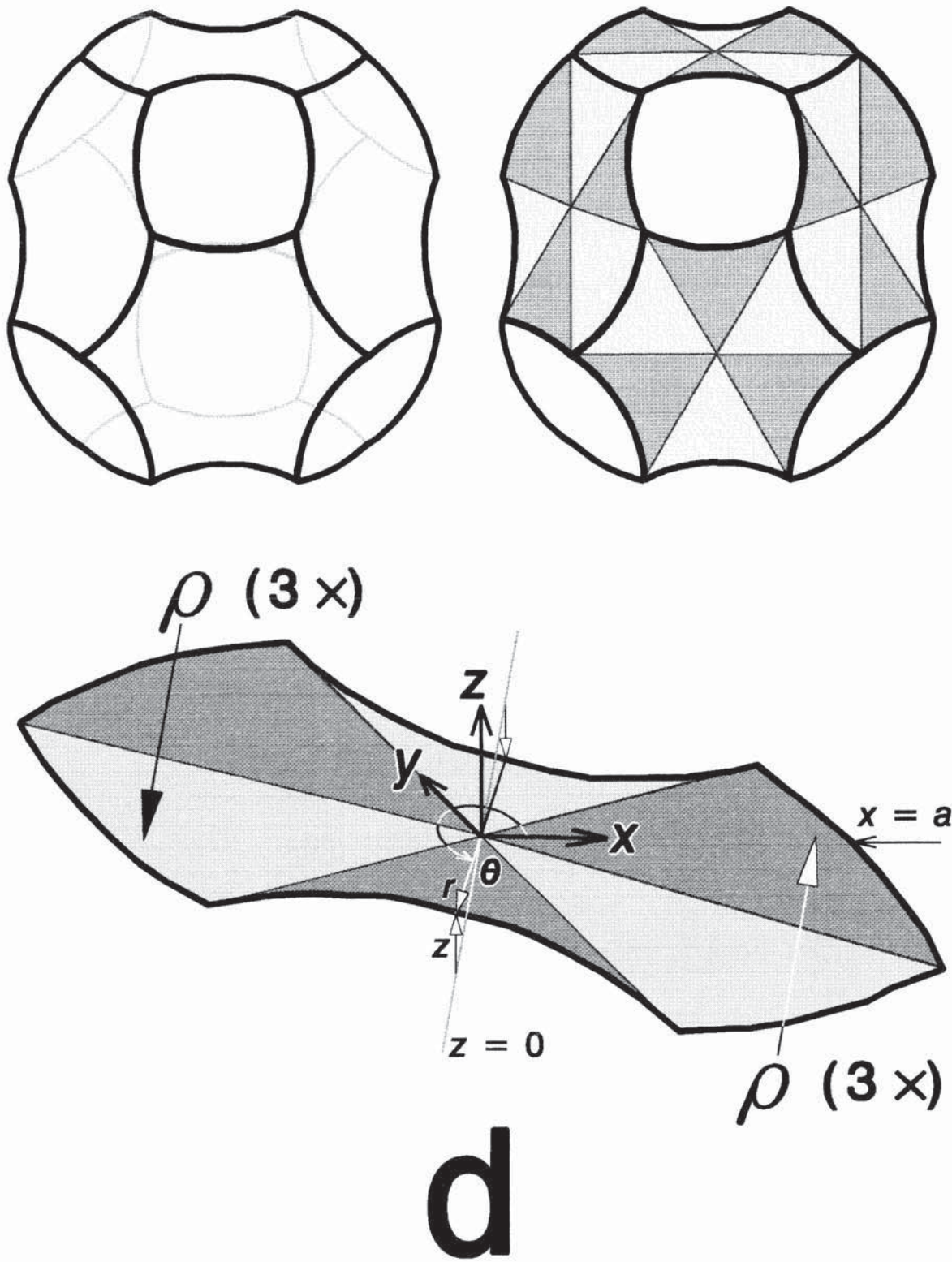


Figure 2 (Continued).



**Figure 2** (Continued). e) Consider the  $60^\circ$  sector BCB' of the non-planar hexagon; the edges CB and CB' are straight lines and the curved edge BEB' lies in a plane Q, through BB', inclined to the plane BCB' at an angle of  $\tan^{-1}\sqrt{2}$  ( $= 109^\circ 28'$ ). The problem to be solved, after Lord Kelvin (Thomson 1887), is "to find the surface of zero curvature edged by BCB' and cutting at  $120^\circ$  the plane Q all along the intersectional curve." Taking the z-axis as perpendicular to the plane BCB', and z as  $z(x,y)$ , then

$$\nabla^2 z = 0 \quad (\text{i})$$

and

$$dz/dx = \sqrt{2}/2 - \sqrt{3}/8, \text{ for } x = a - z/\sqrt{2}; \quad (\text{ii})$$

here,  $\nabla^2 z = d^2z/dx^2 + d^2z/dy^2$ , and  $a$  is the distance between points E and C. The general solution of equation i is  $z = \sum_m [A\cos m\theta + B\sin m\theta]r^m$ , where  $A$ ,  $B$  and  $m$  are arbitrary constants and  $(r,\theta)$  are polar coordinates for the x-y plane. The hexagonal symmetry requires  $B = 0$  and  $m = 3(2i + 1)$ , where  $i$  is any integer. So approximately

$$z = Ar^3\cos 3\theta + A'r\cos 9\theta, \quad (\text{iii})$$

where  $A$  and  $A'$  are to be determined so as to satisfy equation ii for two points, say  $\theta = 0$  and  $\theta = 30^\circ$ , on the curved edge of the hexagon, BEB'. In polar coordinates  $(r,\theta)$ ,  $dz/dx = (dz/dr)\cos\theta - (dz/d\theta)(\sin\theta)/r$ ; and since  $z$  is very small,  $x \approx a$  and  $r \approx a/\cos\theta$ . Equations ii and iii then give  $A + 3a^6A' = 0.031578a^{-2}$ , from  $\theta = 0$ , and  $A - \frac{6}{2}a^6A' = \frac{3}{2}(0.031578a^{-2})$ , from  $\theta = 30^\circ$ ; thus,  $A = 0.036261a^{-2}$  and  $A' = -0.001561a^{-8}$ . The sought after relation is therefore:

$$z(r,\theta) = 0.03626a^{-2}r^3\cos 3\theta - 0.001561a^{-8}r^9\cos 9\theta. \quad (\text{iv})$$

Equation (iv) is plotted here.

Figure 2 (Continued).

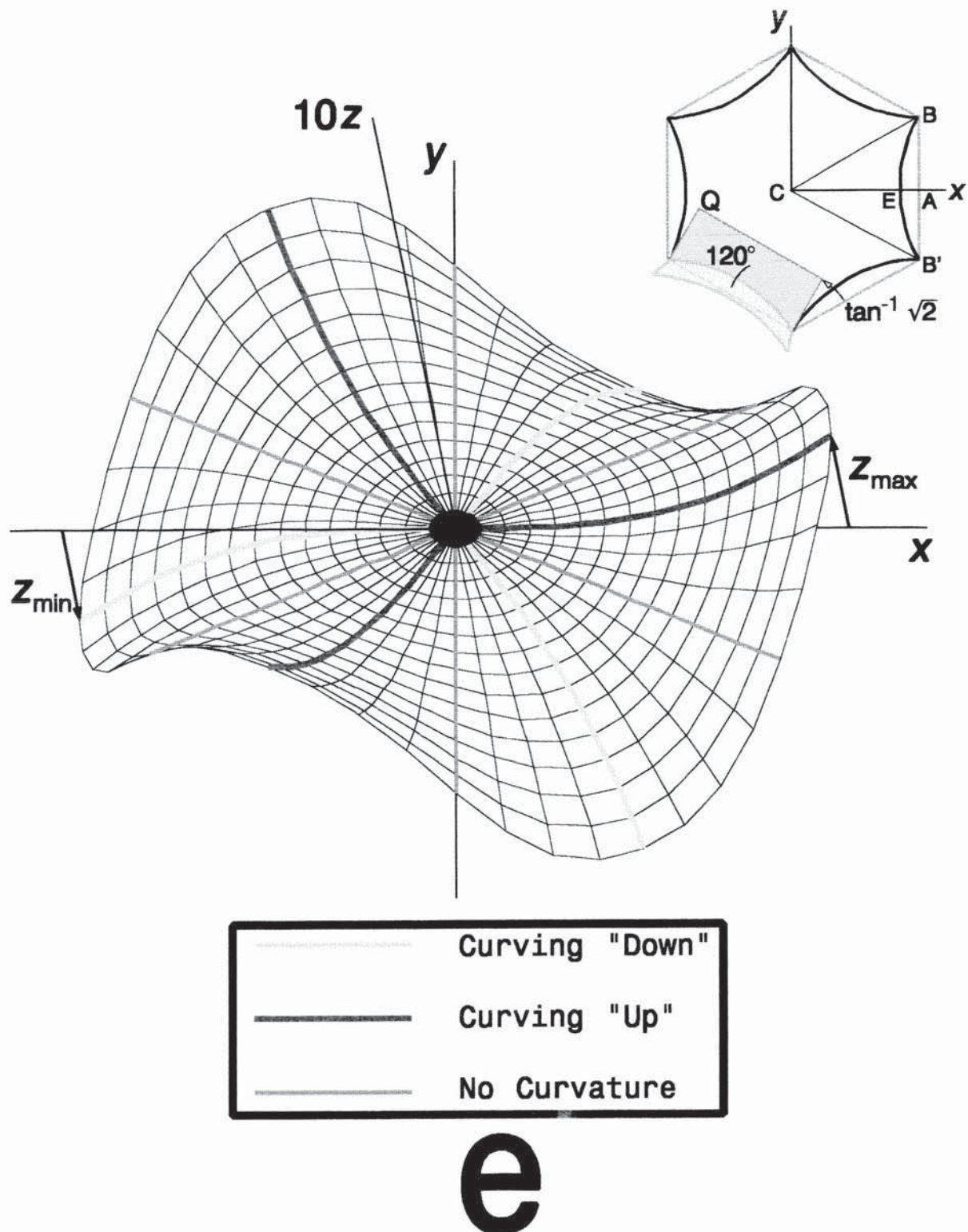
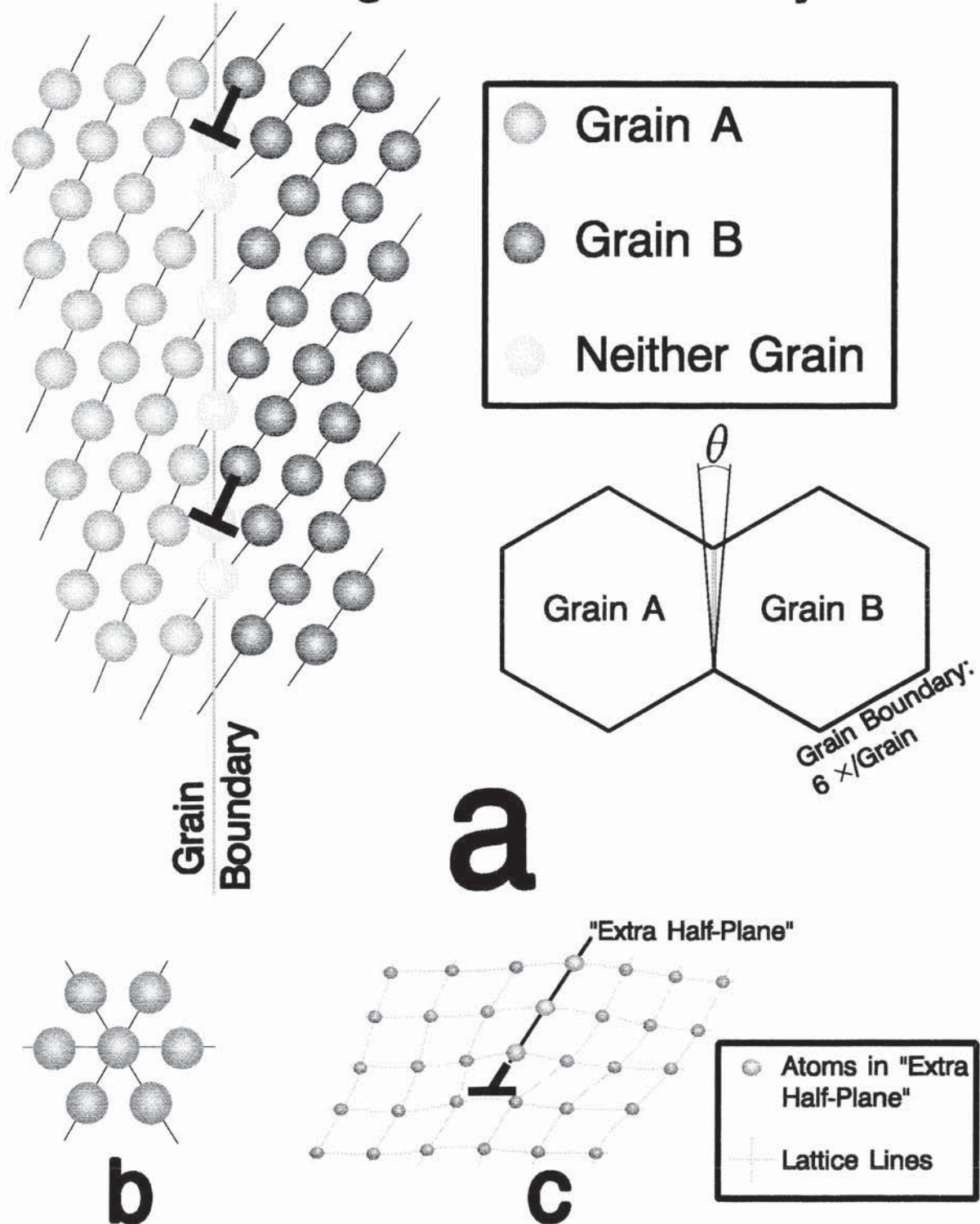


**Figure 3.** Grain boundary model for lattice with *sixfold* symmetry. **a)** A simple tilt grain boundary is comprised of a wall of edge dislocations, but only two of these defects are shown here. Lattice 'A' is rotated from lattice 'B' by angle  $\theta$ . A two-dimensional model of a polycrystalline material is a *honeycomb*, or *hexagonal array*. **b)** Motif for construction of lattice with *sixfold* symmetry, such as the close-packed planes in face-centered cubic and hexagonal close-packed crystals. **c)** The *edge dislocation* used in 'a'.

Figure 3 (Continued)

## Low-Angle Grain Boundary



# Crystallographic Coordinates

*X,Y,Z* are parameterizations

of the lattice planes with

the same crystallographic

orientation.

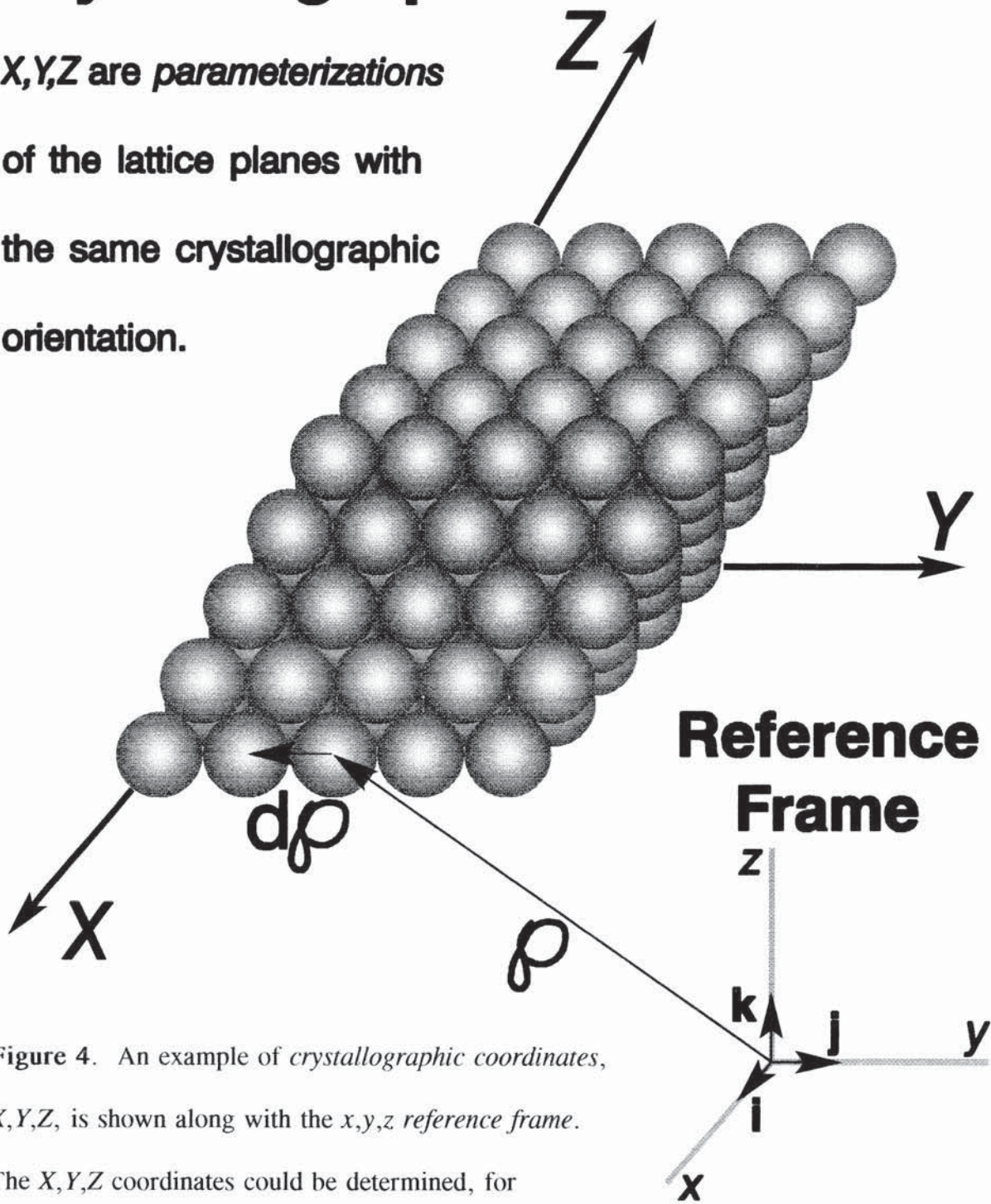


Figure 4. An example of *crystallographic coordinates*, *X,Y,Z*, is shown along with the *x,y,z* reference frame.

The *X,Y,Z* coordinates could be determined, for

example, by x-ray diffraction.

**Figure 5. Conventional and Primitive Unit Cells.** **a)** The *body-centered cubic* (BCC) crystal structure. The *lattice vectors* of the conventional unit cell are  $\mathbf{A}_x = A[100]$ ,  $\mathbf{A}_y = A[010]$ ,  $\mathbf{A}_z = A[001]$ , and the magnitudes of these vectors are  $A_x = A_y = A_z = A$ . Planes of type  $\{110\}$  are *slip planes*; directions of type  $\langle 111 \rangle$  are *slip directions*: blocks of atoms glide over such planes in these directions. The primitive unit cell shown here is comprised of lattice vectors from the family  $\langle 111 \rangle$  of magnitude  $(\sqrt{3}/2)A$ , and planes from the family  $\{110\}$ . This primitive unit cell moves when a mobile dislocation passes through it. Lattice vectors, or *tangent basis vectors*, or *1-forms*, for the conventional unit cell are shown in the lower left-hand corner. *Cotangent basis vectors*, or *1-forms*, for the conventional unit cell are shown in the lower right-hand corner. **b)** The *face-centered cubic* (FCC) crystal structure. Lattice vectors for the conventional unit cell are again  $\mathbf{A}_x = A[100]$ ,  $\mathbf{A}_y = A[010]$ ,  $\mathbf{A}_z = A[001]$ , and their magnitudes are  $A_x = A_y = A_z = A$ . All three primitive unit vectors  $\mathbf{A}_M$  for the primitive unit cell shown here are of the type  $\langle 110 \rangle$  with magnitude  $A/\sqrt{2}$ , and all planes of this cell are of the type  $\{111\}$ . In the FCC crystal structure the family of directions  $\langle 110 \rangle$  are close-packed and the  $\{111\}$  family of planes are close-packed; slip directions in this crystal structure are  $\langle 110 \rangle$  and slip planes are  $\{111\}$ .

Figure 5 (Continued).

## The Unit Cell Body-Centered Cubic

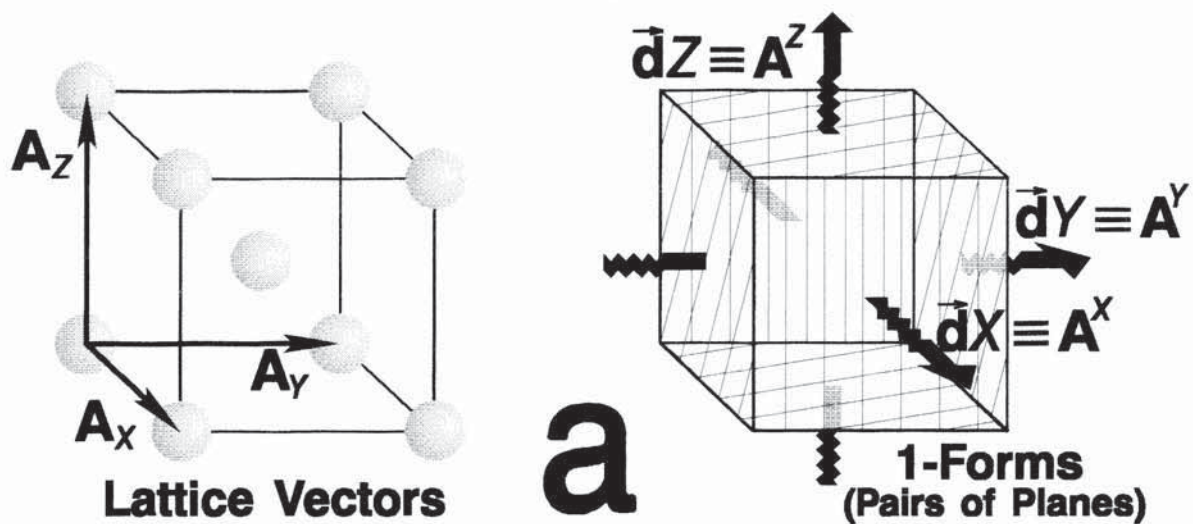
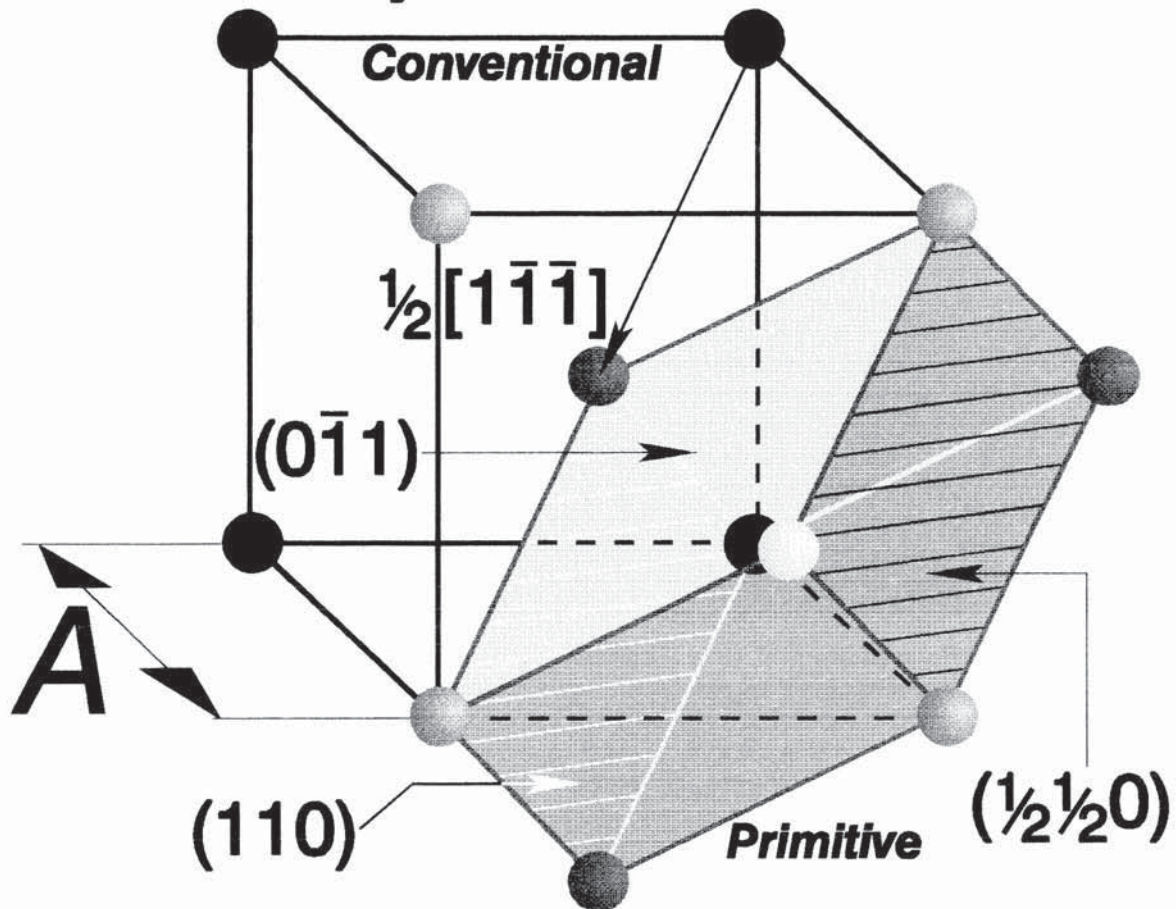
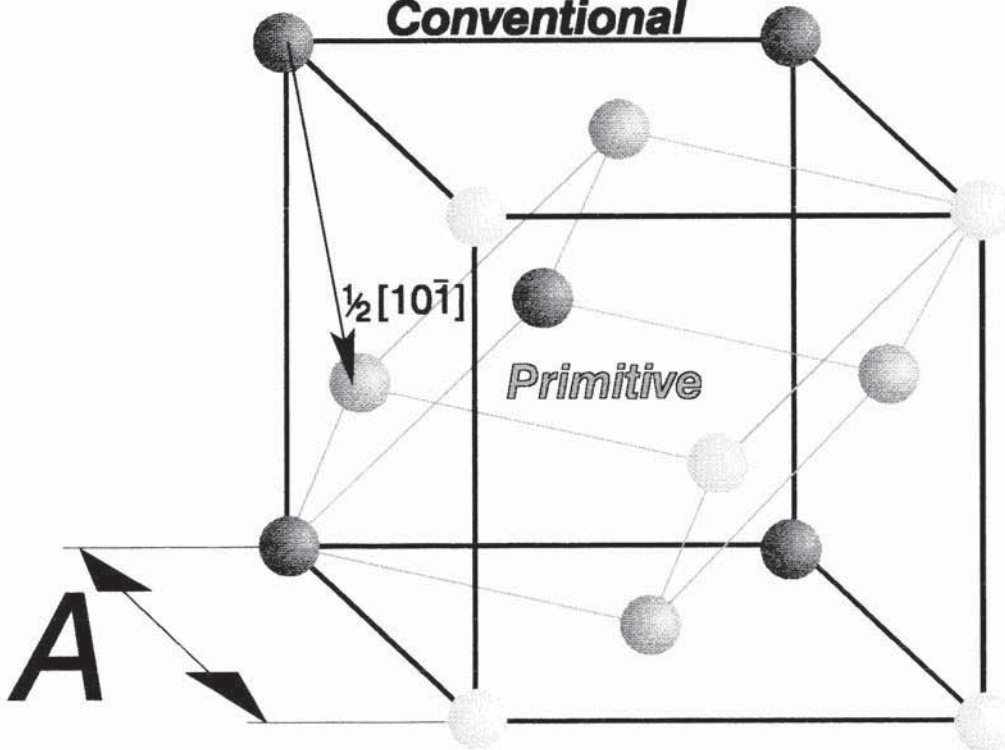


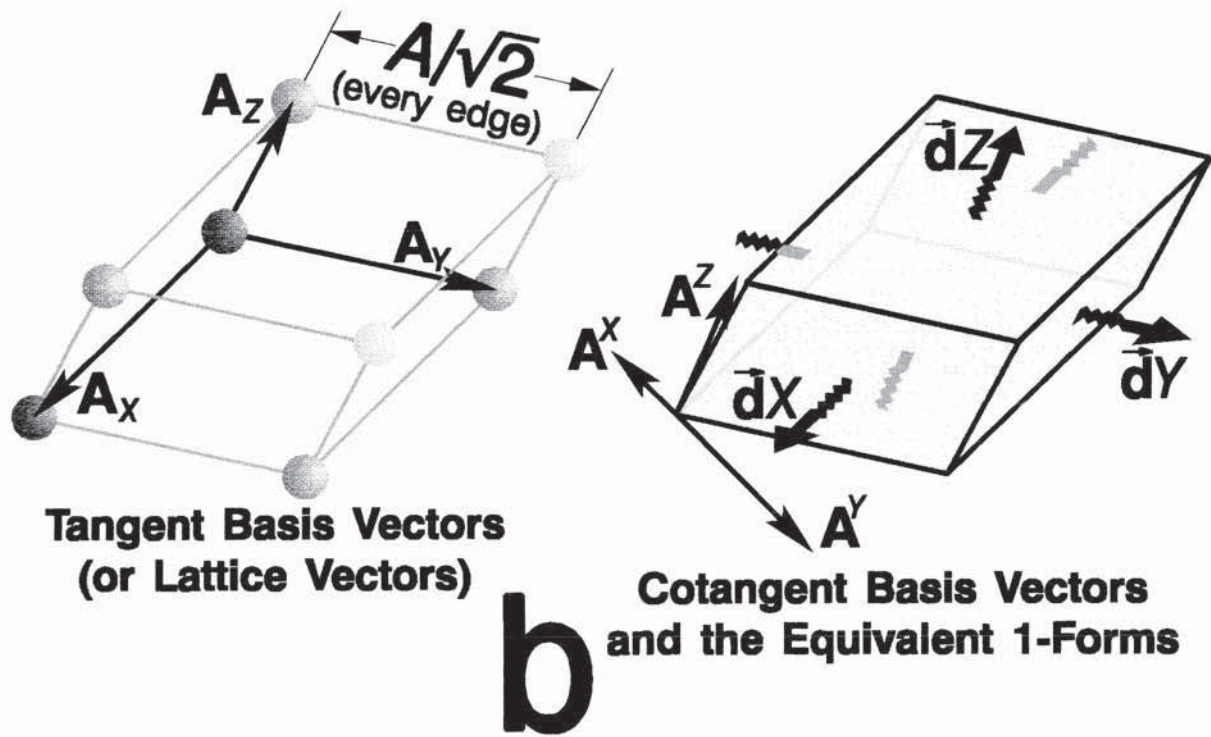
Figure 5 (Continued).

## Face-Centered Cubic

*Conventional*



$\mathbf{A}$



**b**

**Figure 6.** *Wigner-Seitz Primitive Unit Cell* for **a)** The BCC crystal structure and **b)** A two dimensional lattice with *sixfold* symmetry. **c)** Tangent and cotangent basis vectors for the lattice with *sixfold* symmetry.

The Wigner-Seitz primitive unit cells are tetrakaidecahedrons for the BCC crystal structure and hexagons for the lattice with *sixfold* symmetry (Ashcroft and Mermin 1976).

**The definition of a Wigner-Seitz primitive cell requires no reference to basis vectors.**

These Wigner-Seitz primitive unit cells model the grains in a polycrystalline material:

tetrakaidecahedrons for three dimensions and hexagons for two dimensions. Alternative nomenclature (Morral and Ashby 1974): The *lattice graph* of the tetrakaidecahedron is the

BCC conventional unit cell and that of a hexagonal array is a lattice with *sixfold* symmetry.

With respect to the latter, the lattice graph requires the additional line shown dashed, *i.e.*

"space" is *triangulated*. In the lattice graph: cells become vertices of the lattice graph, cell

edges become lines of the lattice graph, and *triple points* (cell junctions) become triangles on

the lattice graph (Morral and Ashby 1974).

Figure 6 (Continued).

## Crystal-Cell "Duality"

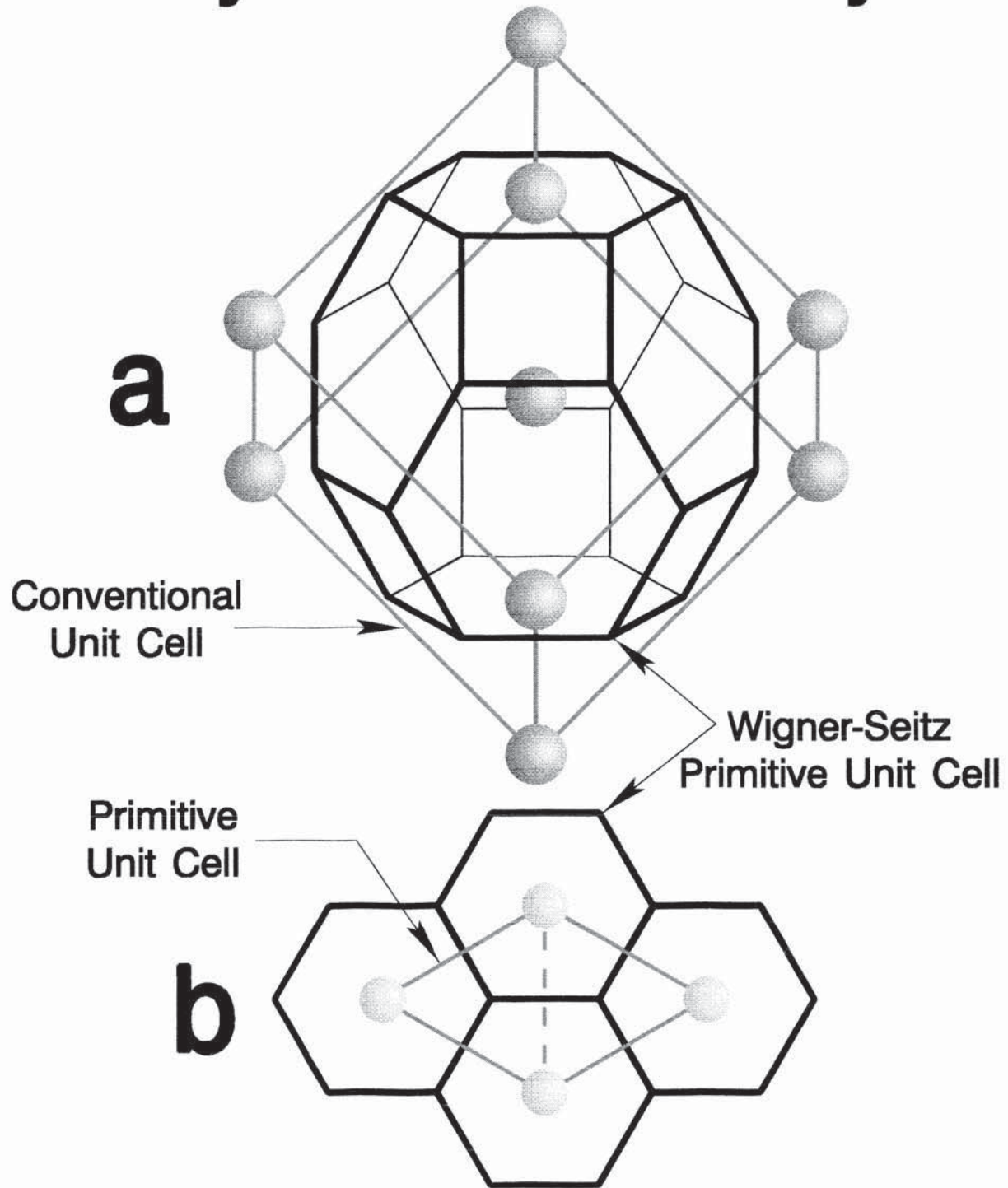
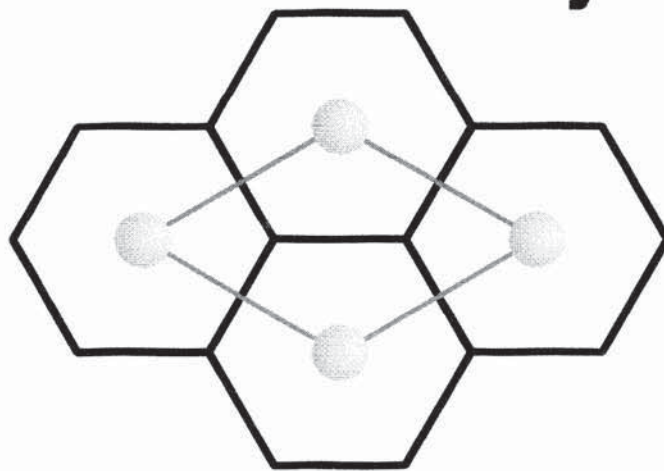
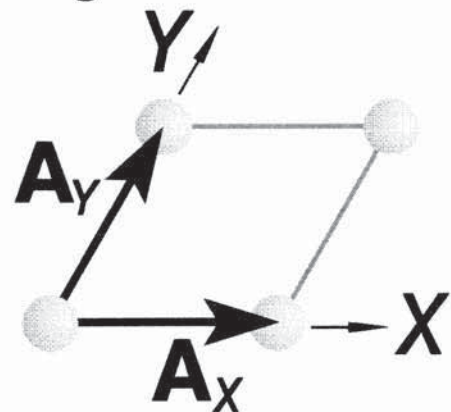


Figure 6 (Continued).

## Lattice With Sixfold Symmetry



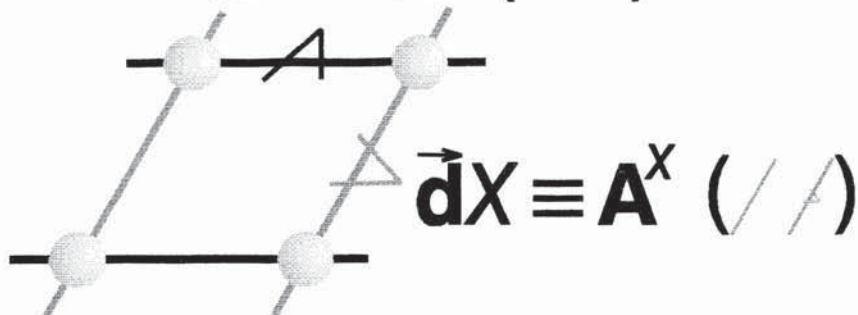
Tangent Basis Vectors



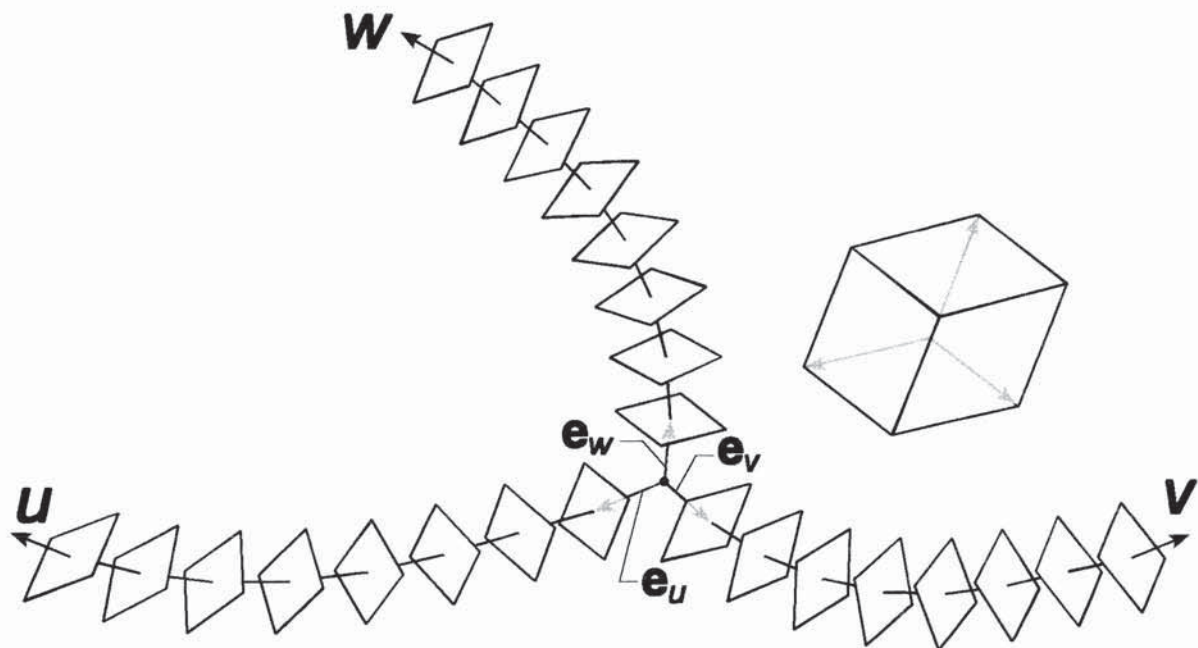
Cotangent Basis Vectors (1-Forms)

$$\vec{d}Y \equiv A^Y (\text{---})$$

C



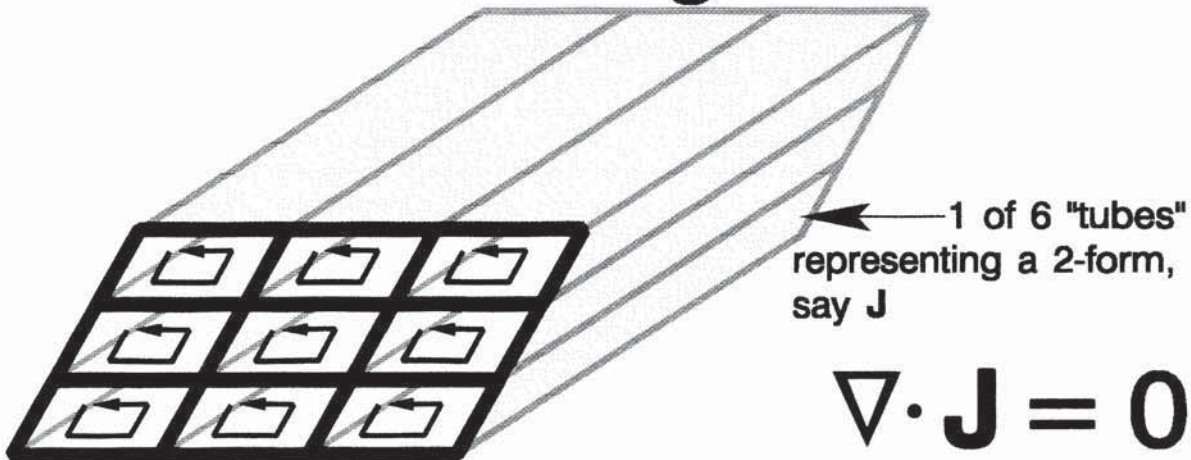
# Pfaff's Problem



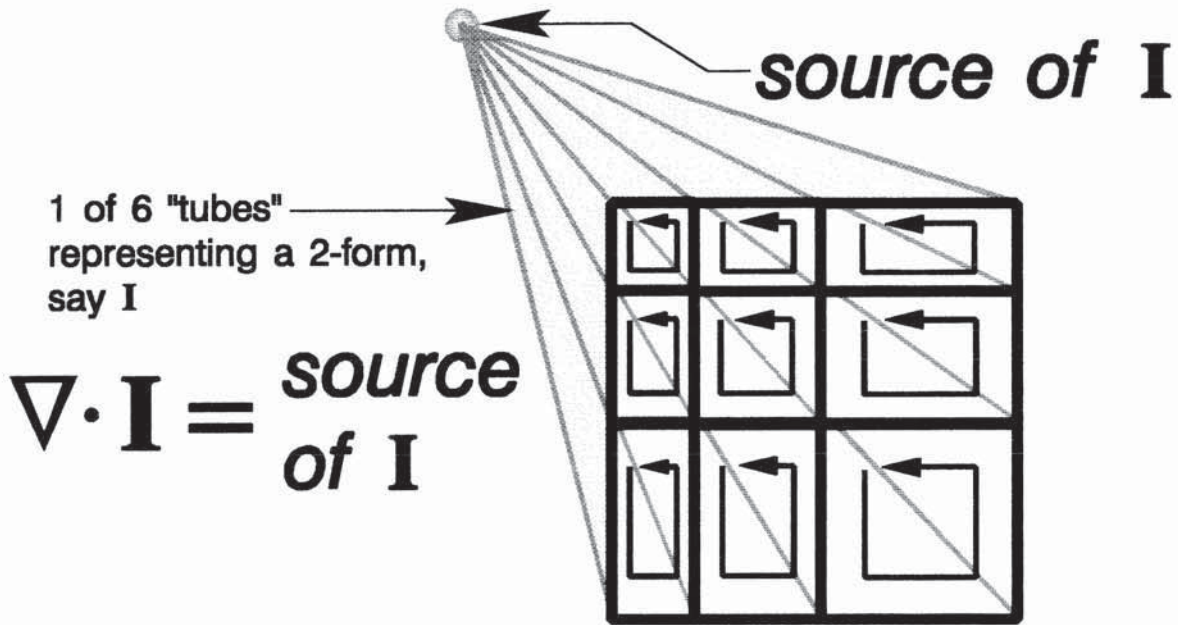
"Curl Free"	"Rotation Free"	Has Rotation
$\text{curl } \mathbf{v} = \mathbf{0}$	$\text{curl } \mathbf{v} = \mathbf{0}$	$\text{curl } \mathbf{v} \neq \mathbf{0}$
$\nabla \times \mathbf{v} = \mathbf{0}$	$\nabla \times \mathbf{v} = \mathbf{0}$	$\nabla \times \mathbf{v} \neq \mathbf{0}$
$V_{[a,b]} = 0$	$V_{[a,b]} V_c = 0$	$V_{[a,b]} V_c \neq 0$
Mesh	Can Be Made to Mesh	Can't Mesh

Figure 7. a) Pfaff's problem is illustrated, after Misner *et al.* (1973);  $v_{[a,b]} v_c \equiv v_{[a,b]} v_c$ .

# No Divergence



# Divergence



**Figure 7 (Continued). b)** Divergence is illustrated, see also Misner *et al.* (1973). Here,  $\mathbf{J}$  and  $\mathbf{I}$  are vector fields, *e.g.*  $\mathbf{J} = J^M \mathbf{i}_M$ , and their associated 2-forms are shown, *e.g.*  $*^b\mathbf{J} = J^M \epsilon_{MNP} \vec{d}X^N \wedge \vec{d}X^P$  is the 2-form dual to the 1-form  ${}^b\mathbf{J} = J_M \vec{d}X^M$ .

# Bianchi Identities

***the boundary of a boundary is zero***

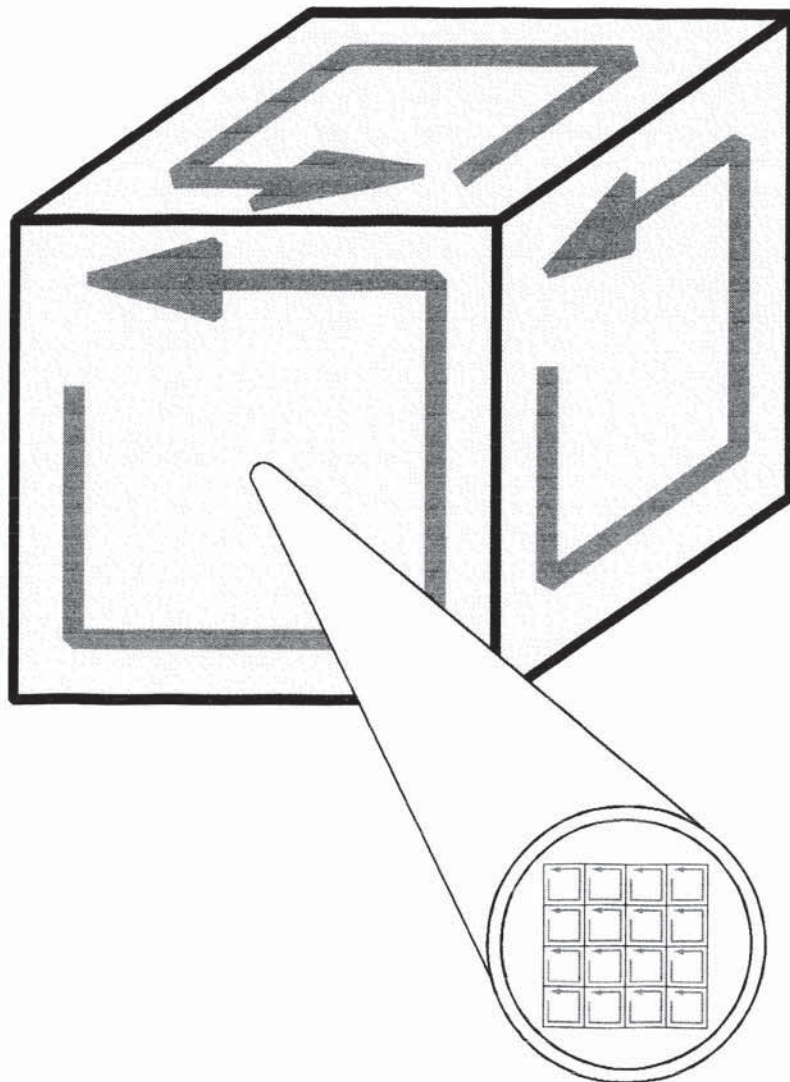
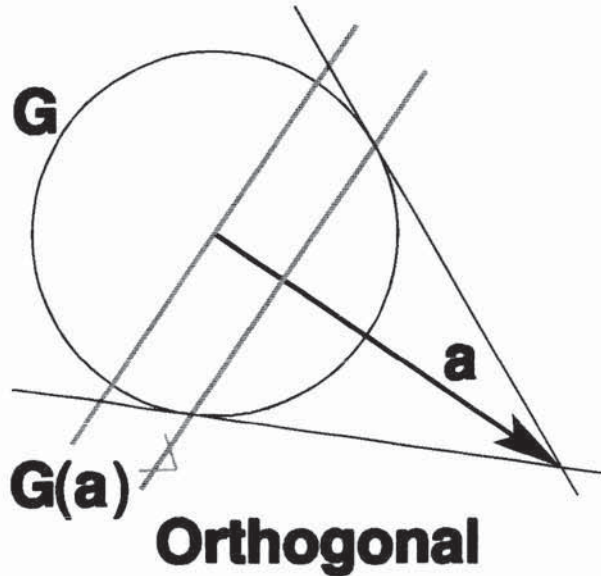
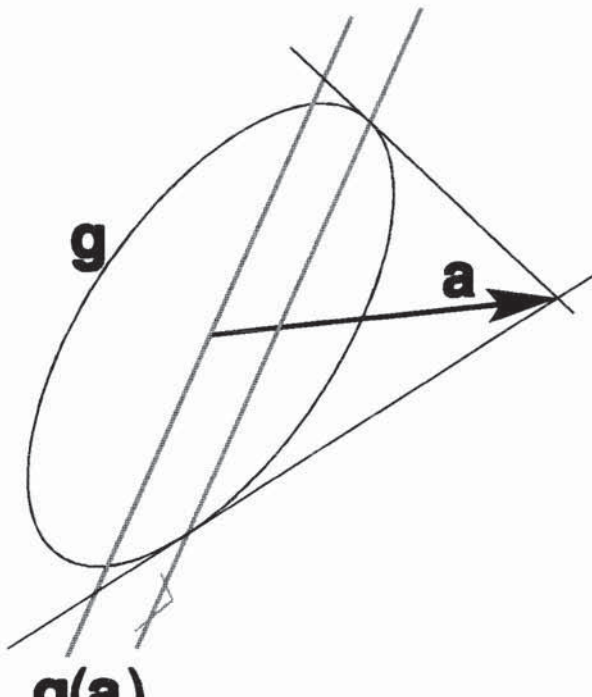


Figure 7 (Continued). c) The meaning of the Bianchi identities is illustrated, after Misner et al. (1973).

# Metric Tensor



**Orthogonal**



**Non-Orthogonal**

Figure 7 (Continued). d) The metric tensor is illustrated, after Burke (1985).

**Figure 8.** *Elasticity of a Lattice.* **a)** Point  $\rho_0 = \mathbf{X}$  of the initial state is *dragged* over the *displacement field*  $\mathbf{u}$  to the point  $\rho = \mathbf{x}$  of the final state. **Coordinates are unaffected by this deformation:** the new coordinates  $x^m$  are related to the old ones  $X^M$  by  $x^m = \delta^m_M X^M$ , so  $x, y, z = X, Y, Z$ . **Basis vectors are, however, affected:** the new cotangent basis vectors are  $\mathbf{a}^m \equiv \vec{d}x^m = \lambda^m_M \vec{d}X^M$  and new tangent basis vectors are  $\mathbf{a}_m = \lambda_m^M \mathbf{A}_M$ , where  $\lambda^m_N = \delta^m_N + \partial u^m / \partial X^N \equiv \delta^m_N + \gamma_{N^m}$ ,  $\gamma_{N^m} \equiv \mathbf{A}_M[u^m] \equiv \partial u^m / \partial X^M$ ;  $\lambda^m_N$  are the *displacement "gradients"* and  $\gamma_{N^m}$  components of the *distortion tensor*. **b)** The initial state is **i** and the final state is **ii**. Tangent basis vectors  $\mathbf{a}_m$  may be greater than or less than the  $\mathbf{A}_M$  for tensile and compressive strains, respectively, while the cotangent basis vectors  $\mathbf{a}^m$  will be less than or greater than the  $\mathbf{A}^M$  for these strains (**planes spaced more widely have smaller cotangent basis vectors** (Burke 1985)).

Figure 8 (Continued).

# Elastic Displacement

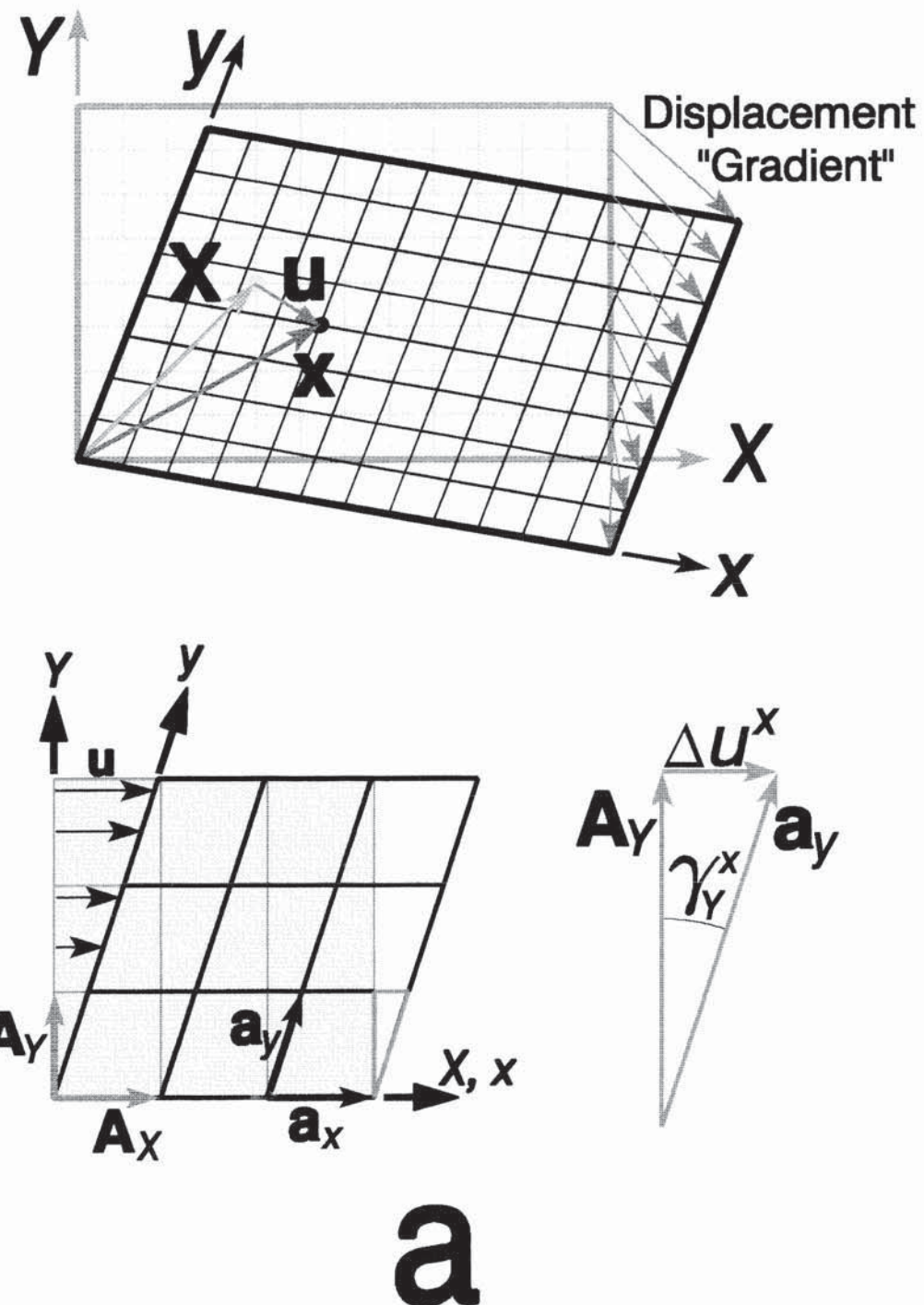
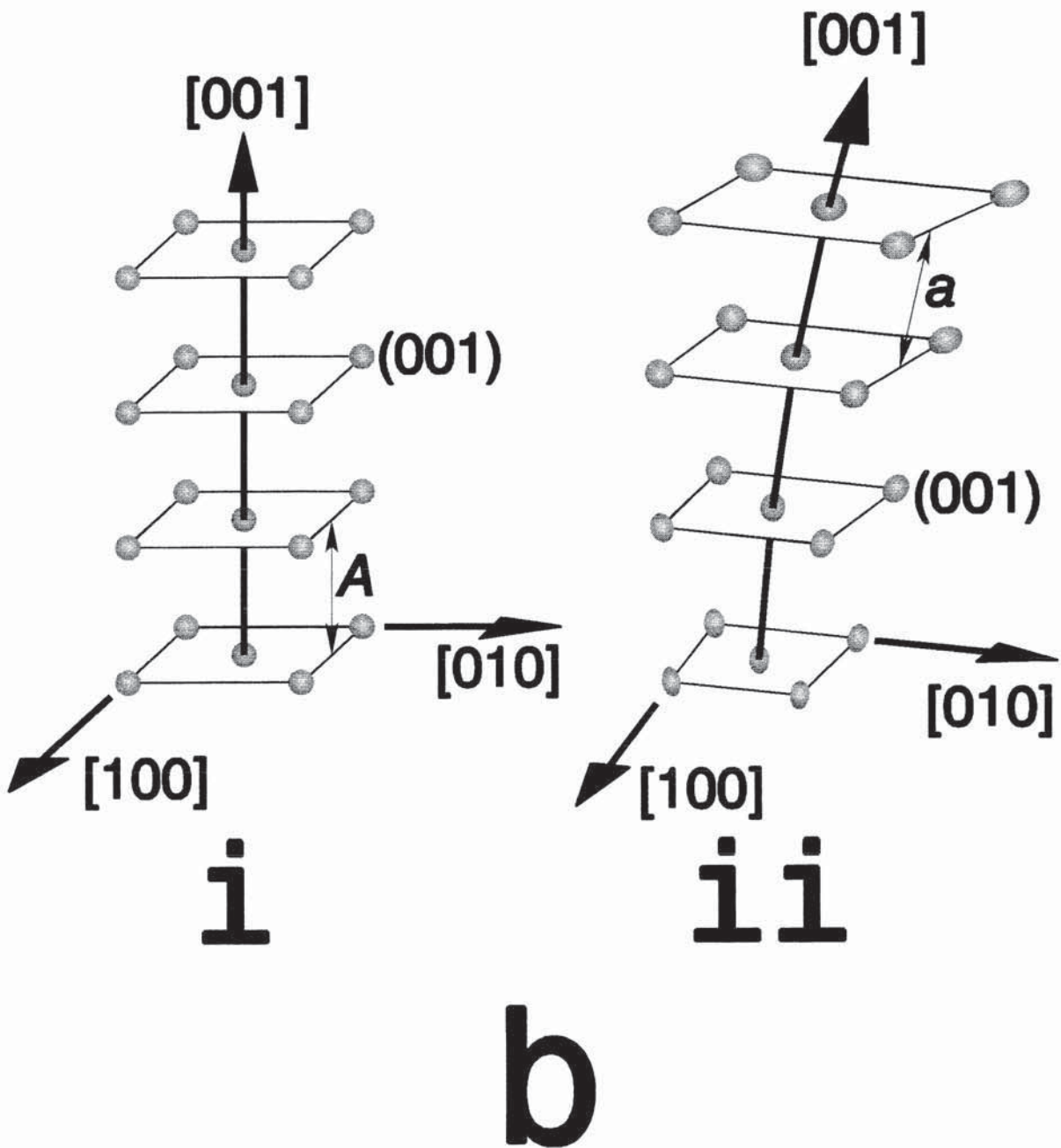
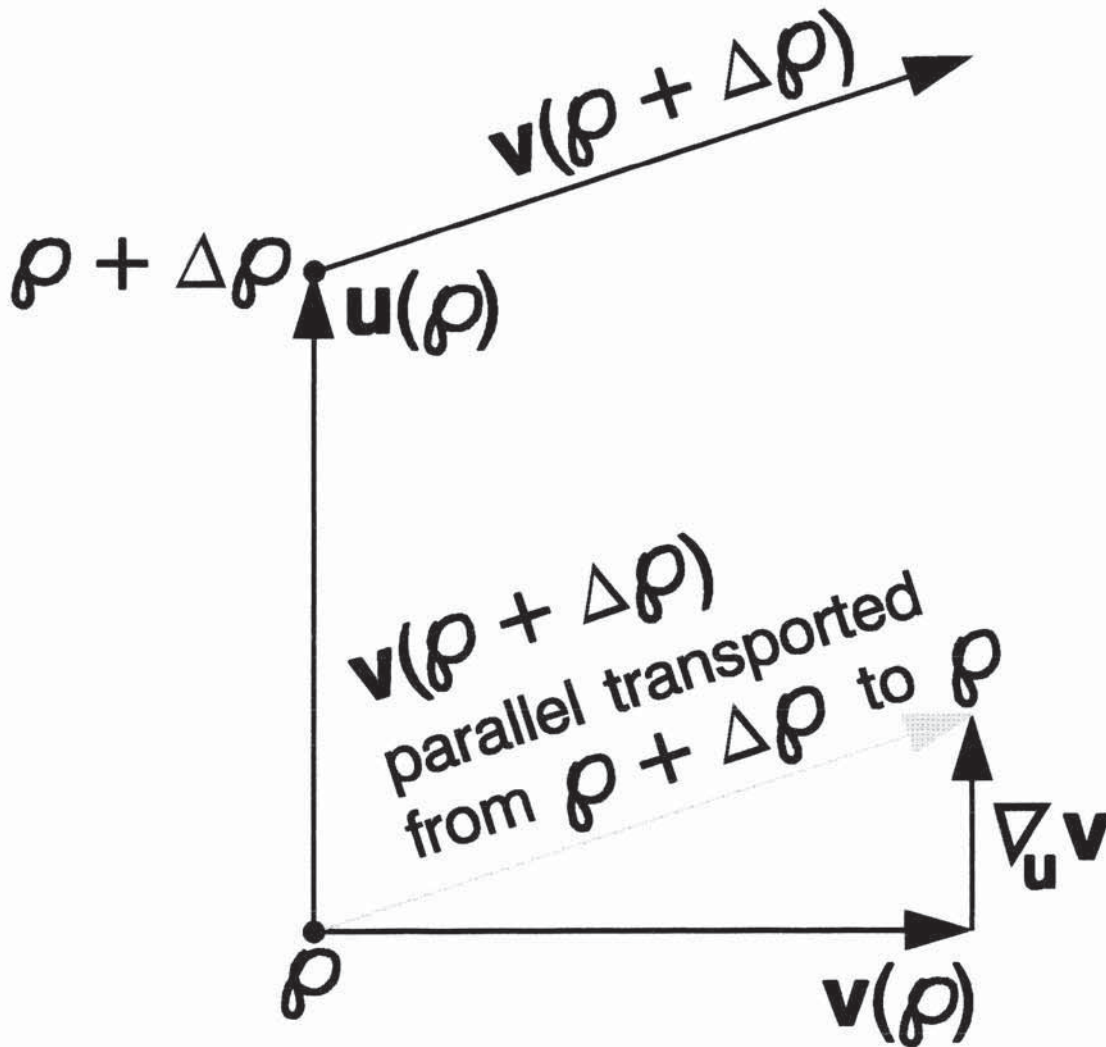


Figure 8 (Continued).

# Elastic Deformation



# Covariant Derivative



**Figure 9.** The covariant derivative of vector  $\mathbf{v}$  in the direction  $\mathbf{u}$ ,  $\nabla_{\mathbf{u}} \mathbf{v}$ , is shown at the point  $\rho$  (Misner *et al.* 1973). For the case where  $\mathbf{u} = d/ds$  is the tangent vector to some curve,

$d\mathbf{v}/ds \equiv \nabla_{\mathbf{u}} \mathbf{v} \equiv$  rate of change of  $\mathbf{v}$  with respect to  $s$ ,

$$\equiv \lim_{\Delta s \rightarrow 0} (\{\mathbf{v}(s + \Delta s)\}_{\text{parallel transported to } s} - \mathbf{v}(s)) / \Delta s.$$

For  $\nabla_{\mathbf{a}_n}$ , just let  $\mathbf{u} \equiv \partial/\partial x^n \equiv \mathbf{a}_n$  in this formula.

**Figure 10. Compatibility:** differential geometry is introduced into Calladine's (1983) treatment. An assembly of small, equal, rectangular plane facets which originally fit together in a planar array. A small strain is imparted to the array. If the facets are not connected to each other after straining (**incompatibility**), an *angular defect* is produced at each vertex. A strain will therefore generally impart some Gaussian curvature, say  $K$ , to the array.

$$\text{Gaussian curvature } \equiv K \equiv R_{xyy}/g, \text{ where } R_{xyy} = g_{mn} R^m_{\quad yy}$$

☞

and  $g$  is the determinant of  $g_{mn}$  (Kreyszig 1991); or

$$K \equiv (\text{angle turned through})/(\text{area circumnavigated})$$

☞

from rotation of a vector parallel transported around a closed path (Misner *et al.* 1973);  $K = 1/r^2$  for a sphere of radius  $r$ . **a)** Here, a shear distortion  $\gamma_x^y \equiv \partial u^x/\partial y$  is applied to the array, and the rectangles each receive their respective shears at their midpoints. The *angular defect* at the vertex, say  $\Psi$ , is  $\Psi = \gamma_y^x - \gamma_{y+\Delta y}^x - \gamma_{y+\Delta y}^{x+\Delta x} + \gamma_{y+\Delta y}^{x+\Delta x} = 10^\circ - 20^\circ - 15^\circ + 5^\circ$ . That is,  $\Psi$  is the sum of the angles inside the cross-hatched area;  $\Psi = -20^\circ$  in the figure, so the vertex has become a gap;  $\Psi = 0 \Rightarrow \text{compatibility}$ . The vertex is represented by the area  $\Delta A = \Delta x \Delta y$ . Thus,  $K \equiv \lim_{\Delta A \rightarrow 0} (\Psi/\Delta A) = \partial^2 \gamma_y^x / \partial x \partial y$ . Superposing tensile strains  $\varepsilon_{xx}$  and  $\varepsilon_{yy}$  onto  $\varepsilon_{xy} \equiv 1/2(\gamma_y^x + \gamma_x^y)$ ,

$$K \equiv \lim_{\Delta A \rightarrow 0} (\Psi/\Delta A) = 2\partial^2 \varepsilon_{xy} / \partial x \partial y - \partial^2 \varepsilon_{xx} / \partial y^2 - \partial^2 \varepsilon_{yy} / \partial x^2.$$

☞

The plane-strain compatibility condition is  $K = 0$ ;  $K = N^{zz}$ ,  $N^{ij} \mathbf{a}_i \otimes \mathbf{a}_j = \text{Incompatibility}$ :

$$\mathbf{N} = -\boldsymbol{\epsilon}^{ikm} \boldsymbol{\epsilon}^{jln} \varepsilon_{mn;lk} \mathbf{a}_i \otimes \mathbf{a}_j \Rightarrow N^{zz} \approx (2\partial^2 \varepsilon_{xy} / \partial x \partial y - \partial^2 \varepsilon_{xx} / \partial y^2 - \partial^2 \varepsilon_{yy} / \partial x^2)/g = R_{xyy}/g.$$

☞

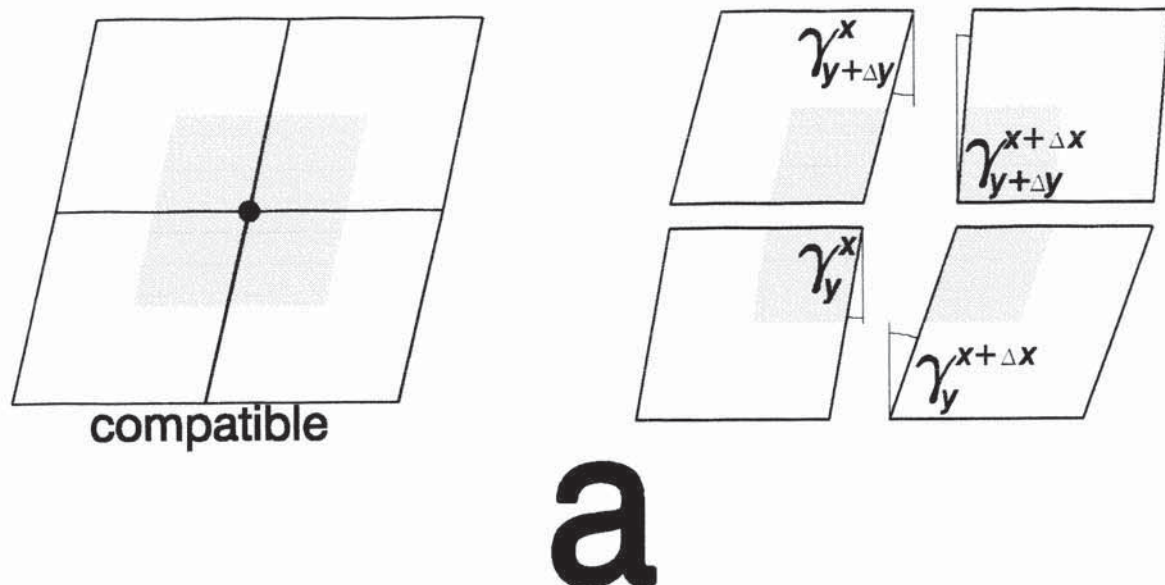
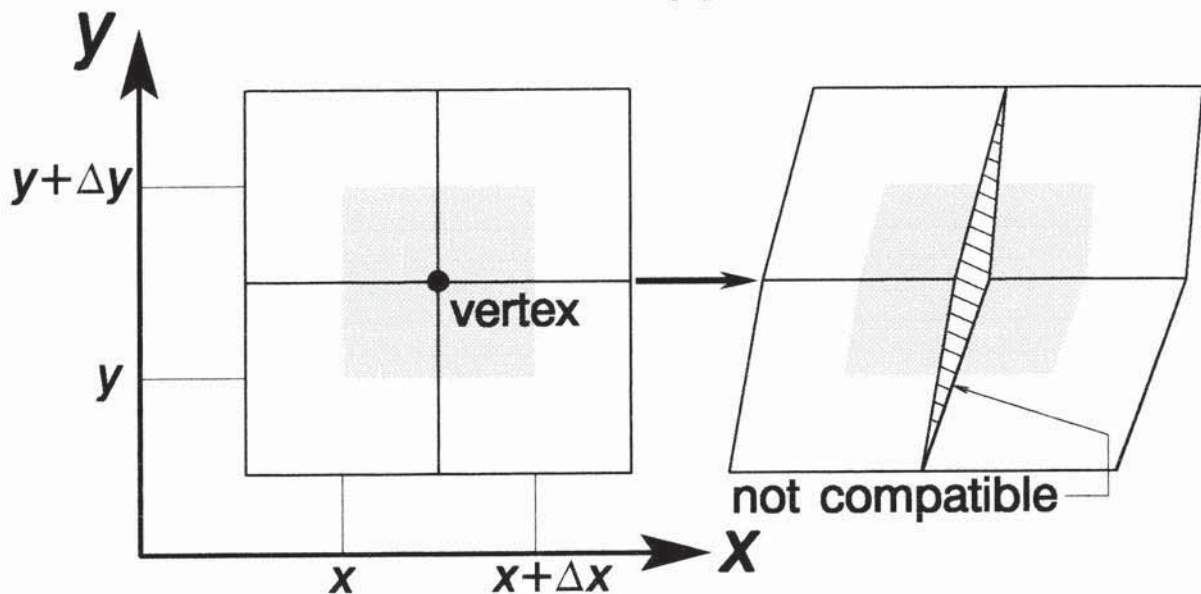
For the compatible case the vertex remains a vertex after straining,  $\Psi = 0 \Rightarrow K = 0$ .

Figure 10 (Continued).

# Compatibility

**Gaussian Curvature = Angular Defect per Unit Area**

$$= g_{xm} R^m y_{xy}/g$$



**Figure 10** (Continued). Mostly Regge (1962): **b)** Each *face*,  $f$ , of a hexagon is a triangle with an *internal angle*,  $\mu$ , of  $\mu = \pi/3 = 60^\circ$ . For any vertex  $v$ ,  $\Psi_v \equiv 2\pi - \sum_f \mu_f$ . Thus,  $\Psi = 0$  for a hexagon. The hexagon can be described with the *polar coordinates*  $r, \phi, Z$ , where  $r^2 \equiv X^2 + Y^2$ , and the metric  $\mathbf{G} = dZ \otimes dZ + dr \otimes dr + r^2 d\phi \otimes d\phi$ . The vertex is the point  $Z = r = 0$ . Since  $\Psi = 0$ ,  $Riemann \equiv R = 0$ ;  $\mathbf{G} = dr \otimes dr + r^2 d\phi \otimes d\phi$  therefore measures all points on the hexagon. A vector, say  $\mathbf{v}$ , is shown being parallel transported along the periphery of the hexagon: at each location  $\mathbf{v}$  is perpendicular to an exterior face. This vector can be so transported for any number of turns around the periphery without changing. **c)** A piece from the hexagon is removed; the angular defect at the vertex is  $\Psi = -60^\circ$ . An "*internal strain*" is applied to join the edges which are then welded together to form the "*buckled*" two-dimensional pentagon. An *incompatible deformation* is obtained. *Parallel transport* vector  $\mathbf{v}$  around the periphery of the pentagon, *i.e.* a path named **C**. No change in the vector results from 1-2-3-4-5; but from 5 to 1  $\mathbf{v}$  changes its angle by  $-\Psi$  (not enough turns). All curvature is associated with the vertex:

$$\Psi_v = \oint_C K dA = 2\pi - \sum_f \mu_f = 360^\circ - 5 \times 60^\circ = 60^\circ = -\Psi,$$

where  $K$  is a Dirac delta function at the vertex and  $dA$  is a differential area. **d)** A slice is made in the hexagon from the vertex to the free surface along an edge so that another triangle can be inserted: the angular defect at the vertex is  $\Psi = 60^\circ$ . Internal strain is applied so that the triangle can be squeezed into place and then welded shut. A "*buckled*" heptagon is obtained. Parallel transport of  $\mathbf{v}$  along periphery **C** results in no change in  $\mathbf{v}$  for the path 1-2-3-4-5-6-7; but from 7-8  $\mathbf{v}$  changes its angle by  $\Psi$  (one turn too many):

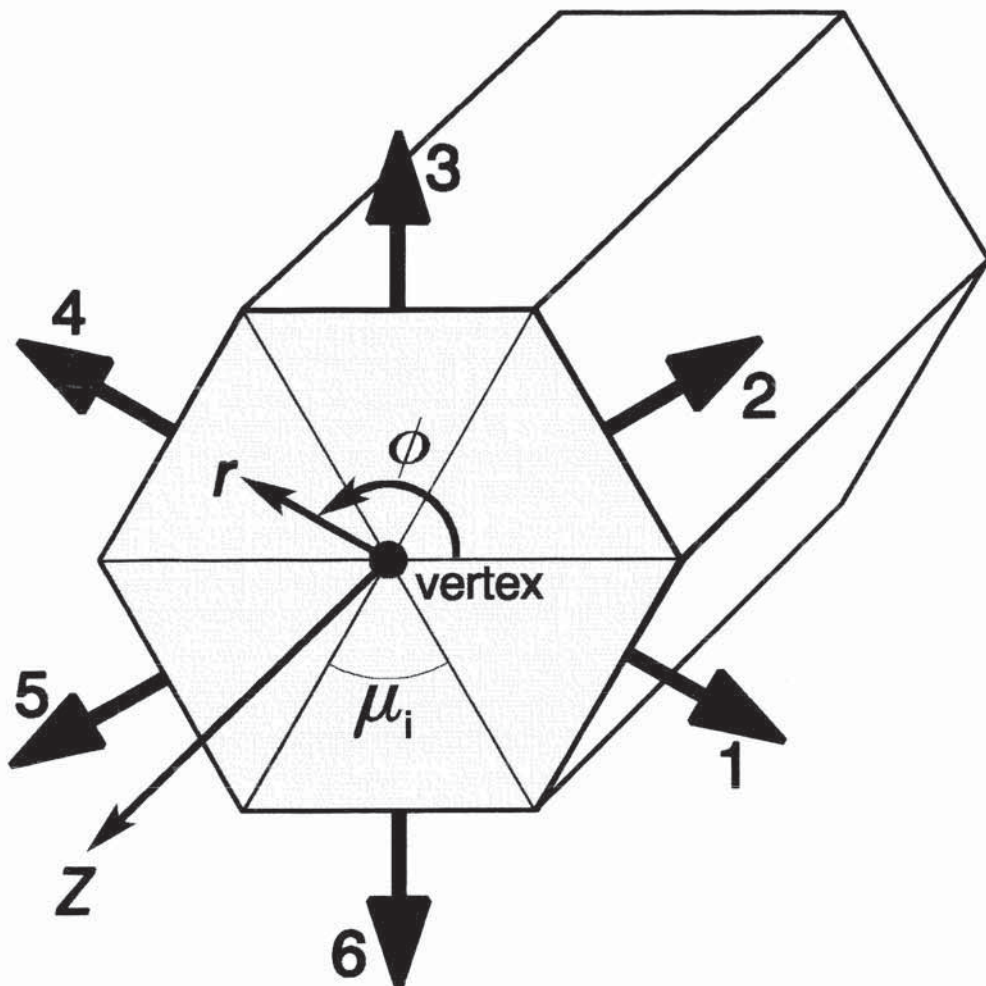
$$\Psi_v = \oint_C K dA = 2\pi - \sum_f \mu_f = 360^\circ - 7 \times 60^\circ = -60^\circ = -\Psi.$$

Figure 10 (Continued).

# Incompatibility

**Gaussian Curvature = Angular Defect per Unit Area**

$$= g_{xm} R^m_{yxy}/g$$



So an array of hexagons is compatible;  $\Psi_6 = 0$ .

b

Figure 10 (Continued).

## Incompatibility (Continued)

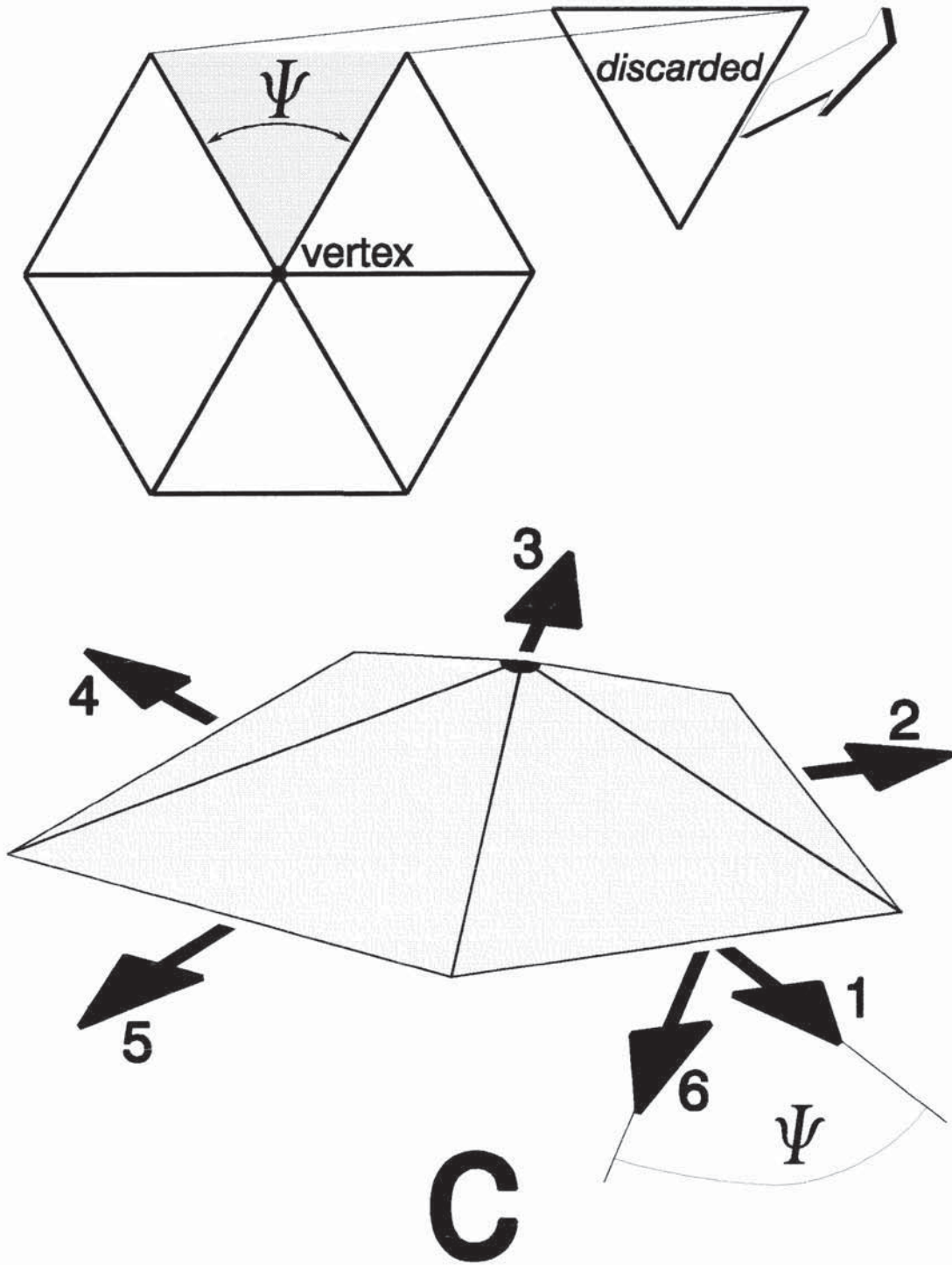
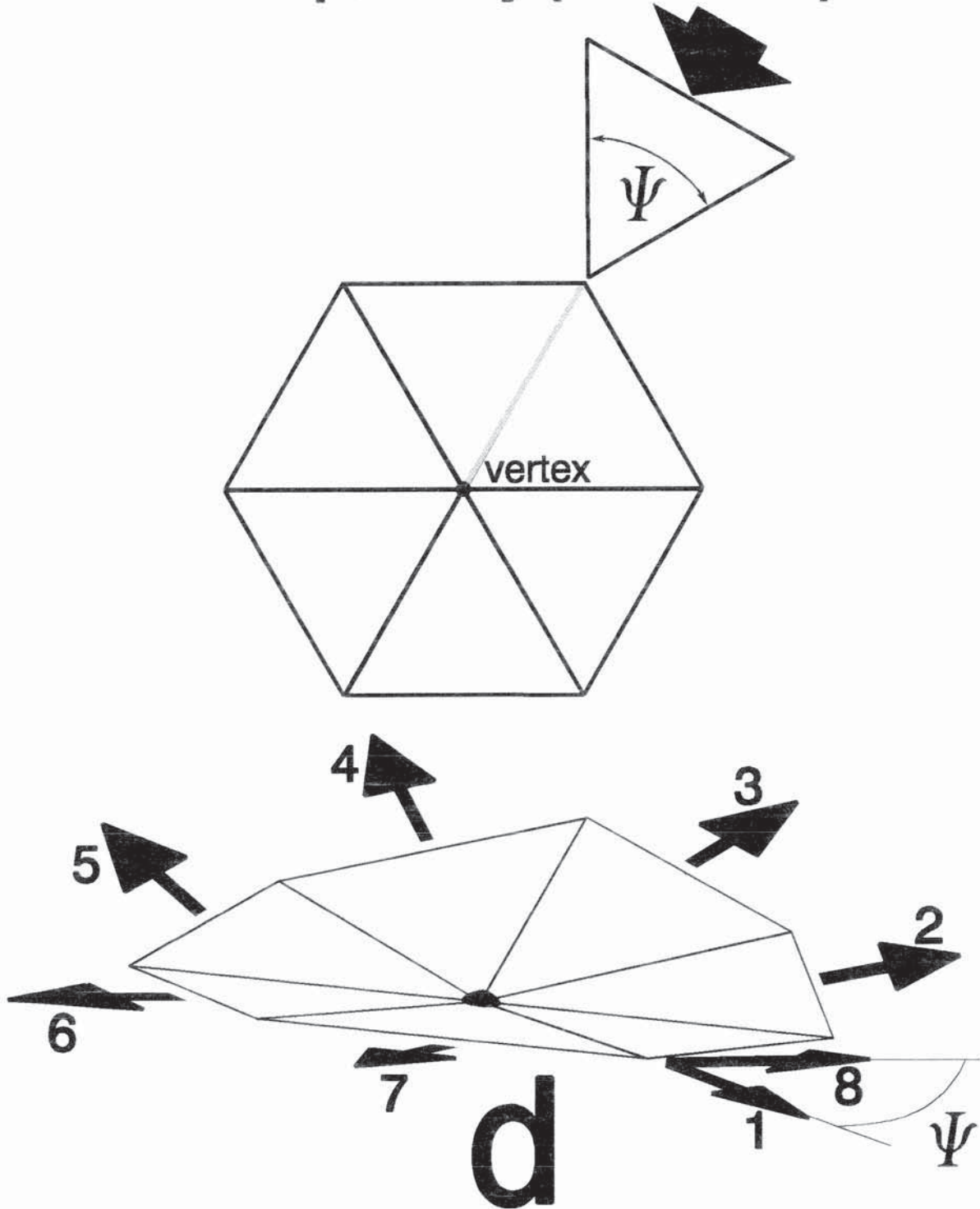


Figure 10 (Continued).

## Incompatibility (Continued)



**Figure 11.** The *Lie derivative* (Misner *et al.* 1973, Burke 1985) of vector  $\mathbf{v}$  in the direction

$$\begin{aligned}\mathbf{u}, \mathbf{f}_\mathbf{u} \mathbf{v} &\equiv (\mathbf{u} \cdot \nabla) \mathbf{v} - (\mathbf{v} \cdot \nabla) \mathbf{u} \equiv [\mathbf{u}, \mathbf{v}] \equiv \mathbf{u}[\mathbf{v}] - \mathbf{v}[\mathbf{u}] \equiv u^m \partial(v^n \partial/x^n)/\partial x^m - v^m \partial(u^n \partial/x^n)/\partial x^m \\ &= (u^m v_{,m} - v^m u_{,m}) \partial/\partial x^n \equiv (u^m v_{,m} - v^m u_{,m}) \mathbf{a}_n, \text{ where } u_{,m} \equiv \partial u^n / \partial x^m \text{ and } \mathbf{a}_n \equiv \partial/\partial x^n.\end{aligned}$$

**a)** Illustration of Lie derivative  $\mathbf{f}_\mathbf{u} \mathbf{v} = [\mathbf{u}, \mathbf{v}]$  for parameterized vector fields  $\mathbf{u} \equiv \partial/\partial s$  and  $\mathbf{v} \equiv \partial/\partial t$ . Top: vectors are shown on the "manifold" (*e.g.* lattice). Bottom: the vectors are shown on the *tangent space* ( $\simeq$  "manifold" for  $(\Delta s, \Delta t) \rightarrow 0$ ). **b)** If  $\mathbf{f}_\mathbf{u} \mathbf{v} = [\mathbf{u}, \mathbf{v}] = 0$ , then the vector field  $\mathbf{v}$  is *dragged* over the vector field  $\mathbf{u}$ . Here,  $[\mathbf{A}_x, \mathbf{A}_y] = [\mathbf{A}_y, \mathbf{A}_x] = 0$  and  $[\mathbf{a}_x, \mathbf{a}_y] = [\mathbf{a}_y, \mathbf{a}_x] = 0$ ; *i.e.* the basis vectors are dragged over each other. The basis vectors  $\mathbf{a}_x$  and  $\mathbf{a}_y$  define the *bivector*  $\mathbf{a}_x \wedge \mathbf{a}_y = \mathbf{a}_x \otimes \mathbf{a}_y - \mathbf{a}_y \otimes \mathbf{a}_x$ , or oriented area. **c)** The *commutator* of the covariant derivatives  $\nabla_\mathbf{u}$  and  $\nabla_\mathbf{v}$ ,  $[\nabla_\mathbf{u}, \nabla_\mathbf{v}] \equiv \nabla_\mathbf{u}(\mathbf{v}) - \nabla_\mathbf{v}(\mathbf{u})$ , is shown: if the connection coefficients are symmetric,  $\Gamma^m_{np} = \Gamma^m_{pn}$ , then  $[\nabla_\mathbf{u}, \nabla_\mathbf{v}] \equiv \nabla_\mathbf{u}(\mathbf{v}) - \nabla_\mathbf{v}(\mathbf{u}) = [\mathbf{u}, \mathbf{v}]$ . For an asymmetric connection,  $\Gamma^m_{np} \neq \Gamma^m_{pn}$ ,

$$[\nabla_\mathbf{u}, \nabla_\mathbf{v}] \equiv \nabla_\mathbf{u}(\mathbf{v}) - \nabla_\mathbf{v}(\mathbf{u}) = [\mathbf{u}, \mathbf{v}] + \mathbf{T}(\dots, \mathbf{u}, \mathbf{v}),$$

where  $\mathbf{T}$  is the torsion tensor. **d)** The Lie bracket obeys the *Jacobi identity*,

$$[\mathbf{u}, [\mathbf{v}, \mathbf{w}]] + [\mathbf{v}, [\mathbf{w}, \mathbf{u}]] + [\mathbf{w}, [\mathbf{u}, \mathbf{v}]] = \mathbf{0},$$

which is illustrated here for two cases. In each case the unit cells fill space with no gaps, *i.e. compatibly*, see exercise 9.12 from Misner *et al.* (1973), *A Chip Off The Old Block*. Top:  $\mathbf{u}, \mathbf{v}, \mathbf{w} = \mathbf{A}_x, \mathbf{A}_y, \mathbf{A}_z$ , where  $\mathbf{A}_M$  are the constant basis vectors for an undeformed lattice; bottom:  $\mathbf{u}, \mathbf{v}, \mathbf{w} = \mathbf{a}_x, \mathbf{a}_y, \mathbf{a}_z$ , where  $\mathbf{a}_m = \mathbf{a}_m(x^n)$  are the basis vectors for a deformed, defect-free lattice.

Figure 11 (Continued).

## Lie Derivative = $[u, v]$

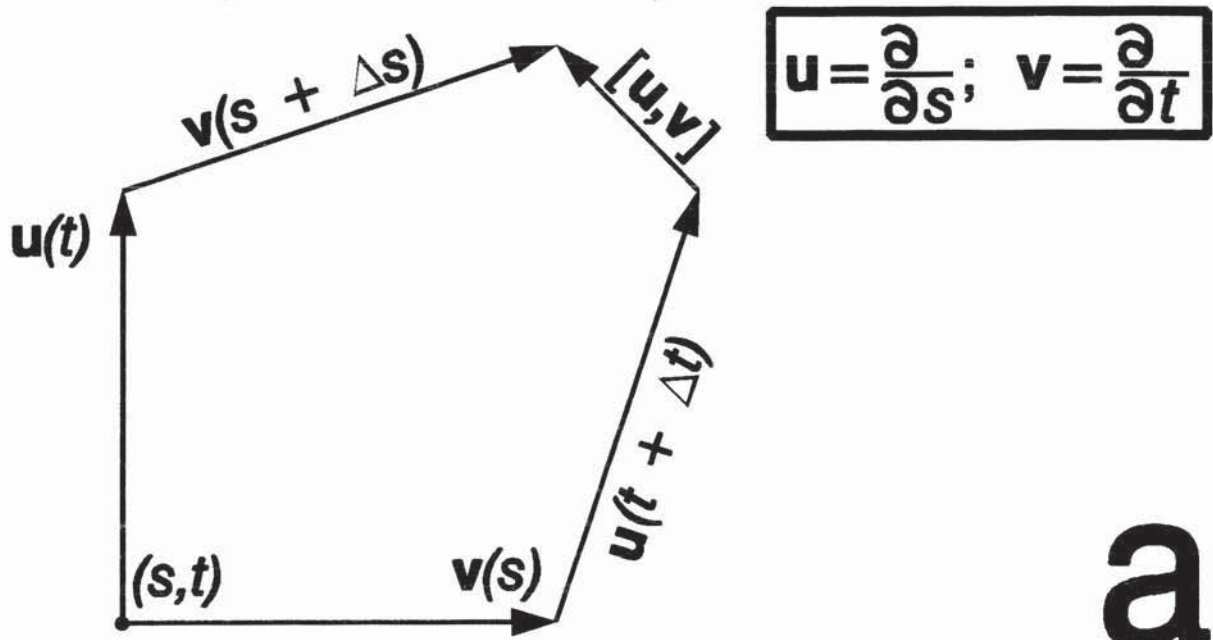
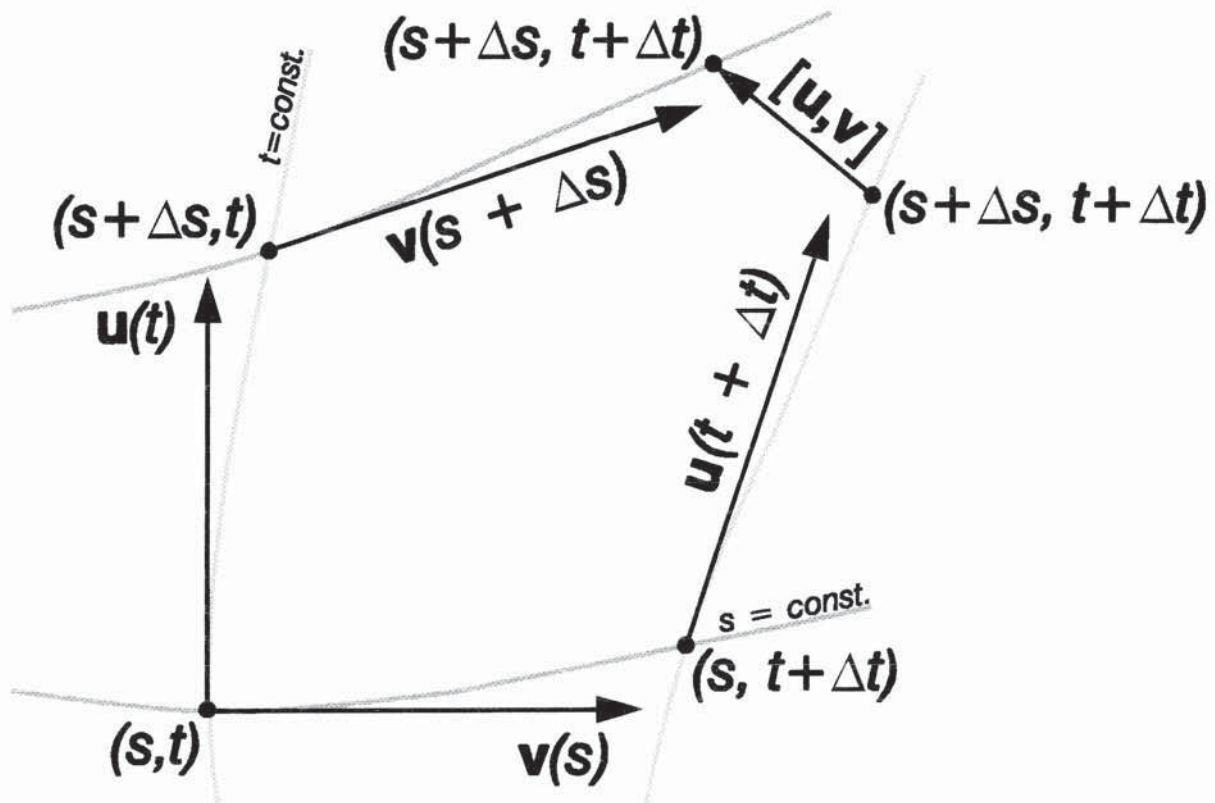


**Figure 11** (Continued).

# Dragging

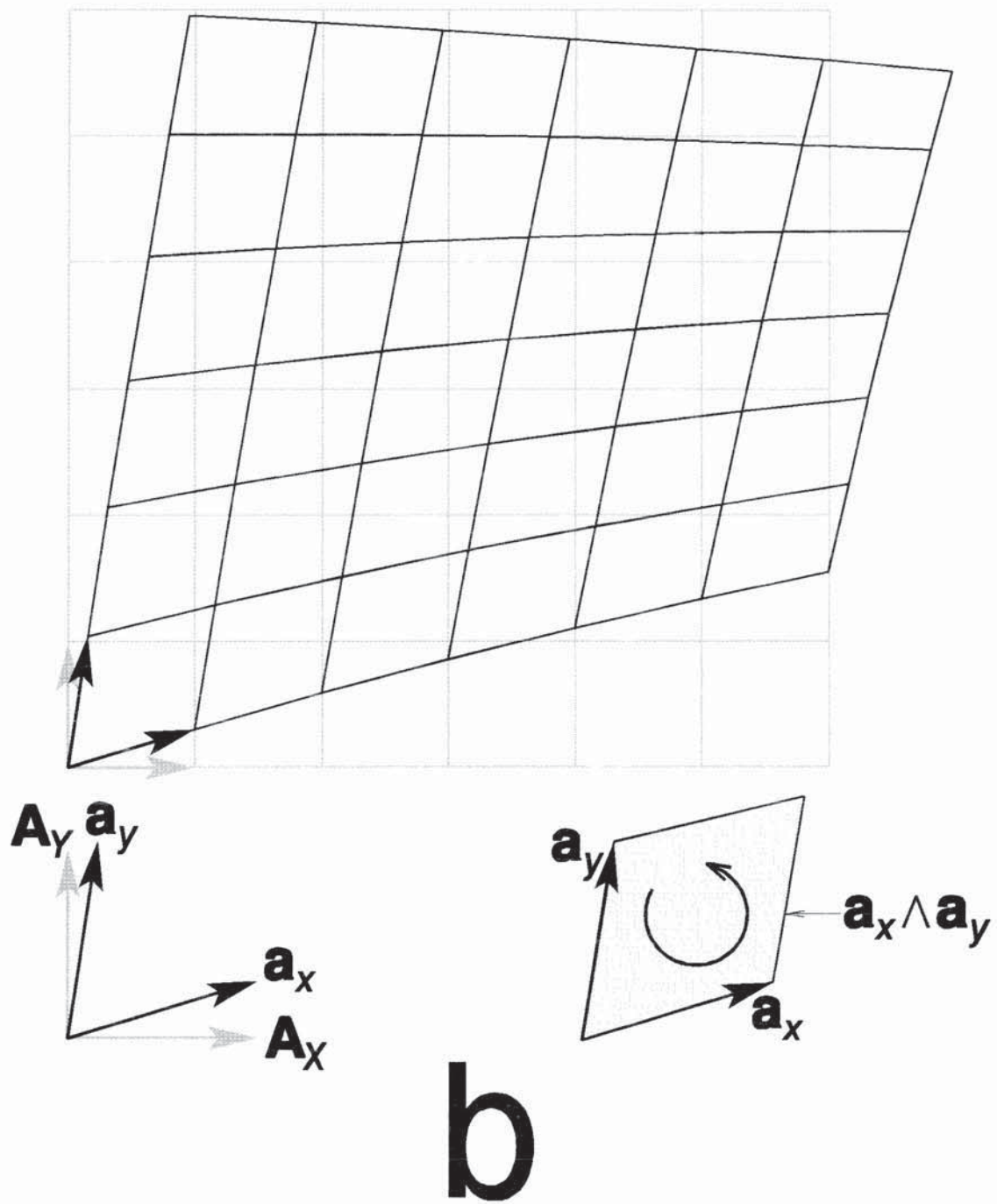
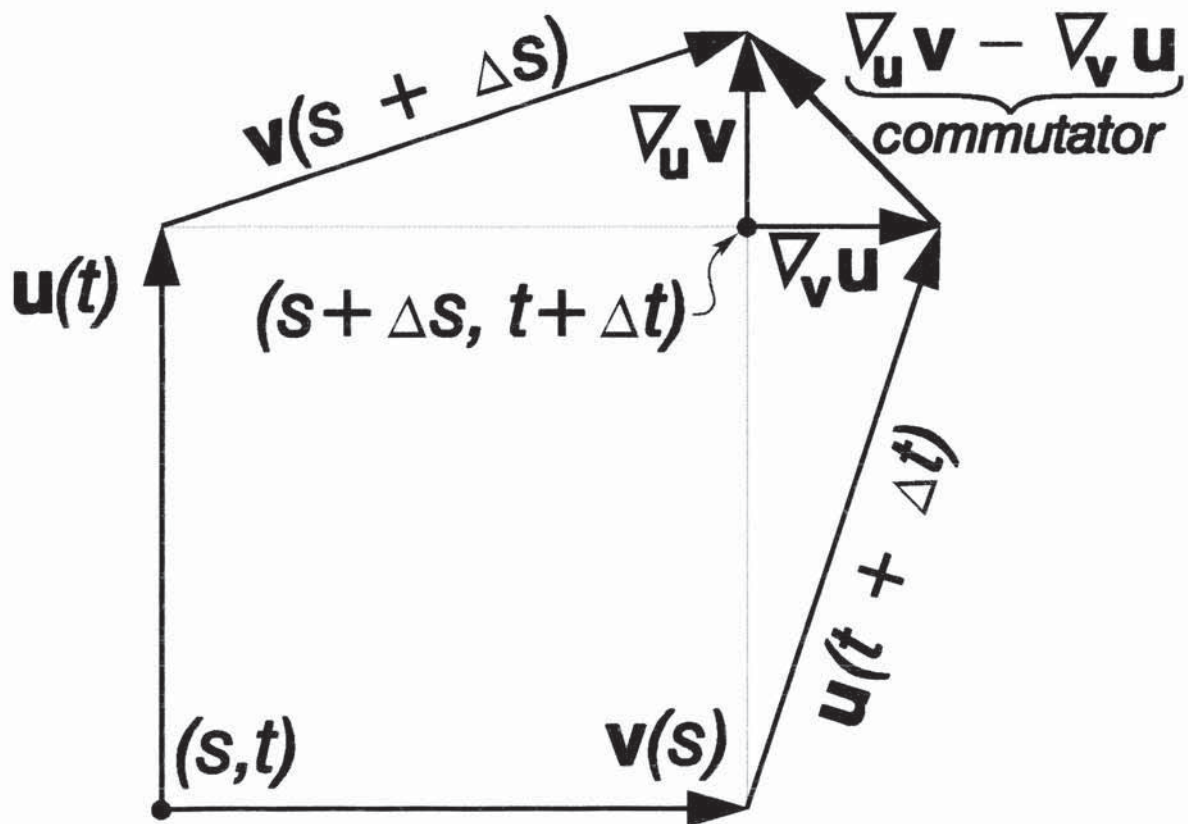


Figure 11 (Continued).

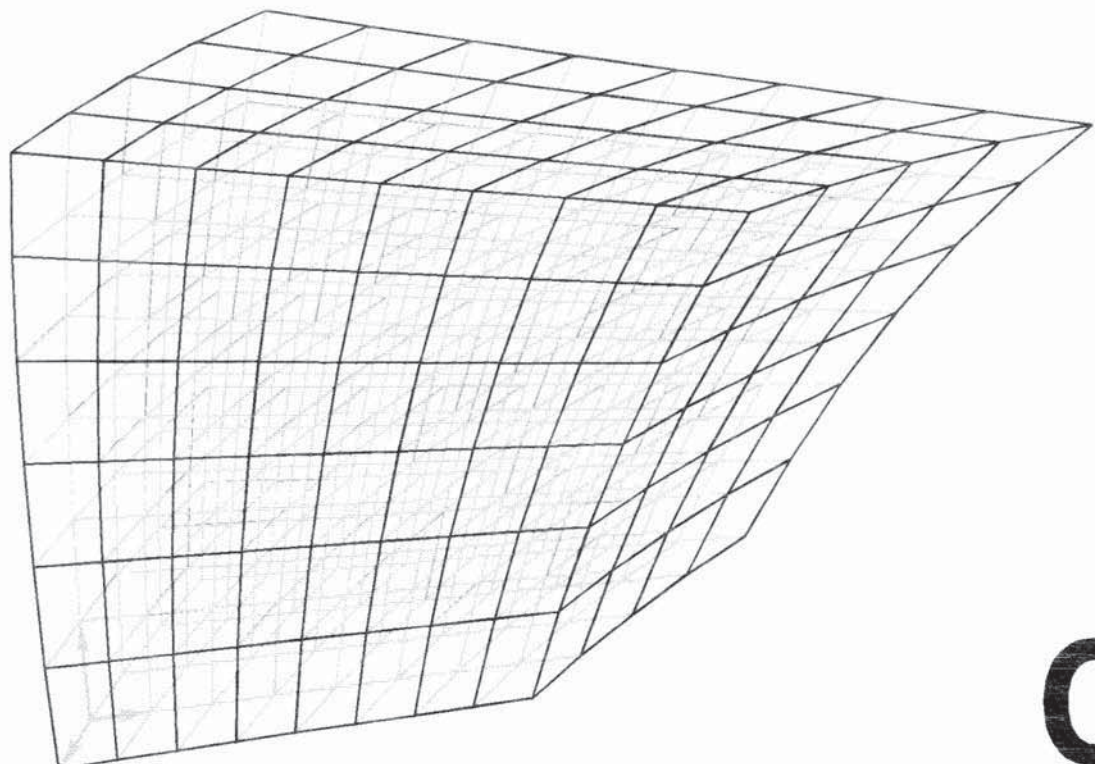
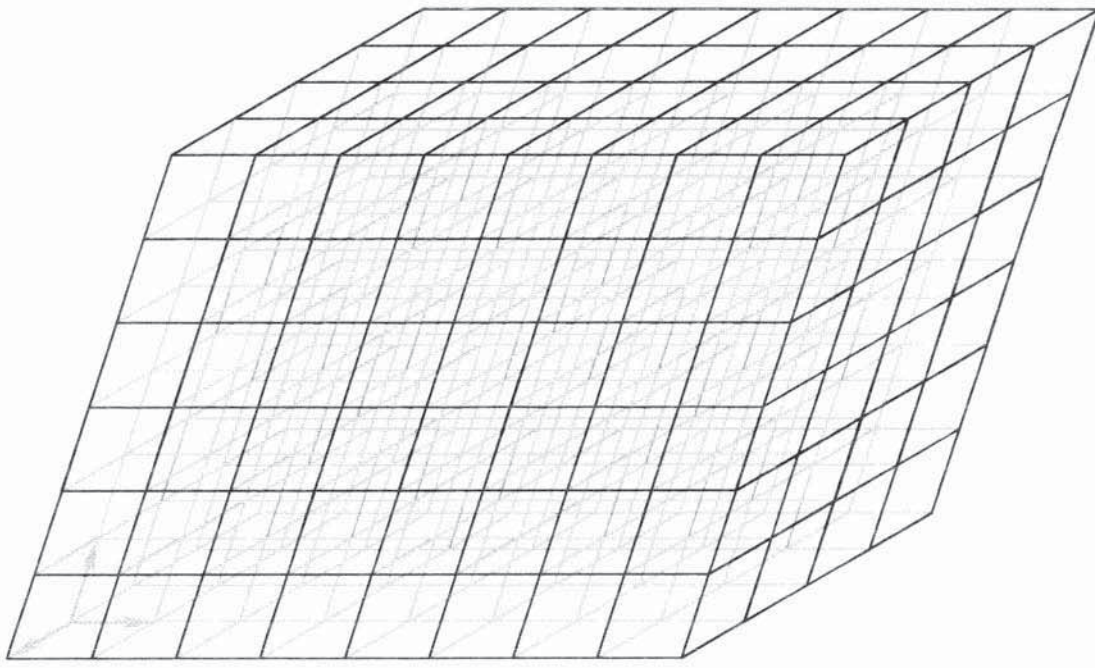
# Commutator of Covariant Derivatives



C

**Figure 11** (Continued).

# Jacobi Identity



**d**

**Figure 12.** *Holonomy* (Burke 1985): Successive "transformations" generally do not commute, *anholonomy* then results. If successive "transformations" do commute, then they are *holonomic*. **a)** Top (anholonomic):  $\mathbf{AB} + \mathbf{A}^{-1}\mathbf{B}^{-1} \neq \mathbf{0}$ . Bottom (holonomic):  $\mathbf{AB} + \mathbf{A}^{-1}\mathbf{B}^{-1} = \mathbf{0}$ . **b)** Geometry of parking a car. In order to get out of the parking space shown on the bottom of the page the driver has two different transformations: **steering**  $\equiv \mathbf{O}$  and **driving**  $\equiv \mathbf{D}$ ;  $\mathbf{O} \equiv \partial/\partial\phi \equiv \mathbf{e}_\phi$  and  $\mathbf{D} \equiv (\cos\theta)\partial/\partial x + (\sin\theta)\partial/\partial y + L^{-1}(\tan\phi)\partial/\partial\theta$ . These transformations act in the *configuration space* shown on top. Steering and driving do not commute:

$\mathbf{OD} - \mathbf{DO} \equiv \mathbf{O}(\mathbf{D}) - \mathbf{D}(\mathbf{O}) \equiv [\mathbf{O}, \mathbf{D}] = (L\cos^2\phi)^{-1}\partial/\partial\theta \equiv \mathbf{R} \equiv \mathbf{rotate}$ ;  
 $\mathbf{rotate} = \mathbf{steer} + \mathbf{drive} + \mathbf{steer}^{-1} + \mathbf{drive}^{-1}$ , where  $\mathbf{steer}^{-1} = \mathbf{steer back}$  and  $\mathbf{drive}^{-1} = \mathbf{drive back}$ . Similarly

$$[\mathbf{D}, \mathbf{R}] = (L\cos^2\phi)^{-1}[(\sin\theta)\partial/\partial x - (\cos\theta)\partial/\partial y] \equiv \mathbf{S} \equiv \mathbf{slide}.$$

Sliding is a displacement at right angles to the car. **c)** "Degrees of freedom" for primitive unit cells. **i.** Reference state. **ii.** *Slip* is a translation analogous to **driving**. **iii.** *Climb* is a translation analogous to **sliding**. **iv.** *Rotation* is analogous to **steering**. **v.** *Shearing* has no analogy with parking a car.

Figure 12 (Continued).

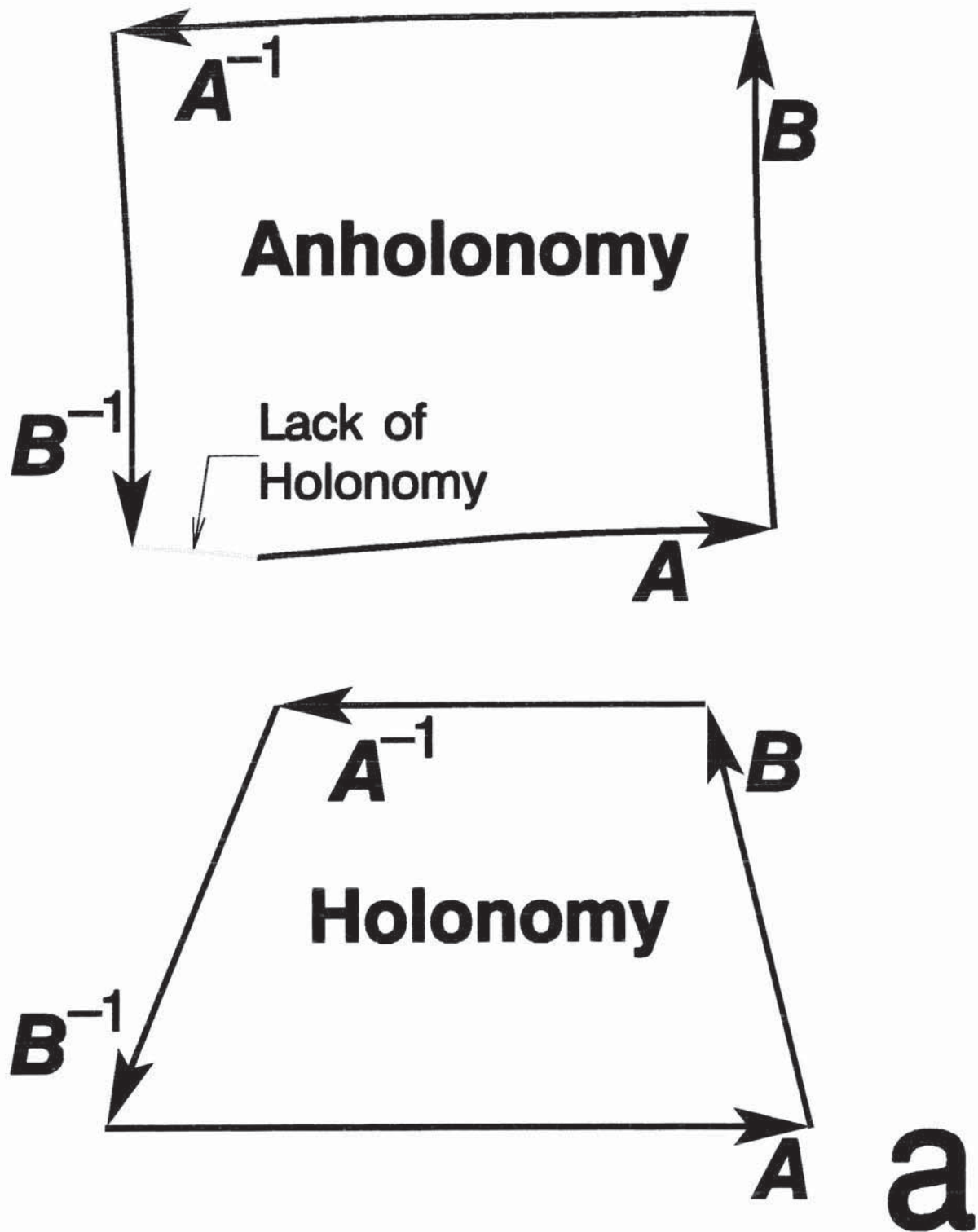


Figure 12 (Continued).

## Parking a Car

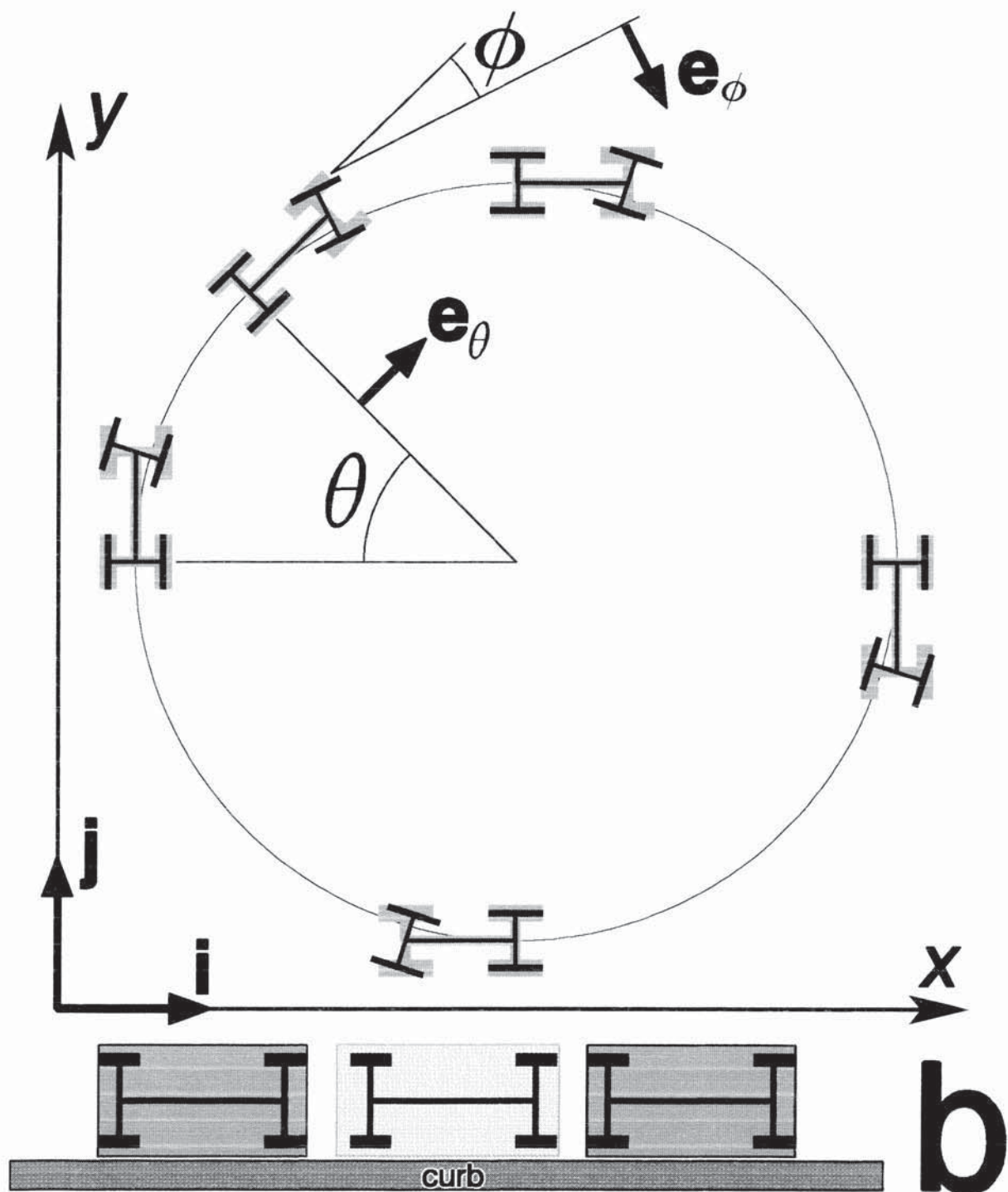
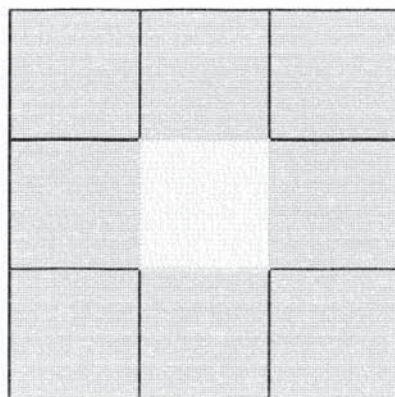
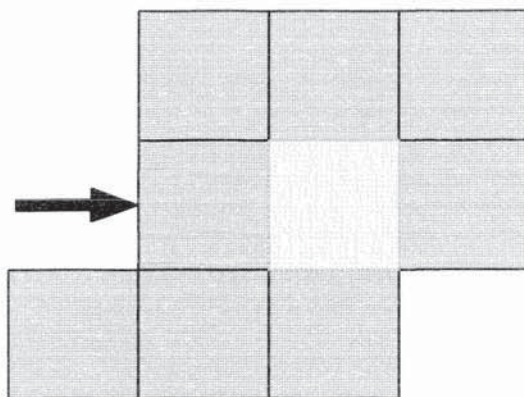


Figure 12 (Continued).

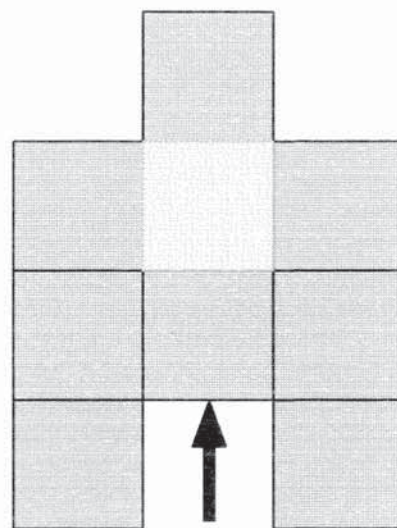
## "Degrees of Freedom" for Unit Cells



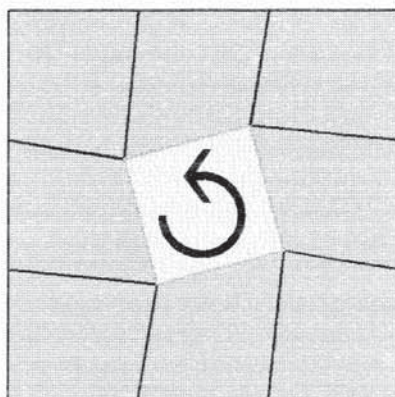
**i**



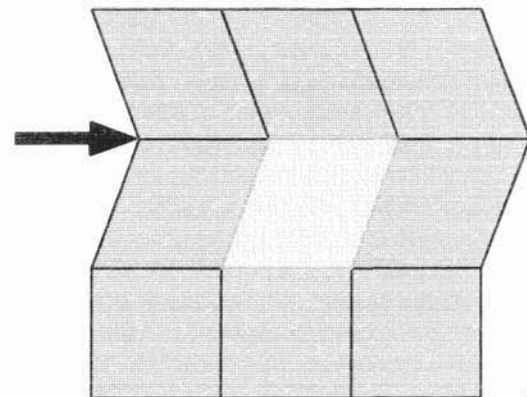
**ii**



**iii**



**iv**



**v**

**C**

**Figure 13.** *Edge Dislocation*, configurations 'a' through 'd': two dimensional view of a line defect that runs into the paper (direction of dislocation axis,  $\xi$ ). **a)** Continuum (Eshelby 1956 and Nabarro 1967): a pie section is cut from the reference state, withdrawn slightly, welded at the right hand side, and remaining material is cut off and discarded, thereby producing the *natural state*. If elastic strains are applied so that the other side of the piece of pie can be welded then the middle configuration is obtained. **b)** Crystal edge dislocation. The reference state does not contain any defects. The dislocated state in the middle was made by removing one-half of a plane of atoms, leaving an *extra half-plane* behind. The natural state shows the missing atoms clearly. The *shape strain* (Bilby 1960) is revealed by attaching a continuum strip around the lattice which has the same elastic properties as the crystal lattice. For the middle configuration the total distortion is the sum of elastic and plastic distortions:  $\gamma = \gamma + \gamma'$ , where  $\gamma'$  corresponds to the dislocation deformation  $\gamma$  in the text and  $\gamma'$  to the internal strain  $\gamma$ ; the elastic strain vanishes in the natural state:  $\epsilon = 0$ . **c)** The *true Burgers vector* (or *Frank's Burgers vector*) results when a closed loop  $C$  around the dislocation line is mapped to the reference lattice where it becomes an open circuit  $M(C) \equiv C'$ . With the *finish-start convention* (Hirth and Lothe 1982):

$$\mathbf{b} \equiv - \int_{M(C)} d\mathbf{l}.$$

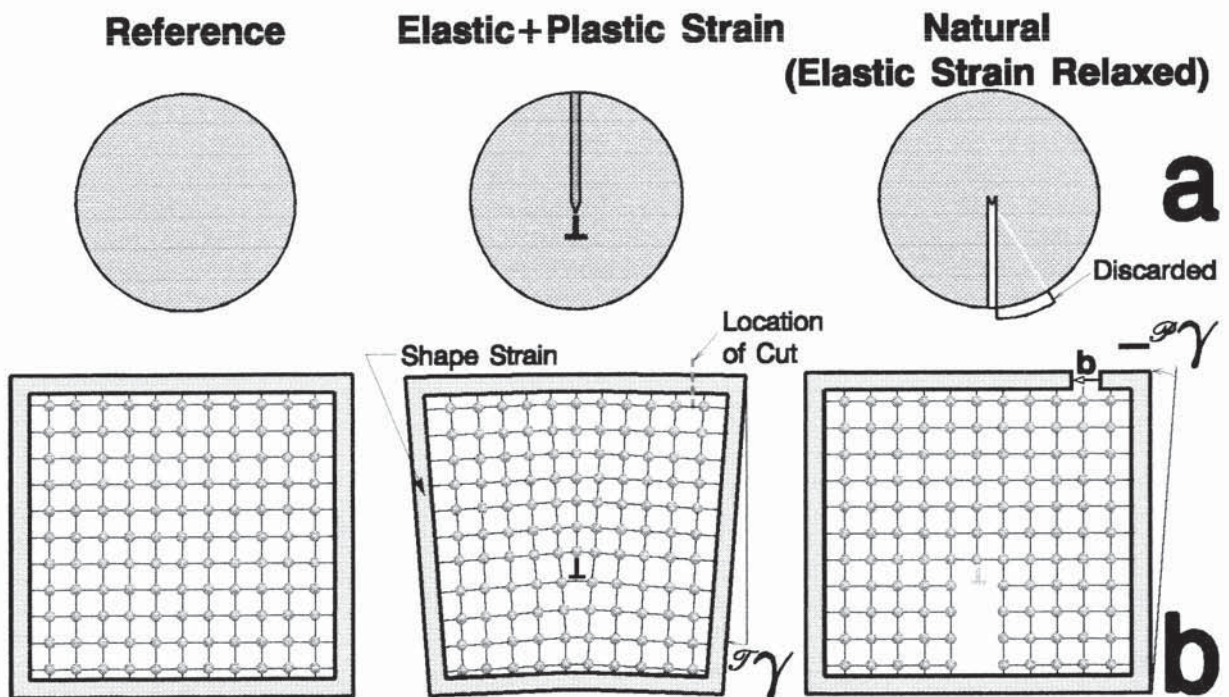
©

**d)** The *local Burgers vector* (or *Read's Burgers vector*) results when a closed circuit  $C'$  from the reference lattice is mapped onto the dislocated lattice,  $C' \rightarrow M(C') \equiv C$ , where it becomes an open circuit. With the *start-finish convention* (Hirth and Lothe 1982):

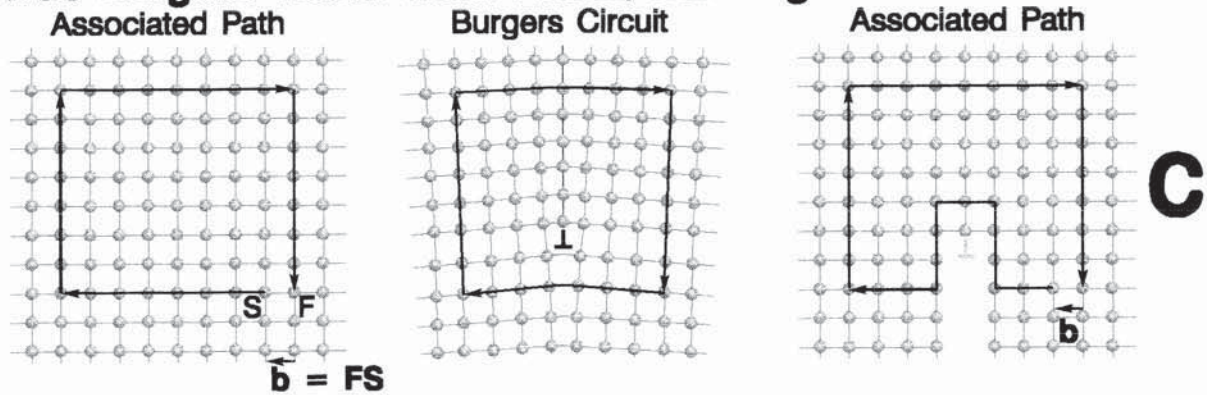
$$\mathbf{b} \equiv \int_{M(C)} d\mathbf{u} = \int_{M(C)} (\nabla \mathbf{u} \bullet d\mathbf{l}),$$

where  $\mathbf{u}$  is the elastic displacement field. See also de Wit (1960) and Kondo (1964).

Figure 13 (Continued).



### True Burgers Vector from Finish/Start Right-Hand Convention



### Local Burgers Vector from Start/Finish Right-Hand Convention

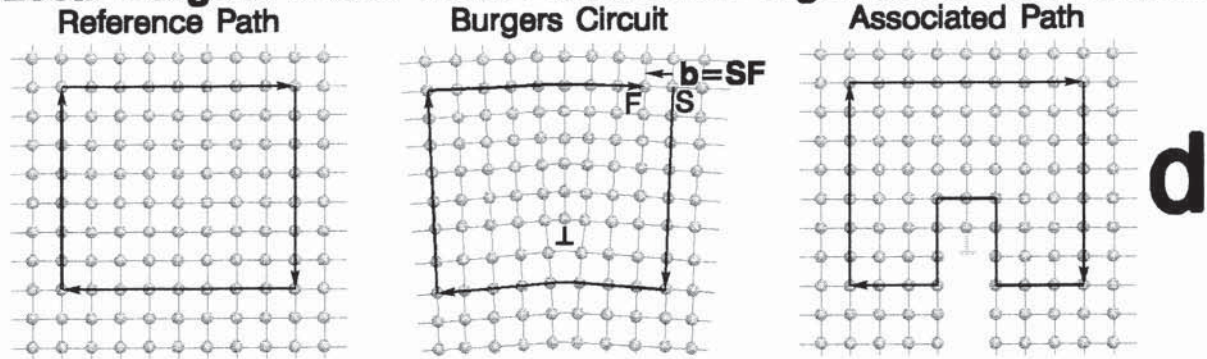
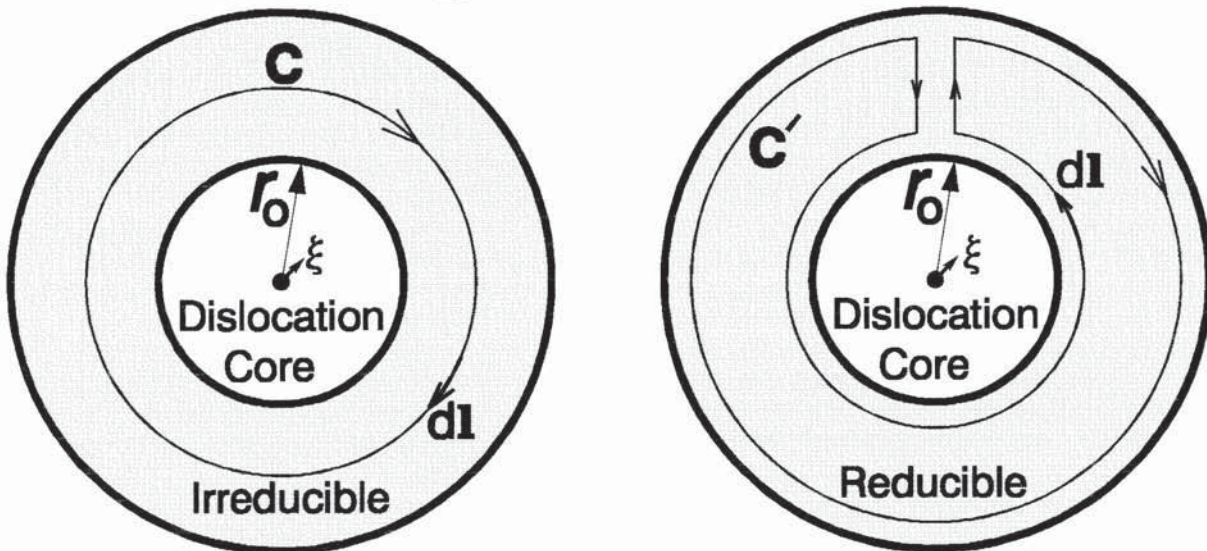


**Figure 13** (Continued). ***Continuum Dislocations***, parts 'e' and 'f'. **e)** *Reducible* and *irreducible* circuits are defined (Cottrell 1953). The unit vector along the *dislocation axis*,  $\xi$ , points into the paper. **f)** The Burgers vector is given for edge and screw dislocations in a continuum. See also Gairola (1979). **g)** Finally, the edge dislocation construction used in 'a' is comprised of a *dipole* of positive and negative *wedge disclinations* (Kröner 1955, Eshelby 1956, Nabarro 1967). The plane-strain condition was called the elastic + plastic strain state in part 'a'.

Figure 13 (Continued).

# Burgers Circuit



**Dislocation axis runs into the paper.**

$$\mathbf{b} = \oint_{\mathbf{C}} (\nabla \mathbf{u}) \cdot d\mathbf{l}$$

$$0 = \oint_{\mathbf{C}'} (\nabla \mathbf{u}) \cdot d\mathbf{l}$$

de Wit (1960, 1981),  
Hirth and Lothe (1982),  
Sherwood (1994),

$$\mathbf{b} = - \oint_{\mathbf{C}} (\nabla \mathbf{u}) \cdot d\mathbf{l}$$

Nabarro (1967).

e

Figure 13 (Continued).

# Continuum Dislocations

**Doubly Connected  
(Deformed)**

**Simply-Connected  
(Natural or Stress-Free)**

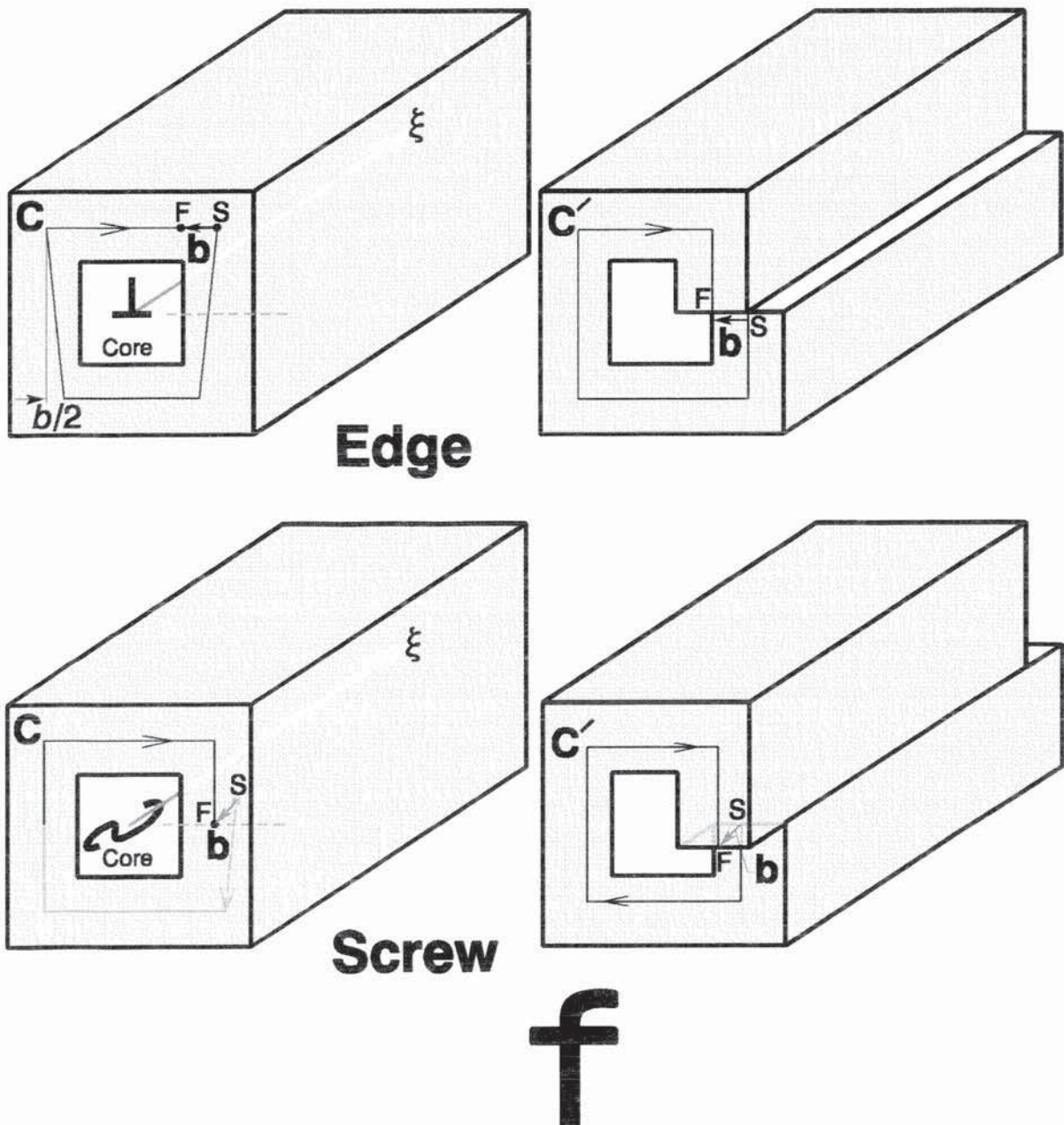
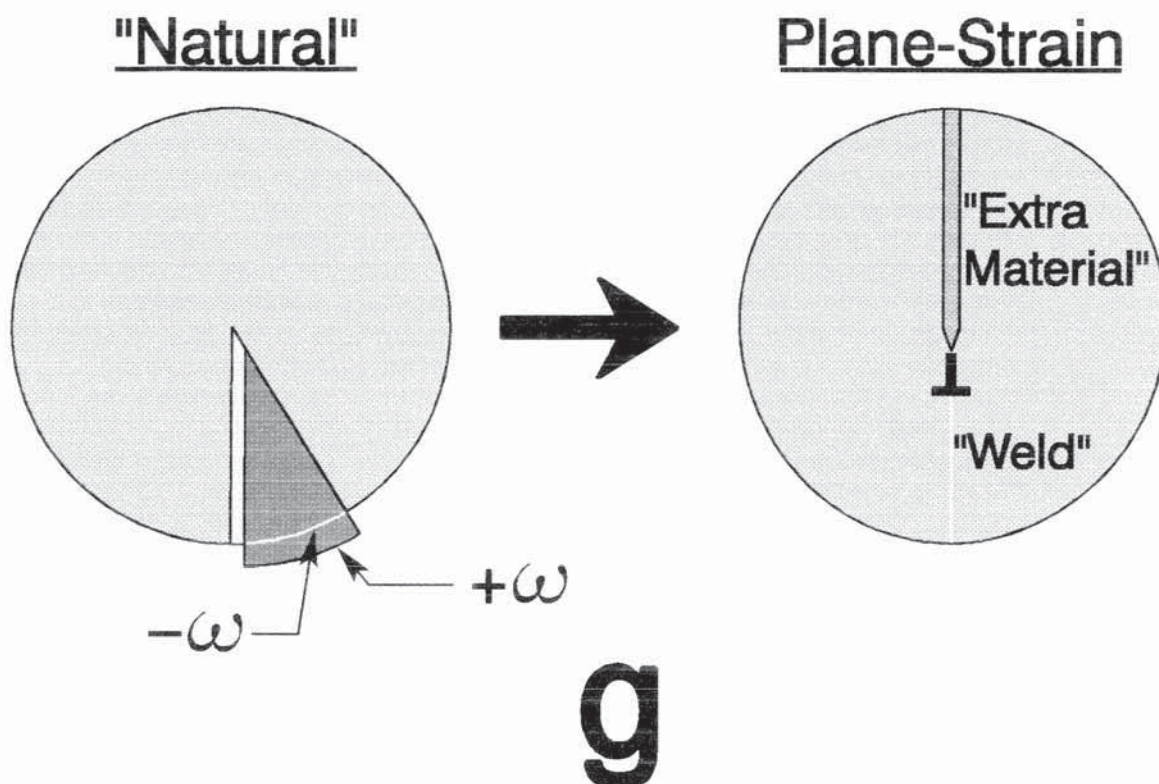


Figure 13 (Continued).

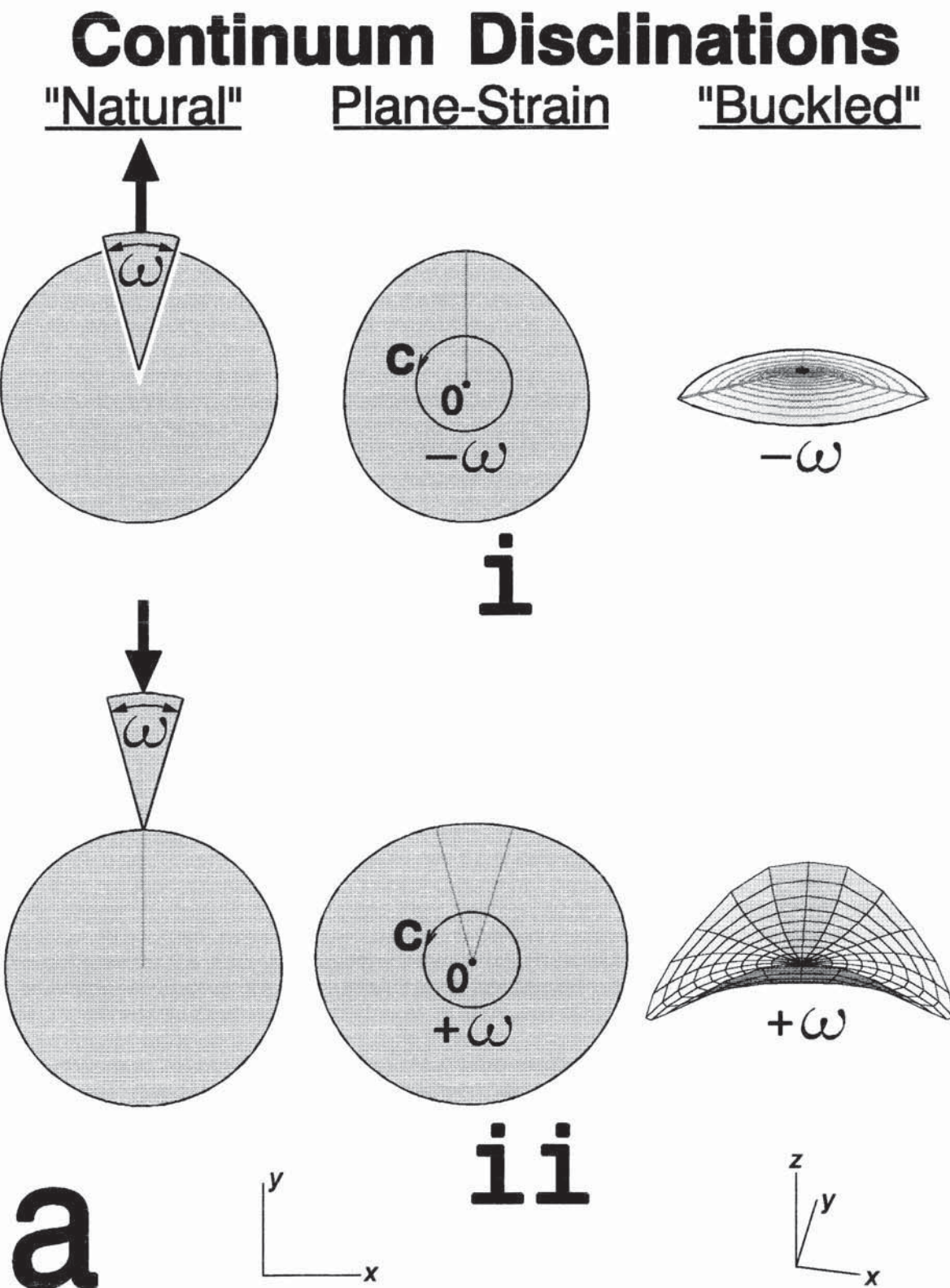
# Continuum Disclination Dipole = Edge Dislocation



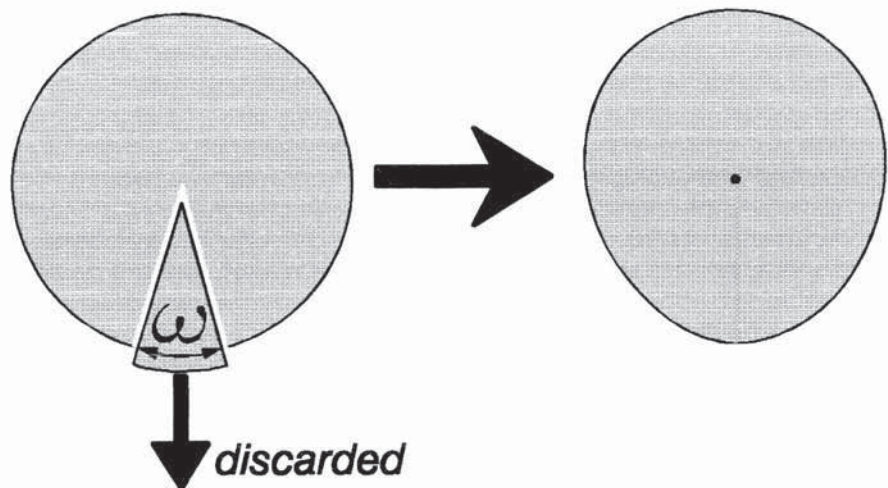
**Figure 14.** **a)** *Disclinations* in a continuum are constructed after Eshelby (1956); see also Nabarro (1967), Kröner and Anthony (1975), Friedel (1979), and Venkataraman and Sahoo (1985). The *negative wedge disclination* (**i**) results from removing a wedge of material from the body and pasting the edges together; this operation can be done in the original plane of the figure (plane-strain) (Eshelby 1956) or out-of-the-plane (Venkataraman and Sahoo 1985) ("buckled"). The *positive wedge disclination* (**ii**) results from making a cut in the material and inserting a wedge of material; this operation can be done in the original plane of the figure (plane-strain) or out-of-the-plane (Venkataraman and Sahoo 1985) ("buckled").

- b)** The negative wedge disclination represents the termination of a tilt grain boundary (Eshelby 1956), here in a simple cubic lattice, after Nabarro (1967); Kröner and Anthony (1975) call it a *partial disclination*. It is comprised of edge dislocations (Li 1972). See Kröner and Anthony (1975) for a drawing of the analogous defect in a face-centered-cubic lattice. **c)**  $\pm 60^\circ$  wedge disclinations in a lattice with *sixfold* symmetry, after Kröner and Anthony (1975). Disclination cores are shown shaded. The lines connecting atoms are crystallographic directions, or *lattice lines*; note that they are not defined at the cores. The  $+60^\circ$  disclination core is at an atom which has seven nearest neighbors; the remaining atoms in the lattice have six nearest neighbors. The  $-60^\circ$  disclination core is at an atom which has five nearest neighbors; the remaining atoms in the lattice have six nearest neighbors.
- d)** Analogously to part 'c', *cellular disclinations* are shown. These defects are either pentagons surrounded by hexagons or heptagons surrounded by hexagons in a honeycomb array (Morral and Ashby 1974, Venkataraman and Sahoo 1985).

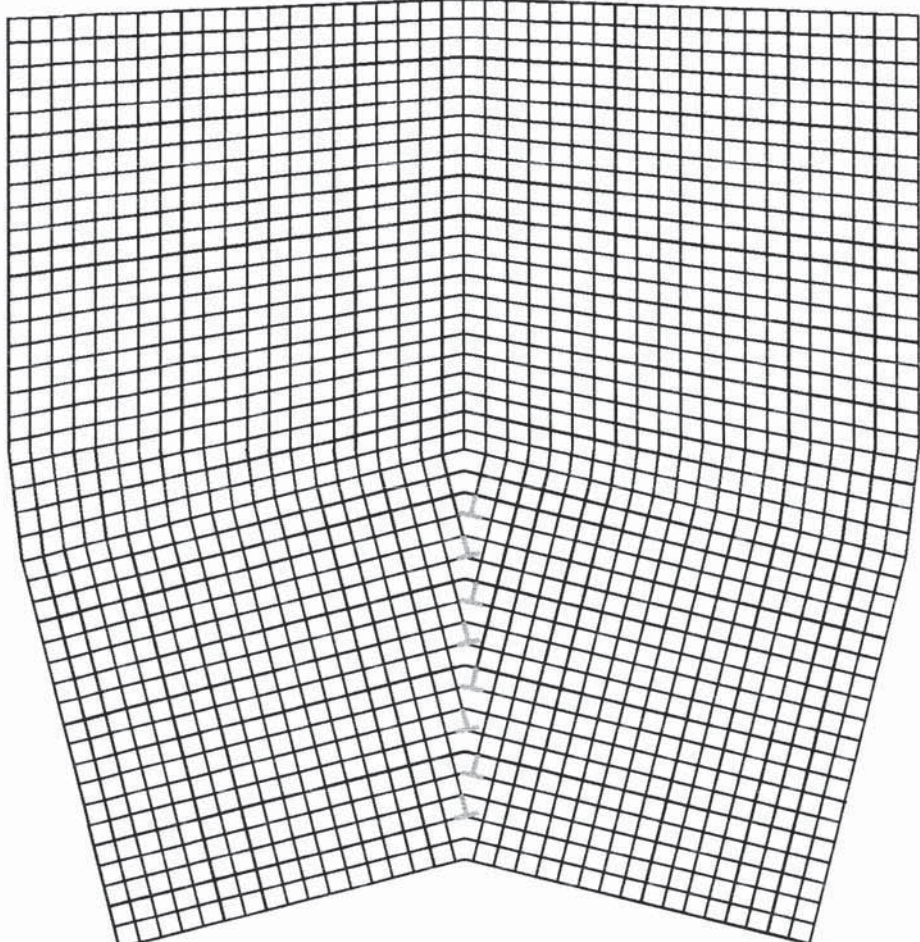
Figure 14 (Continued).



**Figure 14 (Continued).**



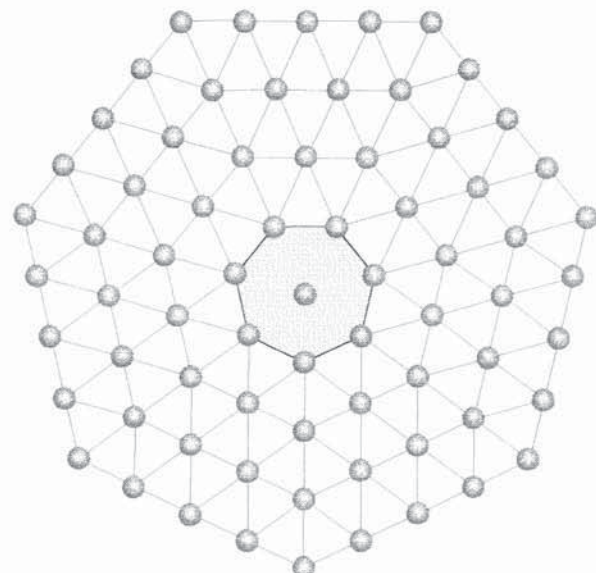
## **Partial Disclination**



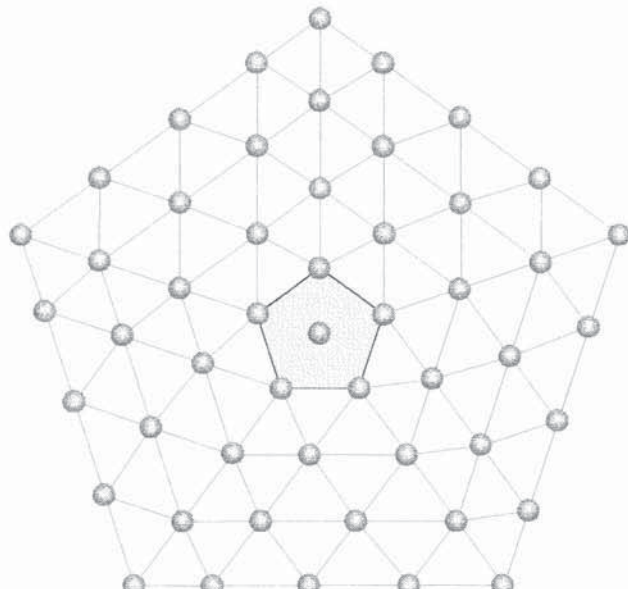
**b**

Figure 14 (Continued).

# Crystal Disclinations



+60°

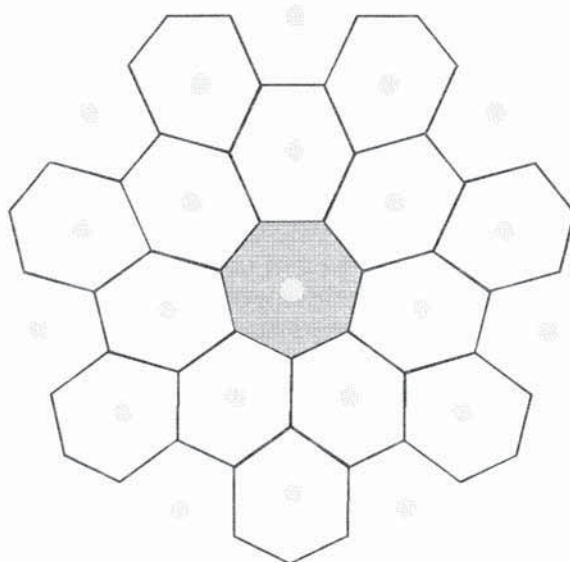


C

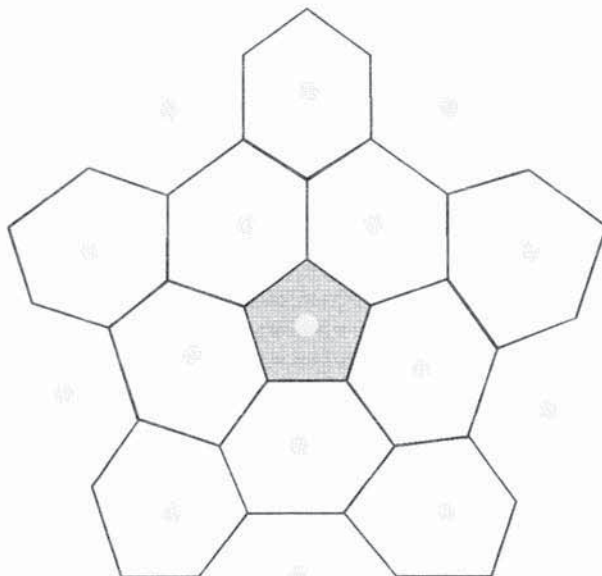
-60°

Figure 14 (Continued).

# Cellular Disclinations



+60°



d

-60°

**Figure 14** (Continued). **e)** After Friedel's (1979) Fig. 12: an edge dislocation in a lattice with sixfold symmetry splits into  $\pm 60^\circ$  wedge disclinations: A pair of disclinations,  $\Omega$  and  $-\Omega$ , is equivalent at long range to a (*translation*) dislocation  $\mathbf{b}$ , where  $\mathbf{b} = \Omega \times \mathbf{l}$ ,  $\mathbf{l}$  denoting the vector separating the disclinations. The shaded wedge shown here is associated with the cutting operations for the production of the analogous defect in a continuum, see Friedel's Fig. 7.

**Weingarten's Theorem** (Kröner and Anthony 1975): (Crystalline line defects can be modelled as strain singularities in an elastic continuum; a dislocation in a continuum can only be made in a multiply-connected body (Nabarro 1967).) Consider a doubly-connected body in a state of self-strain described by a symmetric strain tensor  $\boldsymbol{\epsilon}$ . In a *doubly-connected body* closed circuits  $\mathbf{C}$  are either *reducible* or *irreducible*. "A strain is called *self-strain* if no continuous displacement field  $\mathbf{u}$ , which carries one configuration into another, can be assigned to the points of the strained body. If the body is elastic then the self-strain state is also a self-stress state." Beginning at any point  $\rho$  inside of the self-strained body, along any reducible circuit  $\mathbf{C}'$ ,  $\mathbf{U} \equiv \oint_{\mathbf{C}'} d\mathbf{u} = \mathbf{0}$  and  $\boldsymbol{\Omega} \equiv \oint_{\mathbf{C}'} d\boldsymbol{\omega} = \mathbf{0}$ , then along any irreducible circuit  $\mathbf{C}$ ,  $\mathbf{U} = \mathbf{b} + \boldsymbol{\Omega} \cdot (\rho - \rho_0)$ , which means that the displacement  $\mathbf{U}$  is the sum of a rigid translation  $\mathbf{b}$  and a rigid rotation  $\boldsymbol{\Omega}$  from an arbitrary point  $\rho_0$ . *Dislocations* are defects with  $\boldsymbol{\Omega} = \mathbf{0}$  while *disclinations* are defects with  $\boldsymbol{\Omega} \neq \mathbf{0}$ . The result  $\mathbf{U} \equiv \oint_{\mathbf{C}} d\mathbf{u} = \mathbf{0}$  and  $\boldsymbol{\Omega} \equiv \oint_{\mathbf{C}} d\boldsymbol{\omega} = \mathbf{0}$  for the reducible circuit  $\mathbf{C}'$  are necessary and sufficient conditions for compatibility of the strain field in a doubly-connected body.

Figure 14 (Continued).

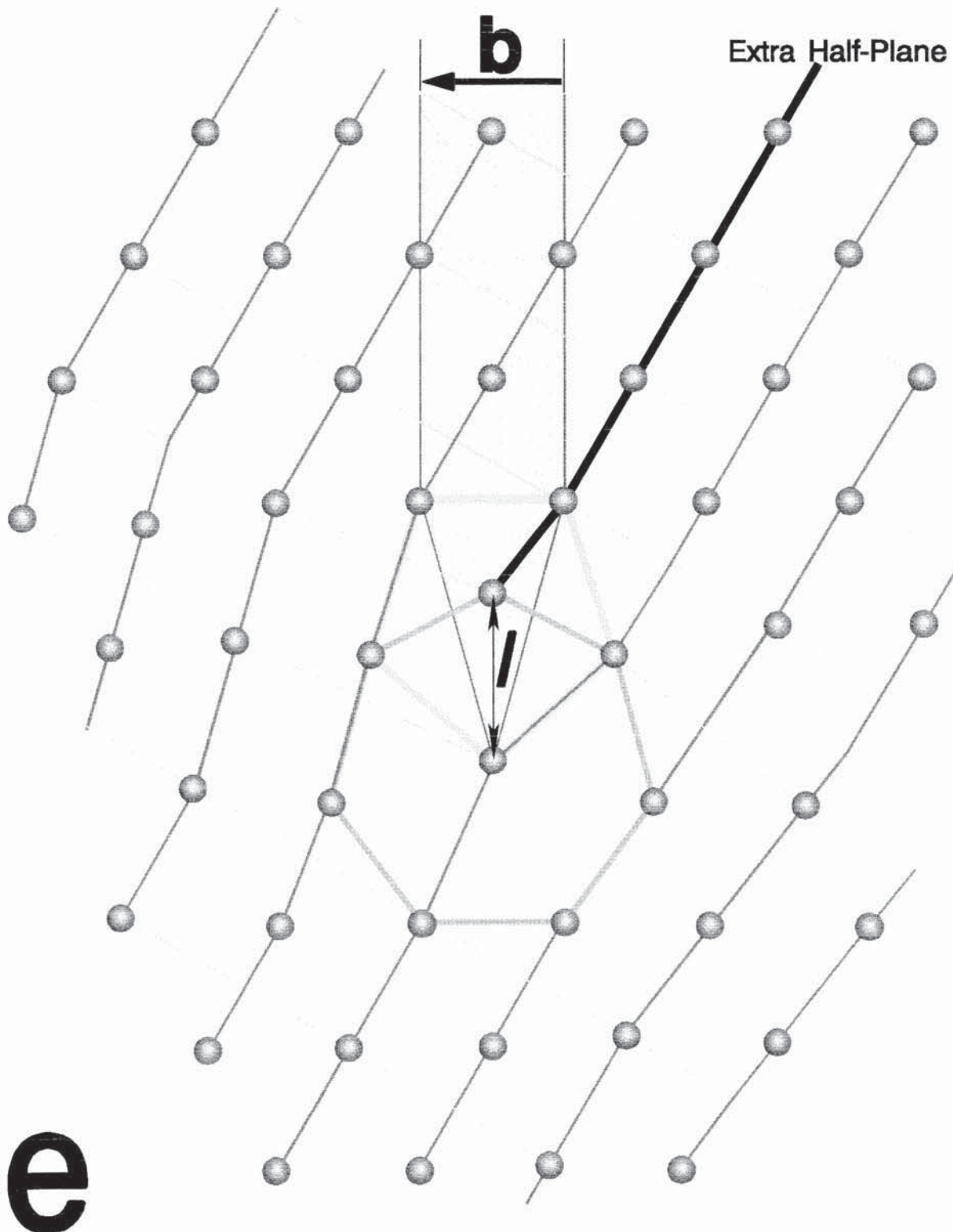


**Figure 15.** Adapted from (Marcinkowski 1979): An edge dislocation, or *singularity* has been introduced into the  $x^m$  coordinates by insertion of an extra half-plane of atoms. The three cells shown darker than the rest are therefore not really unit cells. The boundary of the lattice here is not stress free.

Let  $\mathbf{u}(p)$  denote the vector  $\mathbf{u} \equiv 3\mathbf{a}_x(p)$  at point  $p$  and  $\mathbf{v}(p)$  denote the vector  $\mathbf{v} \equiv 4\mathbf{a}_y(p)$  at point  $p$ . Vector  $\mathbf{u}$  is parallel transported from  $p$  to  $r$  to become the vector  $\mathbf{u}(r) \equiv 3\mathbf{a}_x(r)$ ; during this operation  $\nabla_{\mathbf{u}}\mathbf{u} = \mathbf{0}$  since  $\mathbf{v}(p) = pr$ . (If  $\mathbf{u}$  is parallel transported along  $\mathbf{v}$  then  $\nabla_{\mathbf{u}}\mathbf{u} = \mathbf{0}$  (Misner *et al.* (1973).) Similarly, vector  $\mathbf{v}(p)$  is parallel transported from  $p$  to  $q$  to become the vector  $\mathbf{v}(q) \equiv 4\mathbf{a}_y(q)$ . ( $\mathbf{v}(q)$  is the mirror image of  $\mathbf{v}(p)$ .) The Burgers circuit  $\mathbf{C}$  is  $\mathbf{C} = tq + qp + pr + rs = -\mathbf{v}(q) + -\mathbf{u}(p) + \mathbf{v}(p) + \mathbf{u}(r)$ . This circuit does not close, it is anholonomic. The Burgers vector is  $\mathbf{b} \equiv ts$  and the dislocation axis (row of singularities at the bottom of the extra half-plane; only one of these singularities is shown here) points into the paper.

Figure 15 (Continued).

## Anholonomy: The Edge Dislocation

Extra Half-Plane

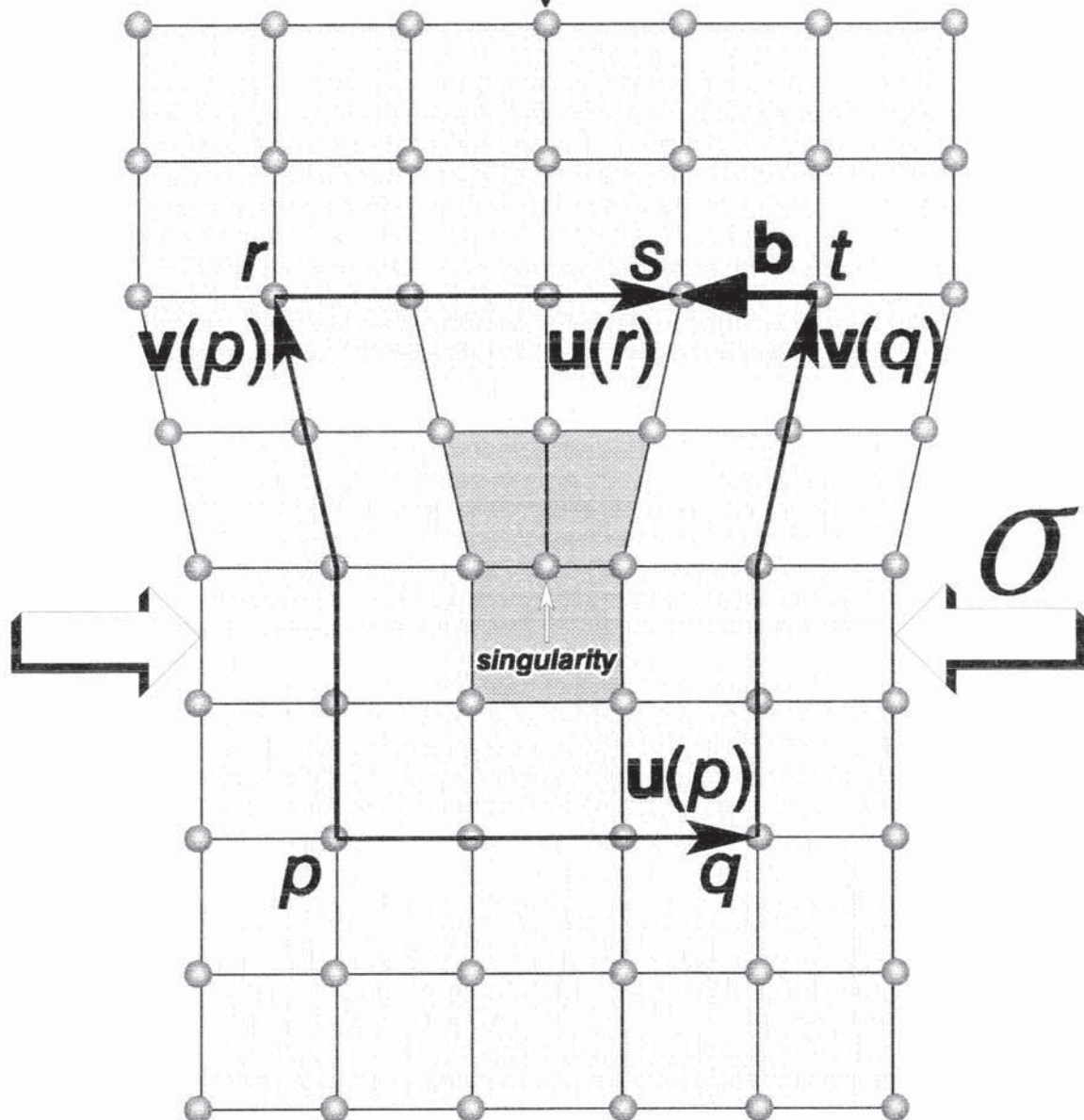


**Figure 16.** Adapted from Marcinkowski (1979), "quantum", or "imperfectly torn" (Kondo 1964) edge dislocation. This state features both "bad" unit cells, which are shown darker than the rest, and "gaps" between some unit cells. **a)** The initial, or reference state is a perfect simple-cubic lattice. **b)** A pair of "quantized" edge dislocations with opposite signs terminating on a single glide plane: a ***dislocation dipole***. **c)** A single (positive) edge dislocation remains after the negative dislocation (the lower one) travels right to the free surface. Atoms in the extra half-plane are shown as black.

Figure 16 (Continued).

## "Quantized" Edge Dislocation

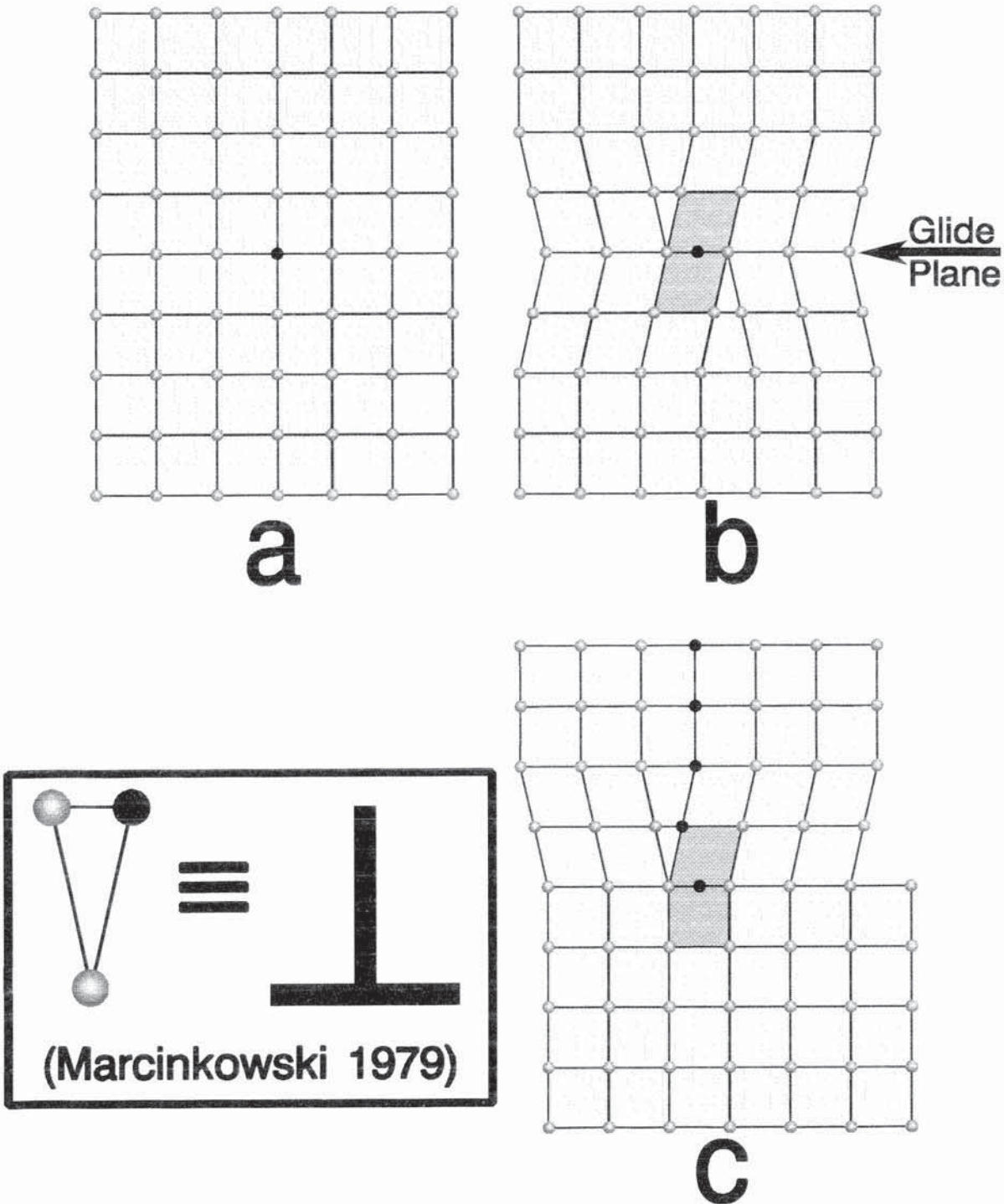


**Figure 17.** **a)** *Dehlinger's Verhakung* (Nabarro 1967) is a pair of edge dislocations, one positive and the other negative, that are separated by one Burgers vector  $\mathbf{b}$ . Atoms in rows one and two and four through six are rigid. Atoms in row four provide a sinusoidal potential energy "trough" in which the atoms in row three move when force  $\mathbf{F}$  is applied at point  $\rho = (\text{column } 9, \text{row } 3)$  to the left. The row three atom in column five has "climbed" to the top of the potential "trough," which corresponds to the *maximal elastic displacement*  $\mathbf{u}$ . Other atoms "climb" in this "trough" by lesser amounts, *i.e.* the displacements are smaller, and atoms very far away from column five are not displaced. So there is a displacement gradient and corresponding elastic strain in the lattice. **b)** Analysis of the potential energy function, say  $\Psi$ , produced by row four atoms and in which row three atoms move from the force. The displacements of the row three atoms follow a smooth curve.

A force  $\mathbf{F}$  can be represented as a 1-form (Burke 1985):

$${}^b\mathbf{F} \equiv -\vec{d}\Psi = -(\partial\Psi/\partial x)\vec{dx} - (\partial\Psi/\partial y)\vec{dy} - (\partial\Psi/\partial z)\vec{dz}.$$

Here,  ${}^b\mathbf{F} = -(\partial\Psi/\partial x)\vec{dx}$ .

Figure 17 (Continued).

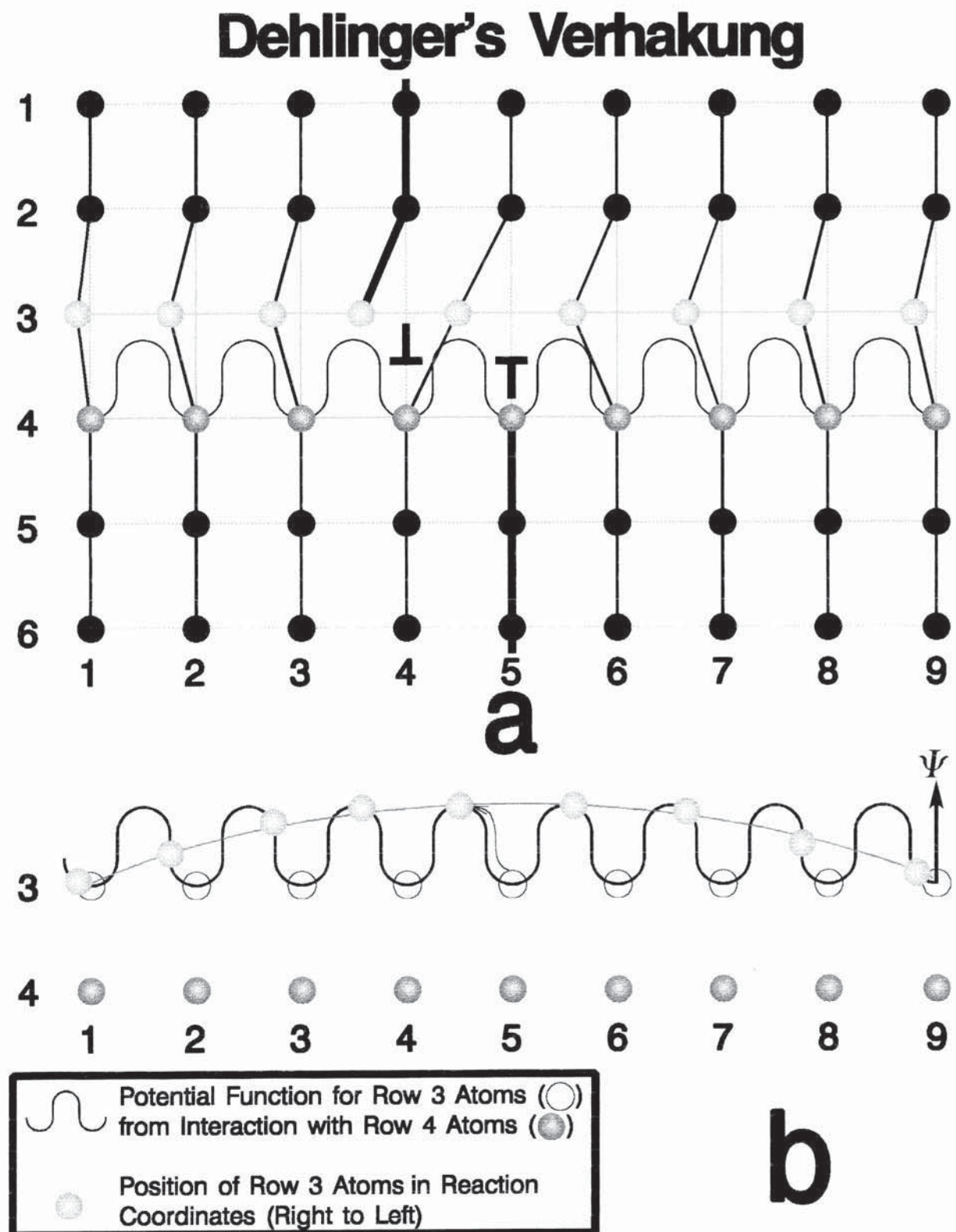


**Figure 18.** After Marcinkowski (1979), in part: **a)** The (undeformed) reference state with  $X^M$  coordinates. The circuit  $\mathbf{C}' \equiv sp + pq + qr + rf$  is open; the Burgers vector  $\mathbf{b} = fs$  closes it (**FS/RH** convention). **b)** A dislocation dipole is nucleated in the reference state. **c)** A single edge dislocation remains after the other has moved to the free surface. The circuit  $\mathbf{C} \equiv sp + pq + qr + rs$  is closed. The vector  ${}^{\text{bot}}\mathbf{v} \equiv rs$  becomes the vector  ${}^{\text{top}}\mathbf{v} \equiv -pq$  when parallel transported in the  $y$ -direction along the vector  $sp$ . The shaded unit cells are elastically deformed. **d)** The geometry of the matrix  $A^m_M$  is shown:  
 $A_x^x = H(y)[\delta(x) + 1] + H(-y)$ , and  $A_y^x = A_z^x = 1$ . **e)** Some of the shaded, elastically deformed unit cells from part 'c' are shown. Note that in this region the  $x^m$  coordinates are obtained from the  $X^M$  coordinates when the latter are dragged over the displacement  $\mathbf{u}$ . Therefore, this region has received a "conservative" deformation;  $\mathbf{a}^m \equiv \vec{\mathbf{d}}x^m = \lambda^m_M \vec{\mathbf{d}}X^M$  and  $\mathbf{a}_m = \lambda_m^M \mathbf{A}_M$ , where  $\lambda^m_N = \delta^m_N + \partial u^m / \partial X^N \equiv \delta^m_N + \gamma_N^m$ ,  $\gamma_N^m \equiv \partial u^m / \partial x^N$ . **f)** A separation vector  $\mathbf{v} \equiv \rho - \rho_0$  between two neighboring points  $\rho$  and  $\rho_0$  pierces  $\langle \omega, \mathbf{v} \rangle$  surfaces of the 1-form  $\omega$  (Misner *et al.* 1973). Thus, the Burgers vector magnitude is  $-b^x = \langle \mathbf{a}^m, {}^{\text{top}}\mathbf{v} \rangle - \langle \mathbf{a}^m, {}^{\text{bot}}\mathbf{v} \rangle = 5\langle \mathbf{a}^m, \mathbf{a}_n \rangle - 4\langle \mathbf{a}^m, \mathbf{a}_n \rangle = (5 - 4)\delta^m_n = 1$ . **g)** The *dislocation density tensor*. **h)** The *dislocation density 2-form*. **i)** *Integration of dislocation density 2-form*. Only three "tubes" of  $\mathbf{a}^x \wedge \mathbf{a}^y$  contribute to  $\int_{\mathcal{V}} \tilde{\rho}^N$ : the upper two "tubes" ("circulations") give  $-2\mathbf{a}_x$  and the lower gives  $\mathbf{a}_x$ , for a total of  $-\mathbf{a}_x$ , "circulations" being added as in "advanced calculus." Note that the Burgers vector is opposite of the integral  $\int_{\mathcal{V}} \tilde{\rho}^N$ . **j)** After parallel transport around the circuit  $pqrstp = -\mathbf{v}(q) + -\mathbf{u}(r) + \mathbf{v}(r) + \mathbf{u}(s) + [\mathbf{u}, \mathbf{v}]$ , the vector  $\mathbf{w}$  changes from  ${}^R\mathbf{w}$  to  ${}^I\mathbf{w}$ . The Lie derivative of  $\mathbf{u}$  with respect to  $\mathbf{v}$  is  $\mathbf{f}_{\mathbf{u}}\mathbf{v} = [\mathbf{u}, \mathbf{v}] = -\mathbf{b}$ .

Figure 18 (Continued).

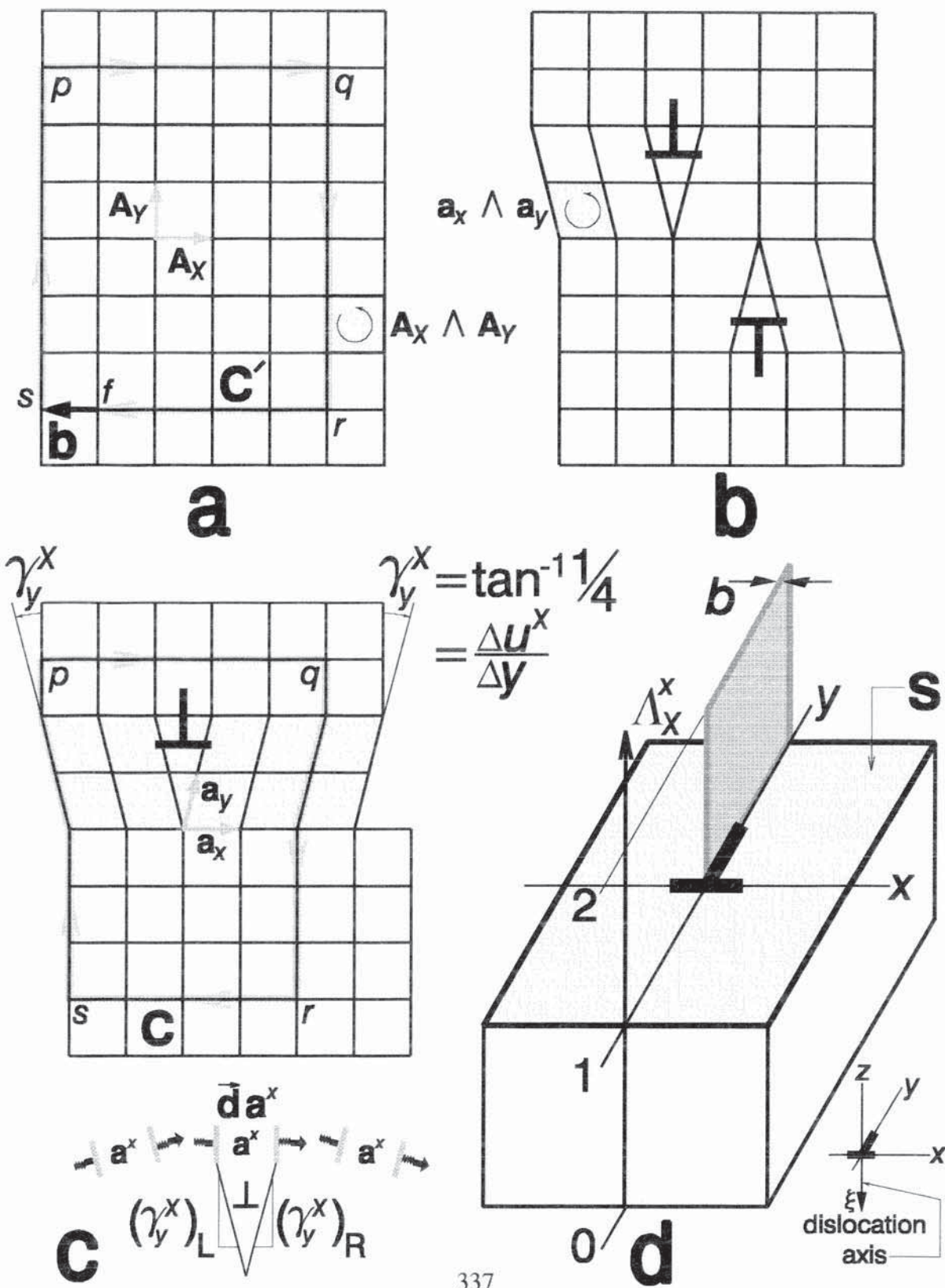


Figure 18 (Continued).

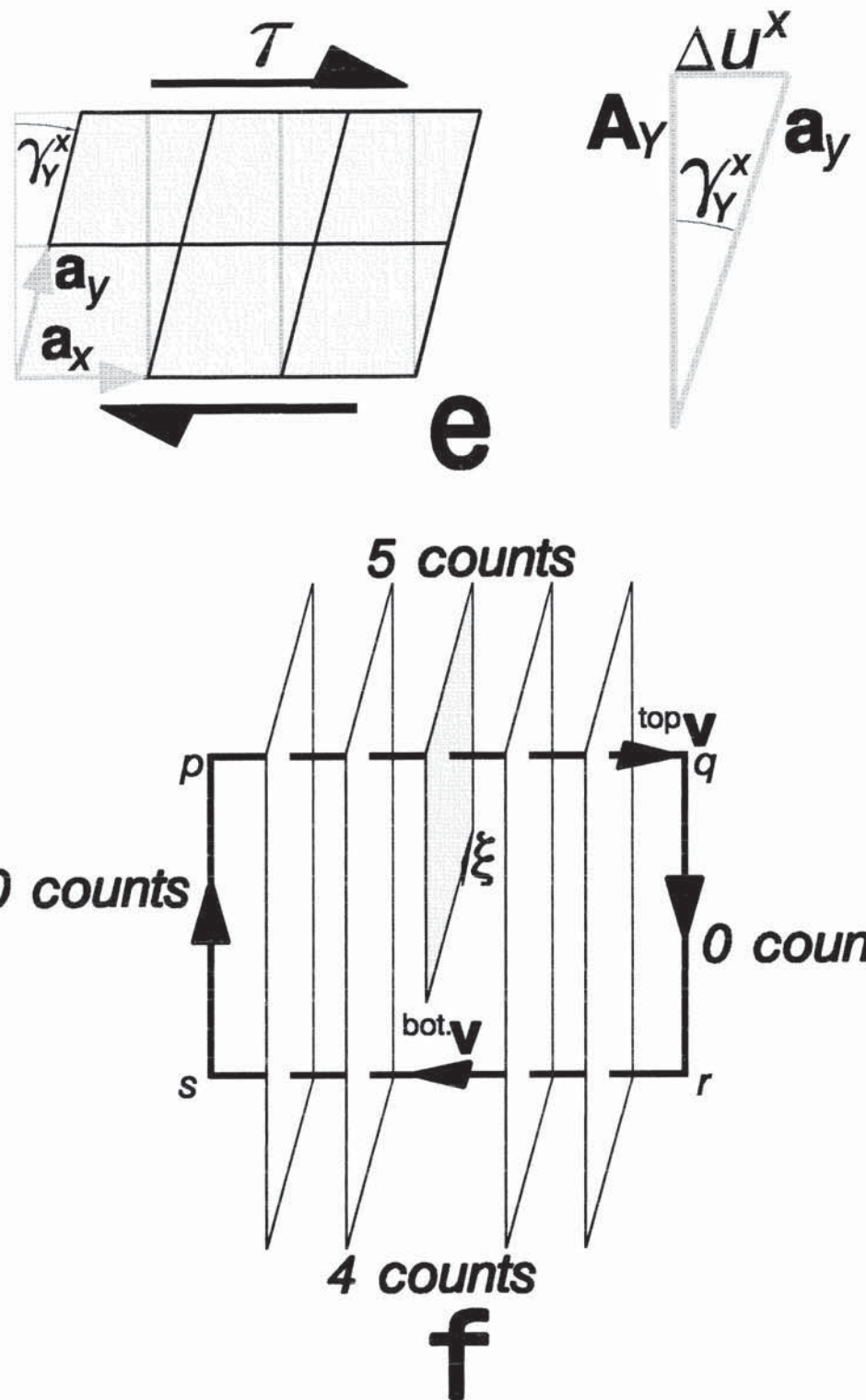


Figure 18 (Continued).

## Dislocation Density Tensor

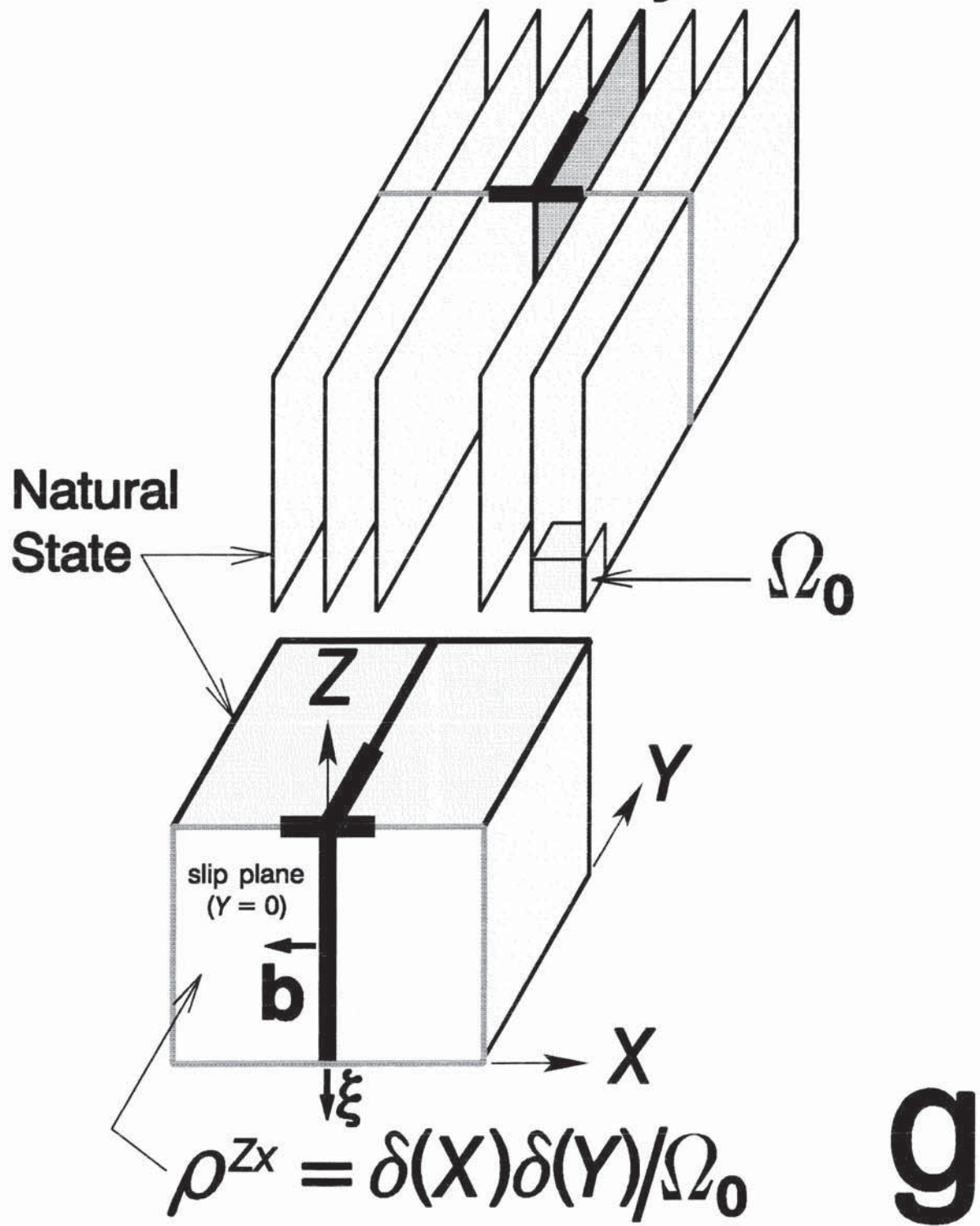


Figure 18 (Continued).

## Dislocation Density 2-Form

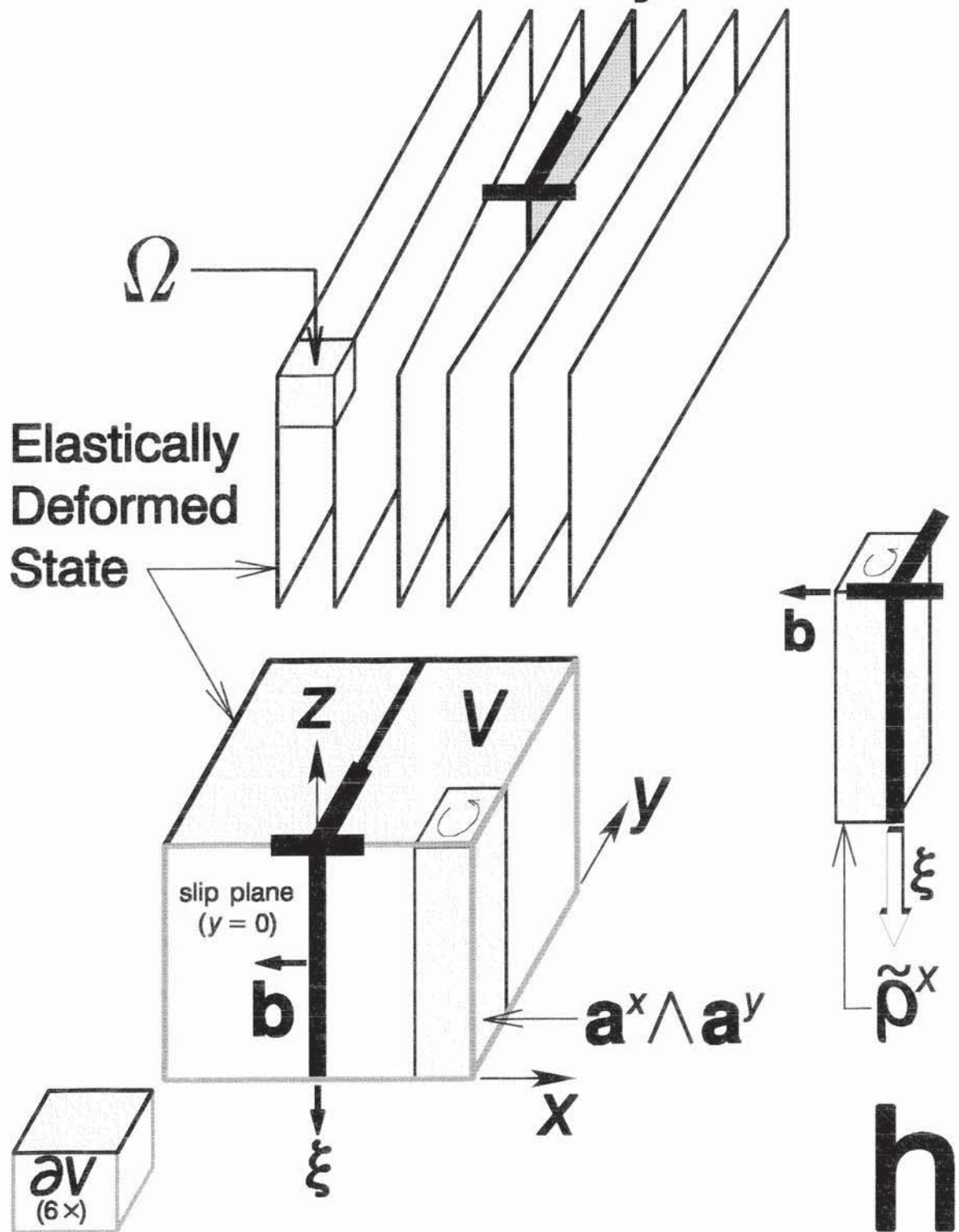


Figure 18 (Continued).

# Integration of Dislocation Density 2-Form

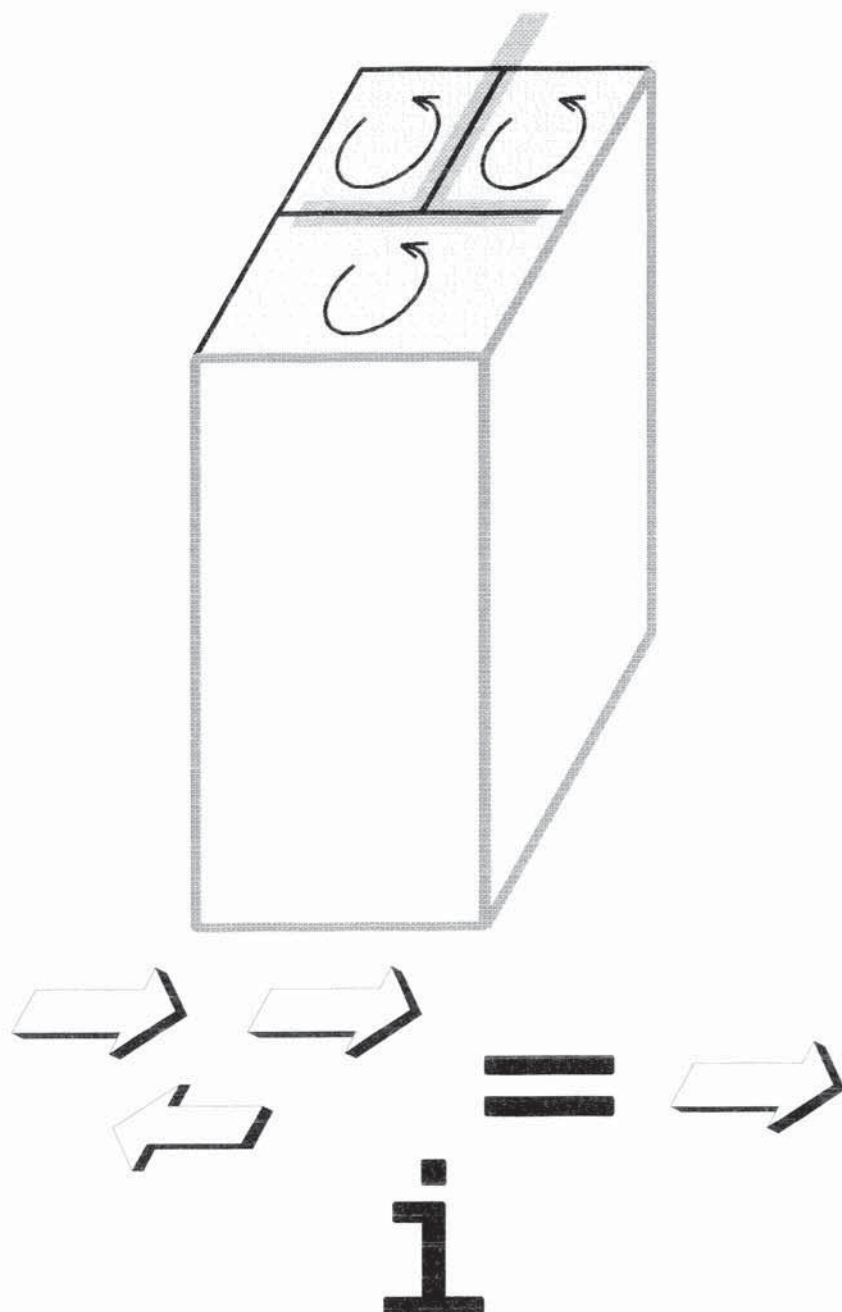
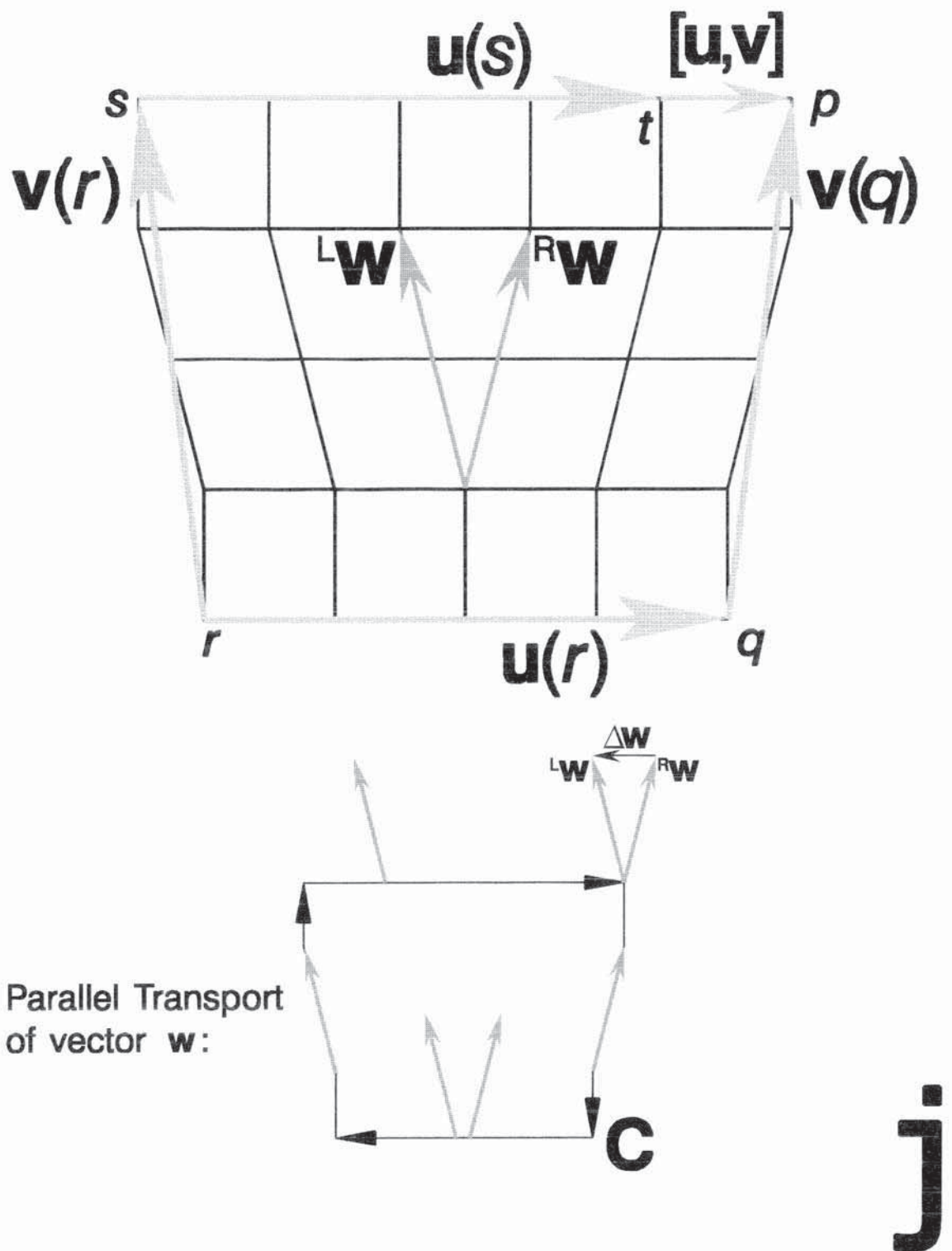


Figure 18 (Continued).



**Figure 19.** *Diffusional Creep* and, *grain boundary sliding and migration*, after Poirier (1985). **a)** The initial condition. A two dimensional array of "grains," or cells, is subjected to a stress,  $\sigma$ , resulting in grain boundary sliding as shown. **b) If there is no matter transport then sliding leaves gaps between the grains.** **c) Matter transport, on the other hand, fills the gaps before they develop, and the deformation is then compatible.** The strain of the array  $\varepsilon$  is the same as that of the individual cells,  $\varepsilon_G$ ;  $\varepsilon = \varepsilon_G$ ,  $\varepsilon_G$  denoting the grain strain. **d) Matter transport to accommodate grain boundary sliding:** **Atomic diffusion occurs because vacancies are not in global equilibrium within the grain.** At top and bottom faces the stress assists vacancy production, increasing the equilibrium concentration of these defects locally, while at the other faces, vacancy production is inhibited, and the local equilibrium vacancy concentration is diminished. A concentration gradient therefore exists which gives rise to the fluxes shown; mass transport also results in grain boundary migration. Mass transport occurs through the lattice for *Nabarro-Herring creep*, or along the grain boundaries for *Coble creep*.

Figure 19 (Continued).

## Diffusional Creep

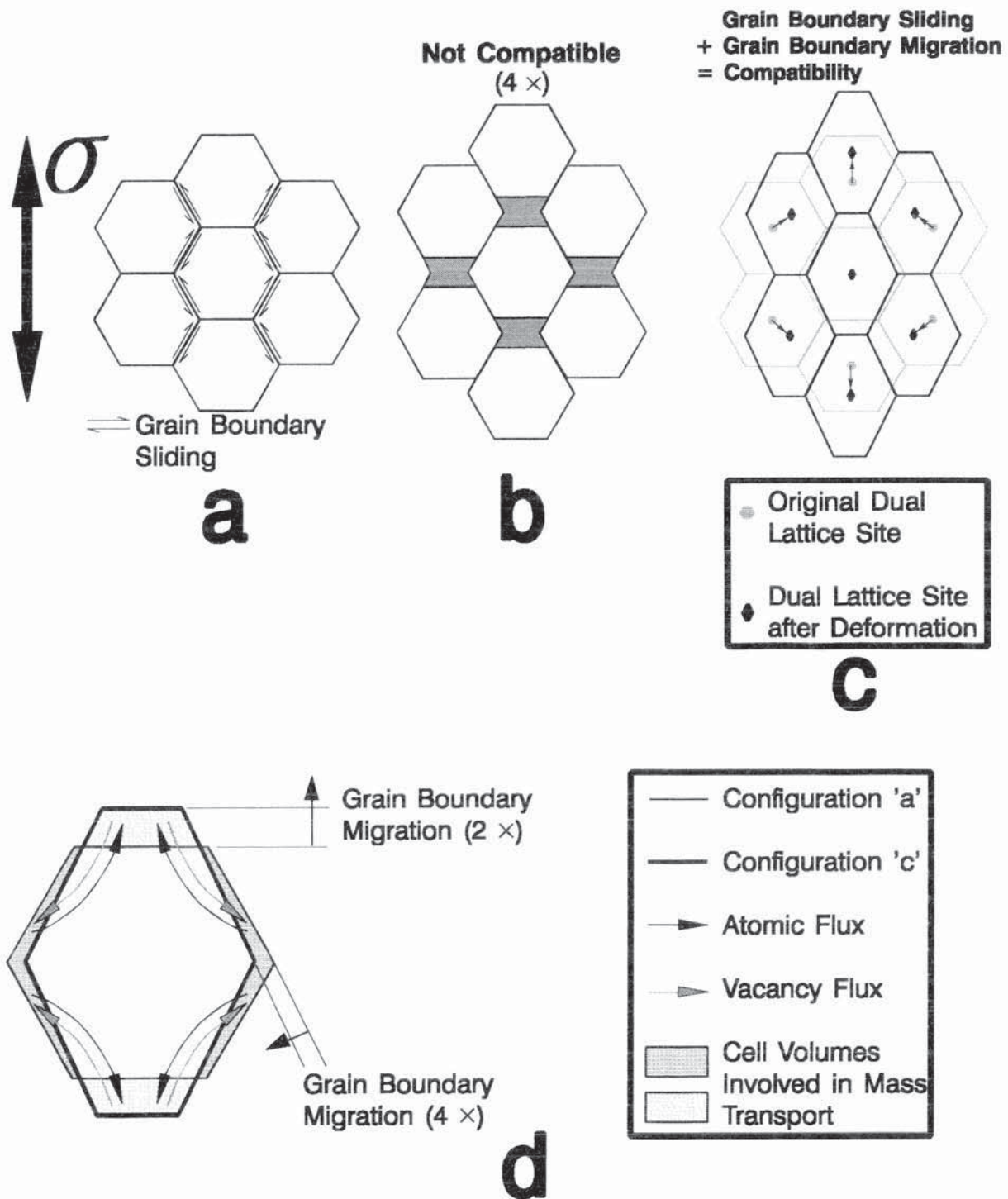


**Figure 20.** a) A grain boundary dislocation in a FCC structure, after Pond *et al.* (1978).

The  $\circ$  and  $\times$  symbols represent atoms in the ...ABAB...  $\{002\}$  stacking sequence of the FCC lattice. Three planes of type  $\{002\}$  are shown by the box in the upper right hand corner; the B plane is  $(002)$  while the A planes are  $(001)$  and  $(00\bar{1})$ . This is a *glissile* (mobile) dislocation loop with Burgers vector  $\mathbf{b} = (a/10)[130]$ ,  $a$  denoting the lattice constant. It glides on a  $(310)$  plane in a  $36.9^\circ$   $[001]\Sigma = 5$  related grain boundary. This grain boundary runs from left to right, with a step up and a step down. *Steps* are at the dislocation core, which, as is the case for dislocations in FCC crystals, consists of two extra half-planes.

b) When the grain boundary dislocation is subjected to a force  $F$ , *e.g.* from an applied stress, the loop expands, so that the upper grain slides over the lower grain (grain boundary sliding). Here, the  $\llcorner$  symbols denote the extra half-planes for the dislocation. When the dislocation expands by  $\|\mathbf{b}\| \equiv b = a/\sqrt{10}$  (unit slip), the grains slide over each other by this amount, and since there is a step in the dislocation core, the boundary migrates simultaneously by  $2d_{\{260\}} = a/\sqrt{10}$ , where  $d_{\{hkl\}} = a/(h^2 + k^2 + l^2)^{1/2}$  is the distance between planes of type  $\{hkl\}$ .

- i. Initial condition.
- ii. The dislocation loop has expanded, the grains have slid over one another, and the boundary between them has risen upwards. Thus, the top grain loses atoms to the bottom grain.
- iii. View showing the two prior configurations of the dislocation loop and grain boundary, and the volume of material added to the bottom grain from the top grain.

Figure 20 (Continued).

## Grain Boundary Dislocation

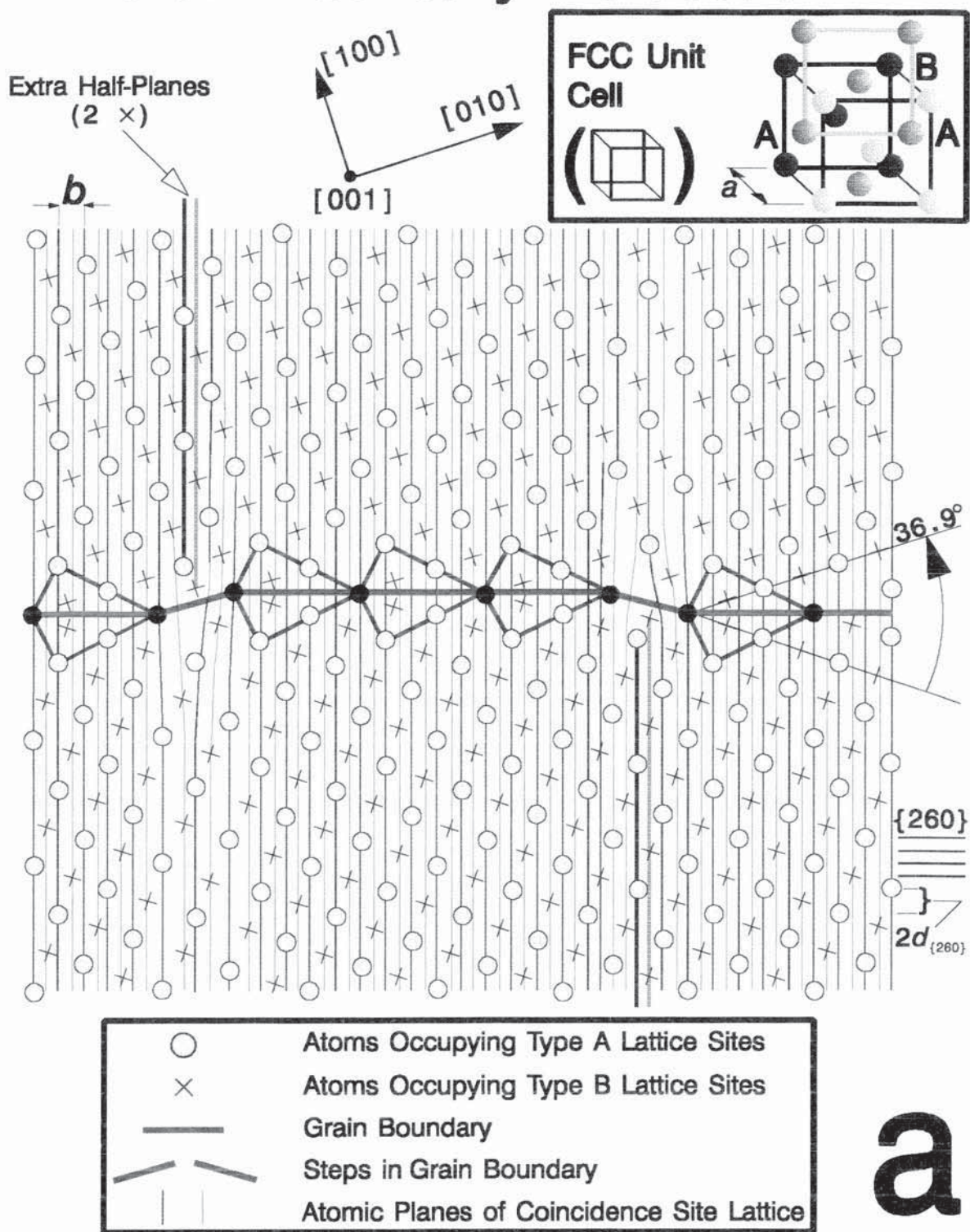
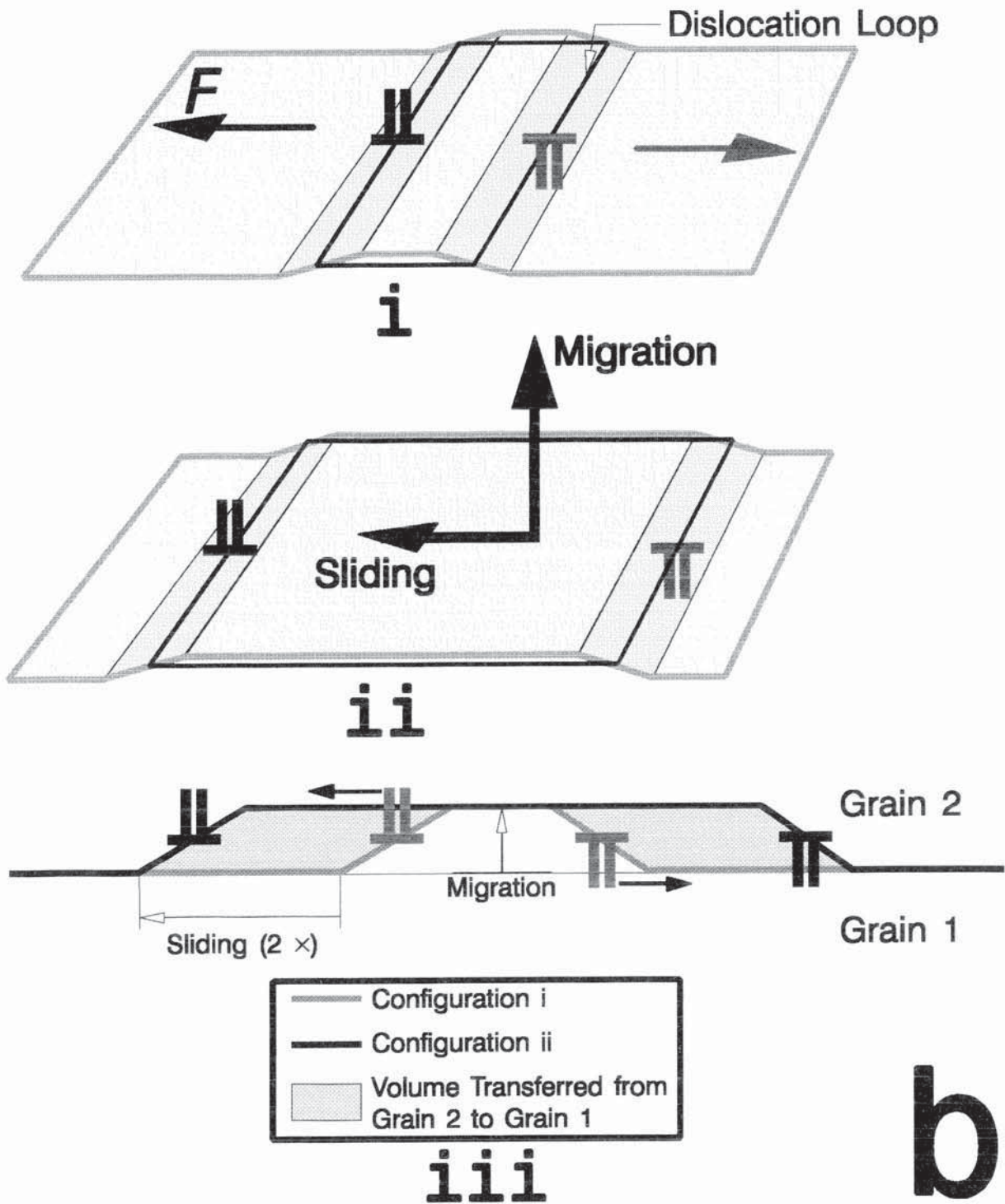


Figure 20 (Continued).

## Grain Boundary Sliding/Migration



**Figure 21. Cellular Dislocation—the 5-7 Combination:** **a)** After Morral and Ashby (1974), a combination of 5- and 7-sided cells in a hexagonal array produces a *cellular edge dislocation*. Far away from the dislocation the cell diameter is  $d$ . The magnitude of the Burgers vector,  $\mathbf{b}$ , is given by  $\mathbf{b} = \sqrt{3} d/2$  (Cahn and Padawer 1965). **S** and **F** denote the start and finish of the Burgers circuit. **b)** Construction of an edge dislocation in a cellular array. See also Morral and Ashby (1974). **i.** The *lattice graph* for a hexagonal array. **ii.** Construction of the lattice graph. **iii.** Edge dislocation in lattice with *sixfold* symmetry. **iv.** Corresponding cellular dislocation and lattice graph. **c) Production of a cellular dislocation pair.** Here:

**Grain boundary sliding (GBS) and migration (GBM) occur only in  
the shaded cells and a pair of cellular dislocations is nucleated.**



Further grain boundary migration results in the configuration displayed next. **d)** Cells from part 'c' are shown along with their *dual*, a lattice with *sixfold* symmetry. The two edge dislocation symbols shown here denote the defects in the cellular array, as opposed to the corresponding defects in the dual lattice. The "lattice lines" drawn on the figure produce a square net, and each square contains one triple point. Other types of "lattice lines" are also possible: see, for example, Hirth and Lothe (1982) and Sato *et al.* (1990).

Figure 21 (Continued).

## Cellular Dislocation

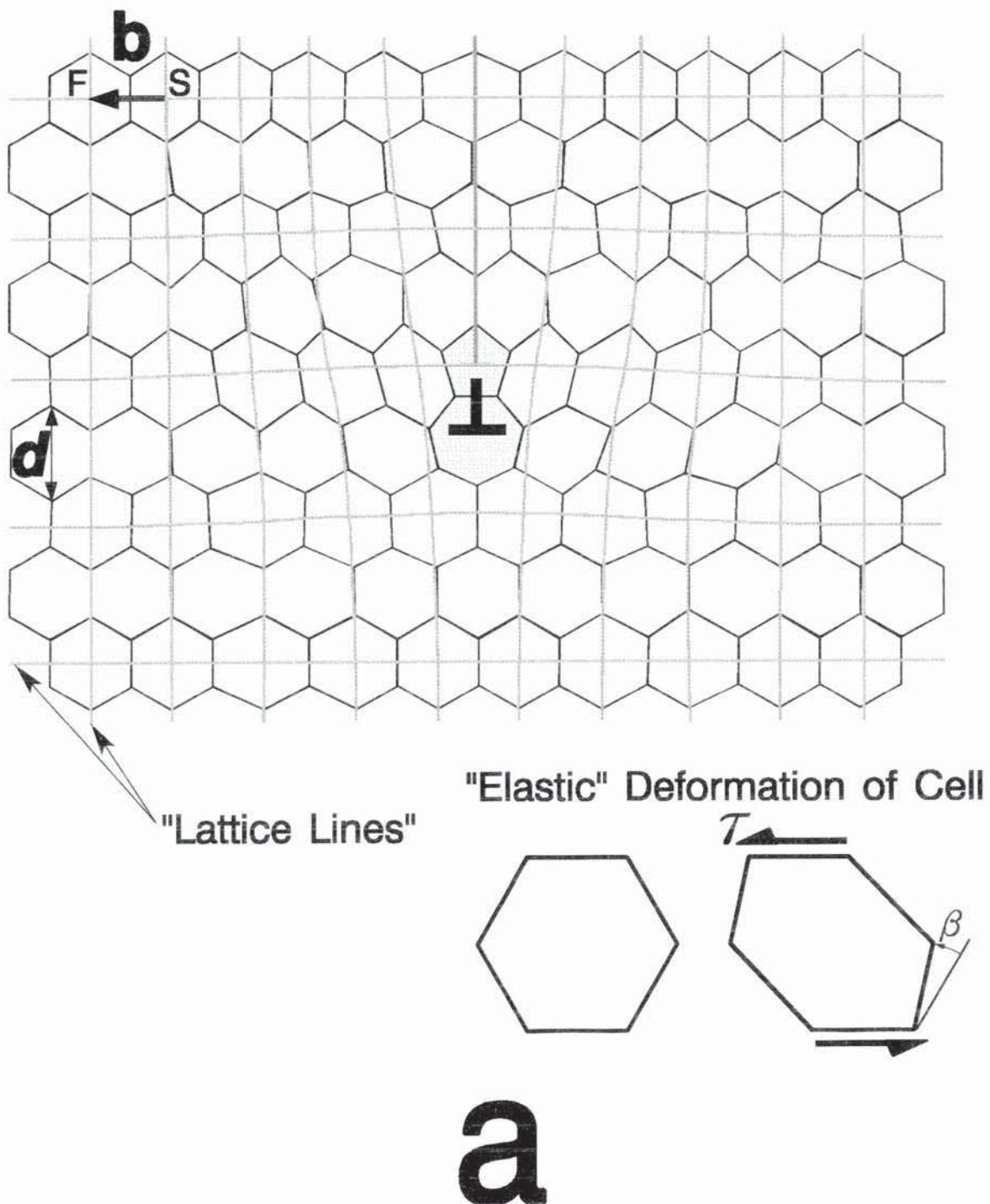


Figure 21 (Continued).

## Construction of Cellular Dislocation

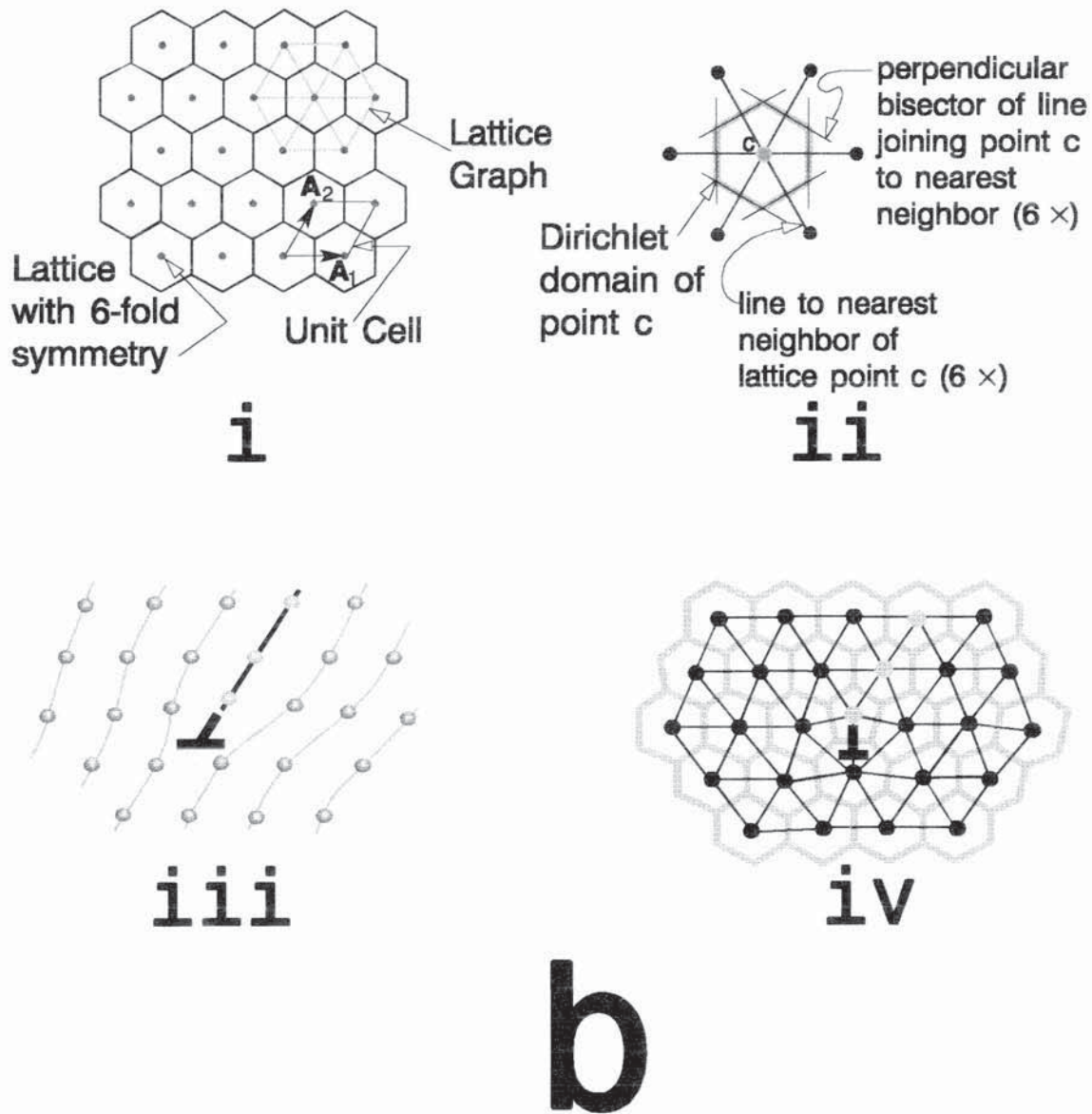


Figure 21 (Continued).

## Production of Cellular Dislocation Pair

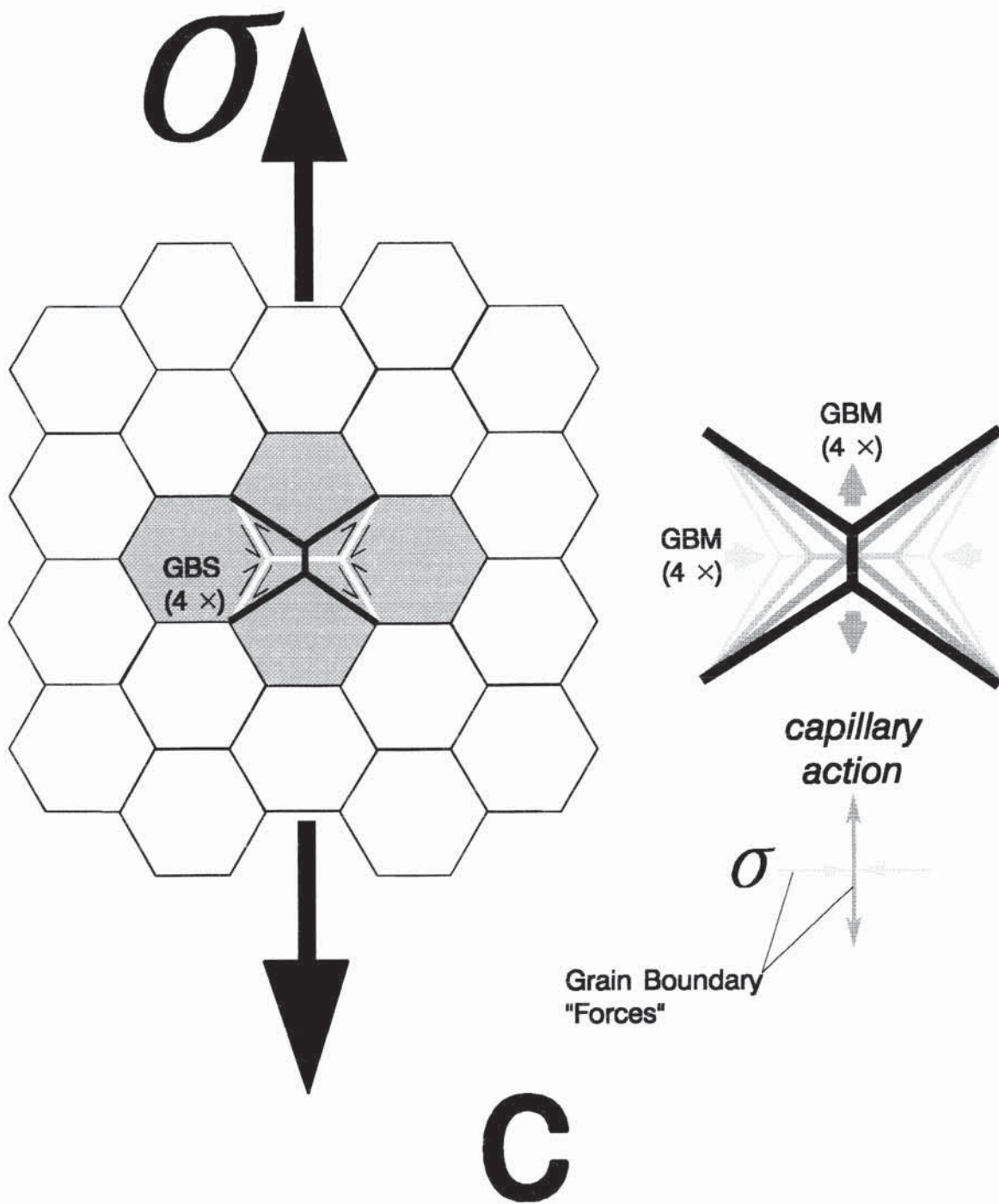
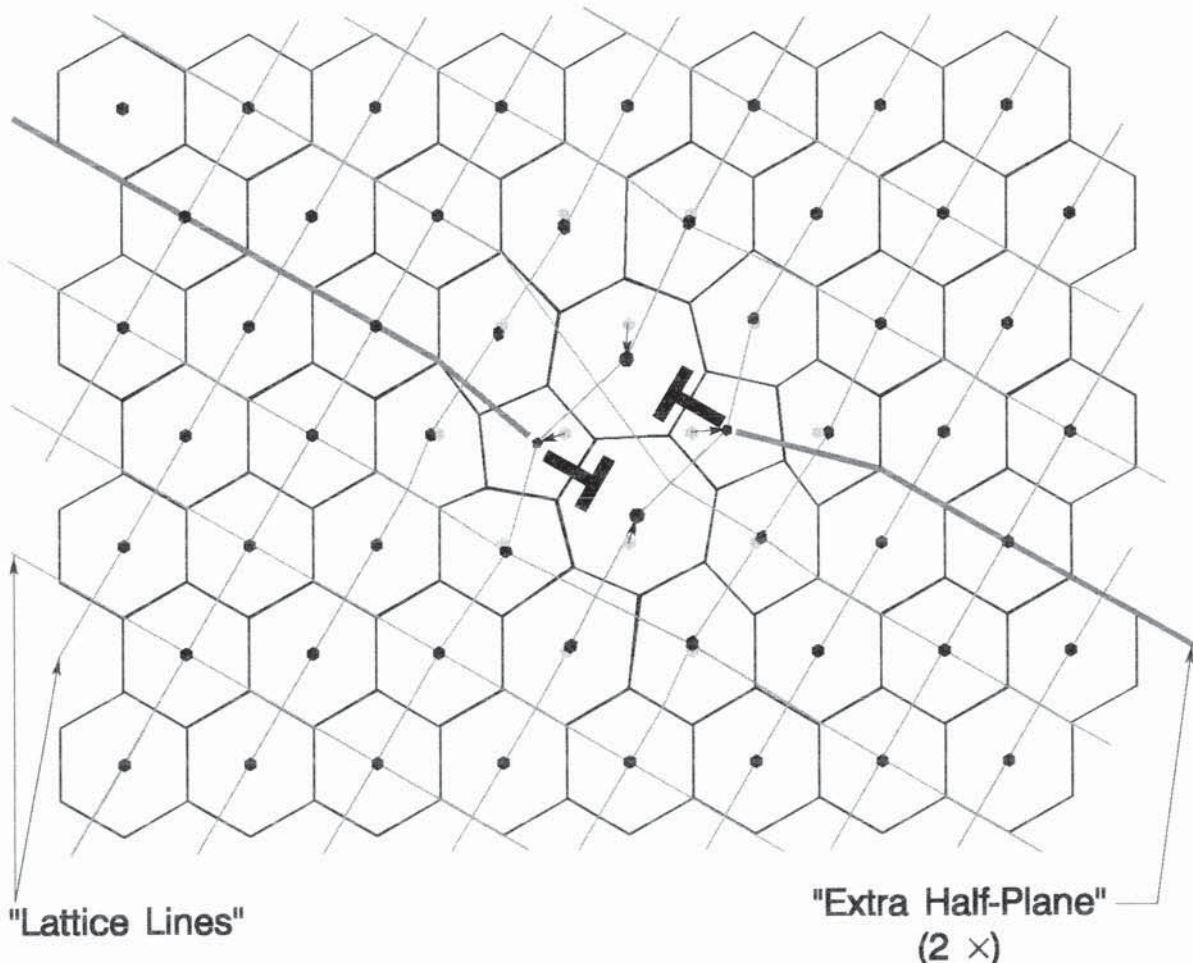


Figure 21 (Continued).

# Cellular Dislocation Pair



d

# Compatibility

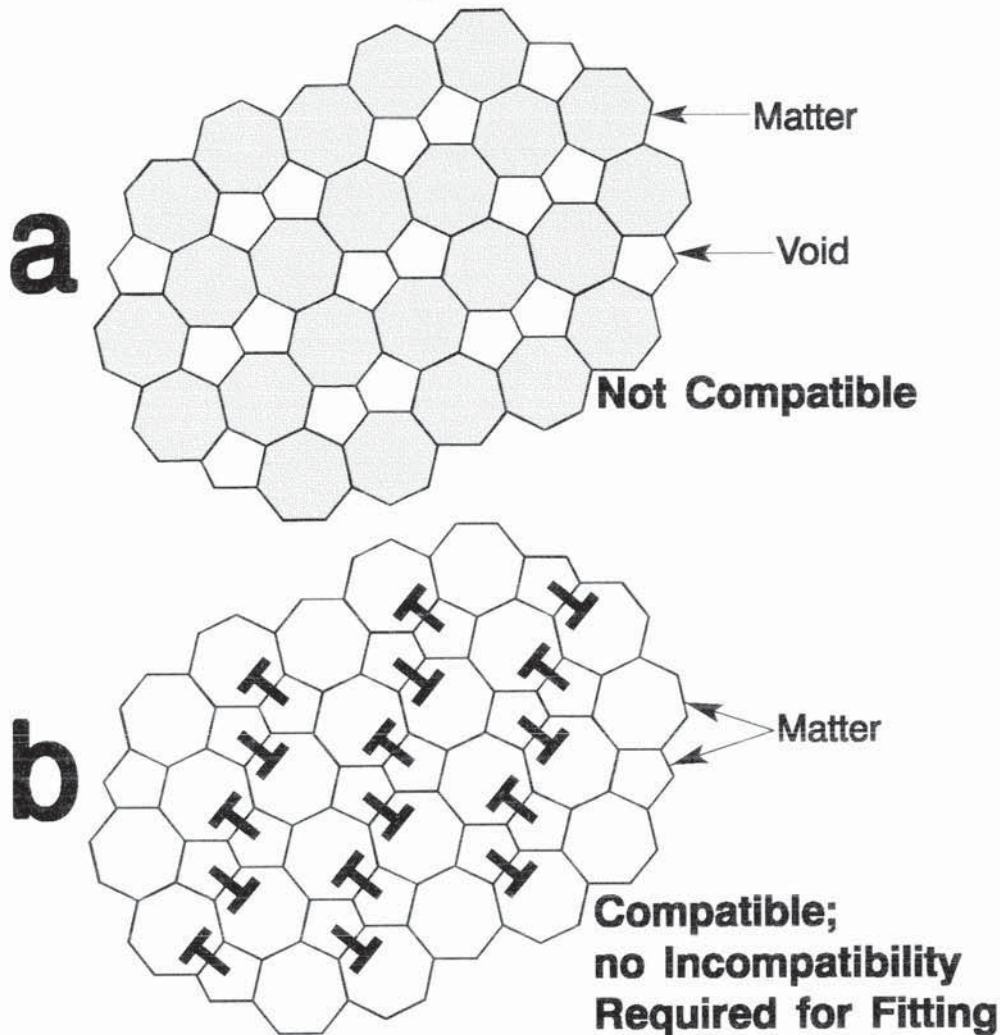


**Figure 22.** Illustration of incompatibility tensor,  $\mathbf{N} = -\epsilon^{ikm}\epsilon^{jln}\epsilon_{mn;lk}\mathbf{a}_i \otimes \mathbf{a}_j$ , (Kröner 1955, Eshelby 1956, Nabarro 1967) for dislocation array. **a)** A plane is tiled with heptagons, but gaps in the shape of pentagons remain. **b)** If the gaps are replaced with pentagons then space is filled with an array of dislocation dipoles and there is no incompatibility,  $\mathbf{N} = 0$ , no curvature  $Riemann = 0$ , and no "net Burgers vector,"  $\int Torsion = 0$ .

## Grain Boundary Dislocation Climb/Glide Mechanism for Grain Boundary Sliding/Migration

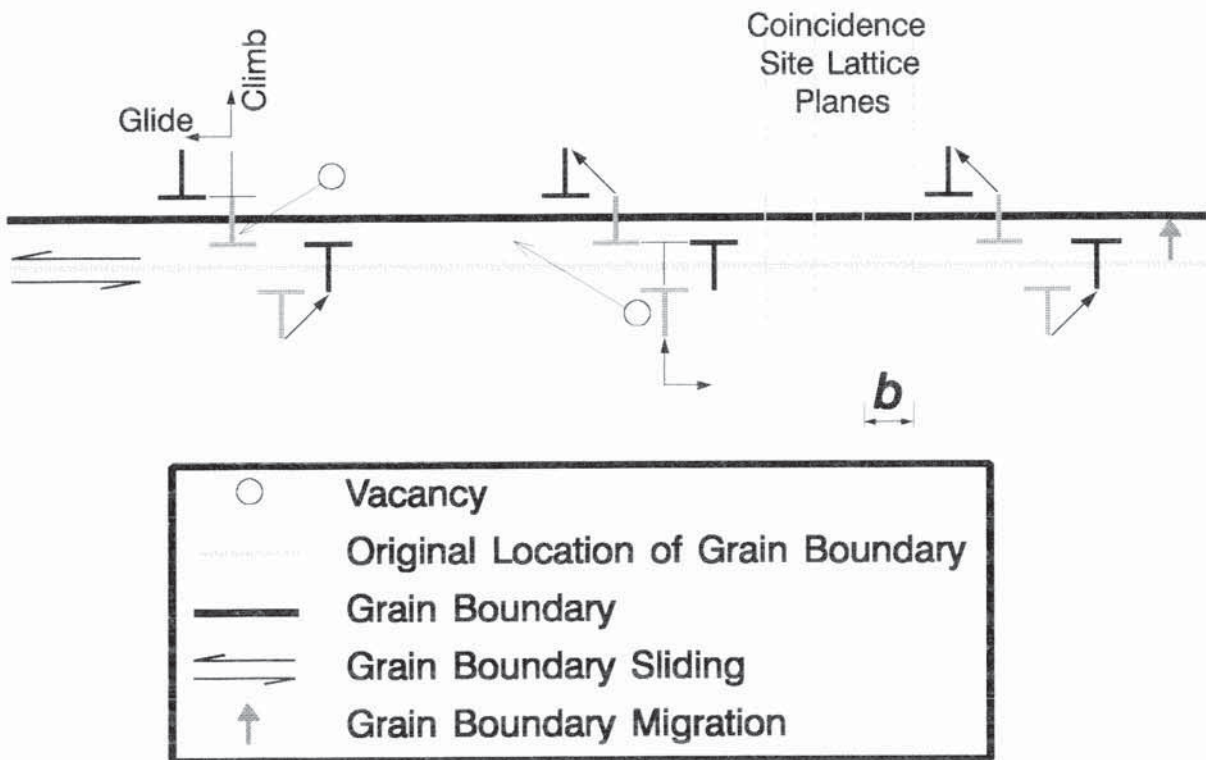


**Figure 23.** After Beeré (1978): The diffusion path between grain boundary dislocations is much shorter than the distance between grain boundaries. This enables grain boundary sliding to rapidly release boundary shear forces during diffusional creep; diffusional creep is then "limited" only by mass transport from grain boundary to grain boundary. Here, grain boundary dislocations climb and glide so that the boundary slides and migrates. Dislocations in the top lattice "climb up" when a vacancy is absorbed while dislocations in the lower lattice "climb down" by emitting a vacancy. Defects help each other move; diffusion paths are short.

**Figure 24.** After Beeré (1978): "Shear forces are likely to develop on grain boundaries during diffusion creep at low stresses near a threshold stress and during stage II superplastic creep. The creep rate will be controlled either by the shear process with rapid relaxation of normal forces or by simultaneous slow relaxation of both normal and shear forces. In both cases the important feature from the point of grain motion is the effect of the shear forces. **The friction which develops between grains leads to rotation of the grain. This is not to be confused with apparent rotation resulting from motion of grain boundaries. The process to be discussed rotates the lattice whereas boundary migration leaves the lattice orientation unchanged.**" a) An array of square "grains" is subjected to an applied stress  $\sigma$  resulting in deformation by grain boundary sliding. i. The initial condition. ii. Grain boundary viscosity is isotropic and the horizontal and vertical boundaries slide by equal amounts:  $S_h = S_v$ , where  $S_v$  and  $S_h$  denote the distance vertical and horizontal boundaries slide, respectively. iii. Vertical grain boundaries are more viscous than horizontal boundaries and therefore only horizontal boundaries slide. The same strain as shown previously can be developed if the grains rotate in addition to sliding along only the horizontal boundaries, as shown. b) Hexagonal array for analysis of grain rotations.

Figure 24 (Continued).

## Grains Rotate When Some Grain Boundaries Are More Viscous Than Others

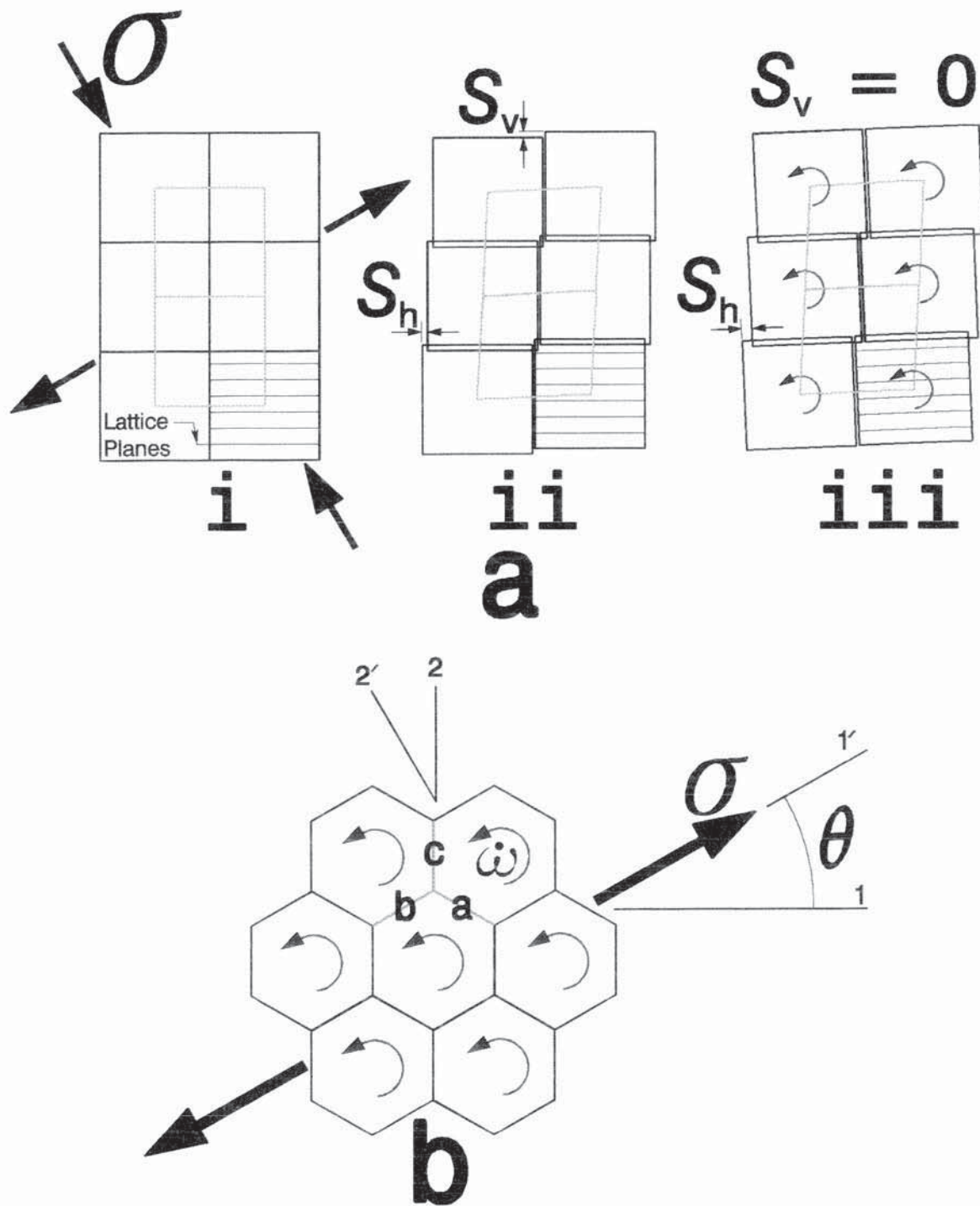
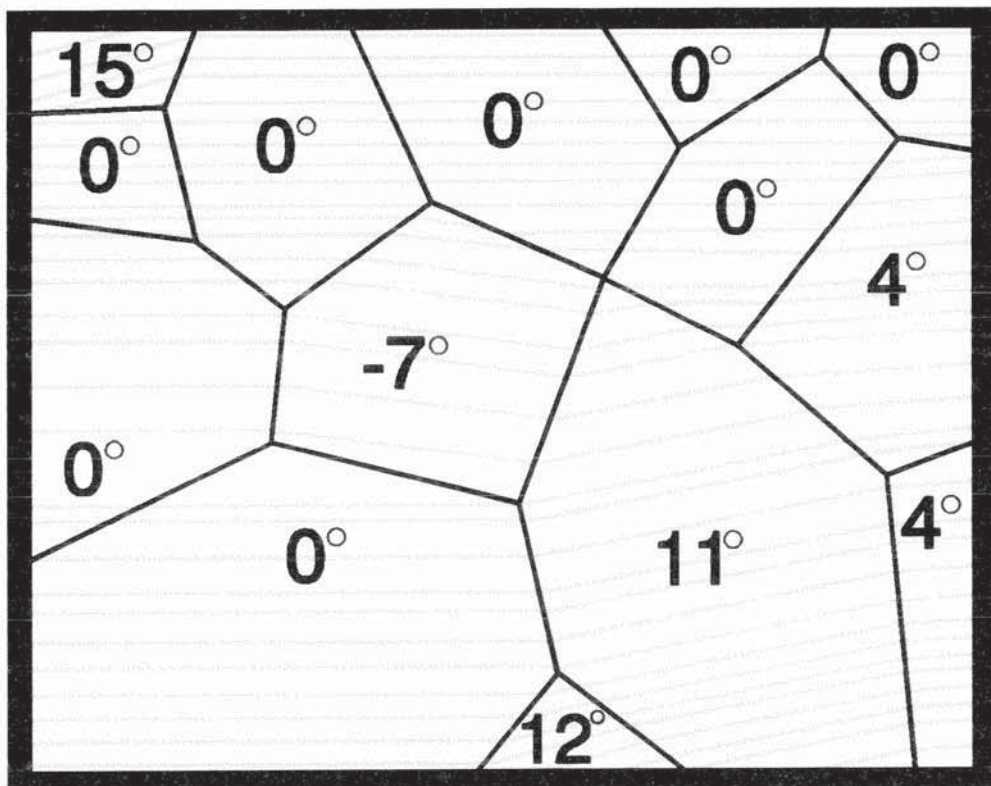
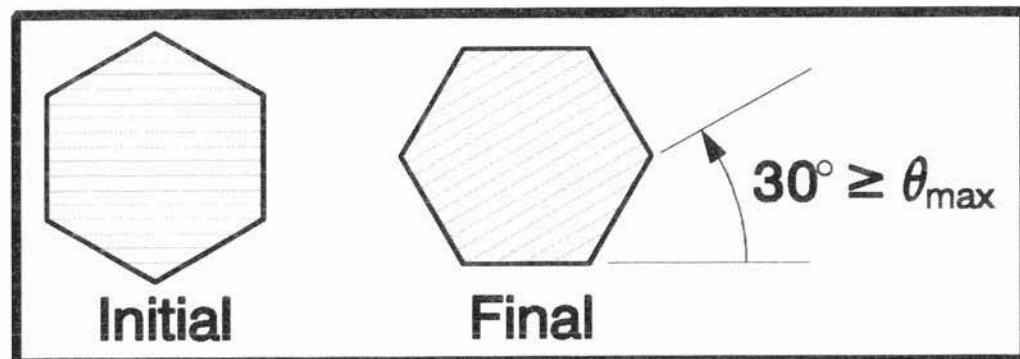


**Figure 25.** **a)** After Beeré (1978): Shear forces develop on grain boundaries during creep because grain boundaries have "friction," resulting in lattice rotations which are probably never in excess of  $30^\circ$ . **b)** After Beeré (1976): Grain rotations are actually observed in crept materials. Here, hydride stringers indicate lattice rotations in a Mg-Zr alloy deformed at  $400^\circ\text{C}$  to a strain of 42%.

Figure 25 (Continued).

## Grain Rotation

a



b

Hydride Stringers  
— Grain Boundary

**Figure 26.** **a)** A bar made of very soft metal is hung up so that it is subjected to the force  $mg = \text{mass} \times \text{acceleration from gravity}$ . Let  $A$  denote the cross-sectional area of the bar and  $A_{\text{sp}}$  the area of the slip plane; the normal ( $\mathbf{n}$ ) to the slip plane makes angle  $\theta$  with the  $h$ -axis so that  $A/A_{\text{sp}} = \cos \theta$ . The slip direction,  $\mathbf{s}$ , makes angle  $\phi$  with the tensile axis. The *resolved shear stress* acting on the slip plane in the slip direction,  $\mathcal{T}$ , is  $\mathcal{T} = \sigma \cos \theta \cos \phi$ ,  $\sigma = mg/A$  denoting the tensile stress, expands the dislocation loops, thereby deforming the bar. The maximum value of  $\mathcal{T}$  occurs for  $\theta = \phi = 45^\circ$ , and then  $\mathcal{T}_{\max} = \frac{1}{2}\sigma$ . The potential energy of the bar,  $\Psi$ , is  $\Psi = mgh$ , where  $h$  is the height of the bar's center of gravity. Deformation reduces the height from  $h_i$  to  $h_f$ , lowering the potential energy,  $\Delta \Psi = mg(h_f - h_i) \equiv mg\Delta h < 0$ , and the capacity for gravity to perform work. The work  $W = \text{force} \times \text{distance}$  that gravity does to the bar is  $W = -mg \times \Delta h > 0$ , and the associated (true) force is  $F \equiv -\nabla \Psi = -d\Psi/dh = -mg$ . The *thermodynamic "force"* acting on each dislocation is  $F = dW/ds$ , where  $s = h/\cos \phi$  is the distance traversed by the (edge components of the) dislocations. Thus,  $F = dW/ds = (\cos \phi)dW/dh = -mg\cos \phi \propto \mathcal{T}$ ; negative-edge components move down.

**b)** Successive states of the dislocation loops shown in part 'a'. Dislocation components of opposite signs annihilate when they meet.

Figure 26 (Continued).

# Thermodynamic "Force"

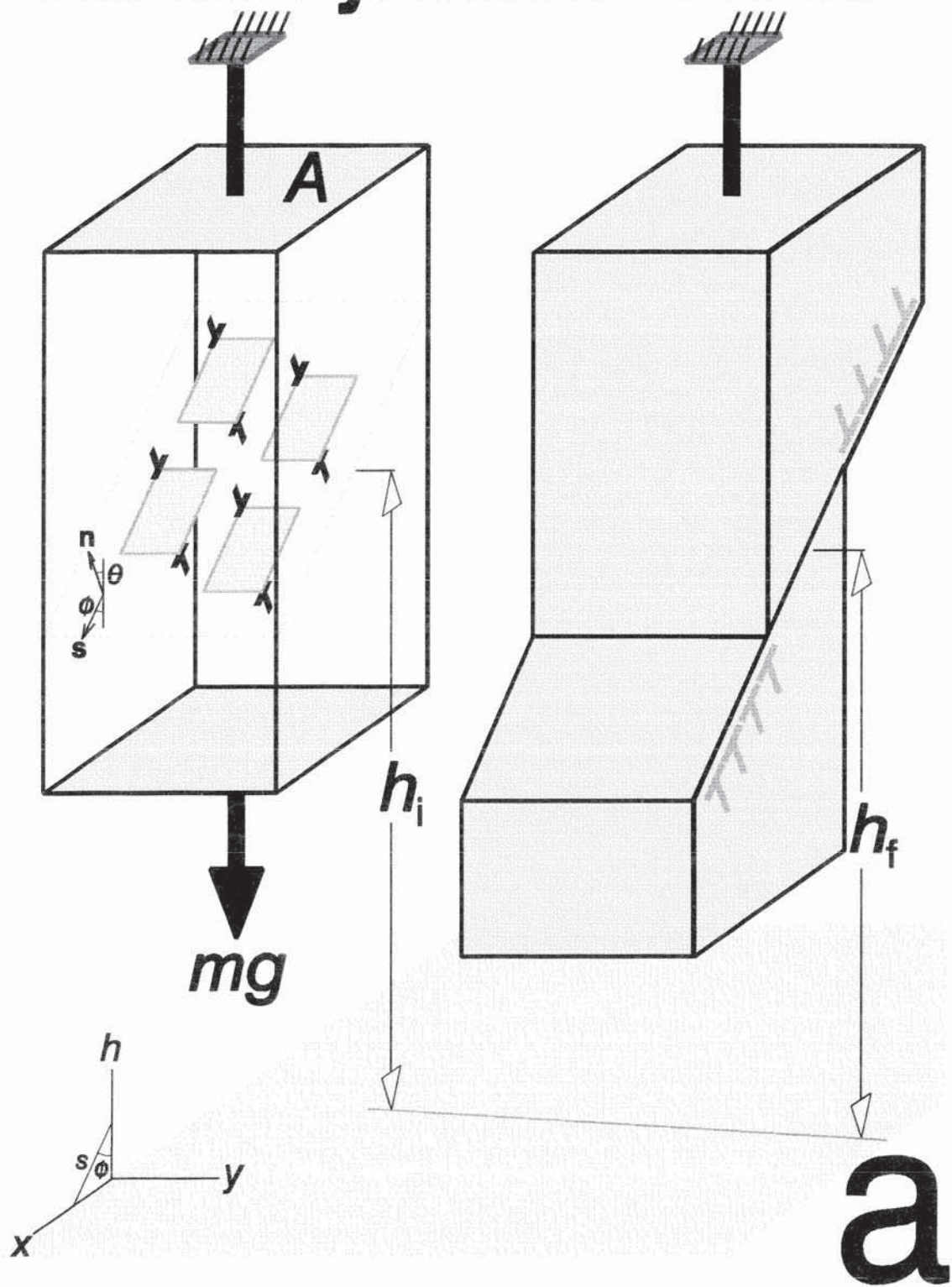
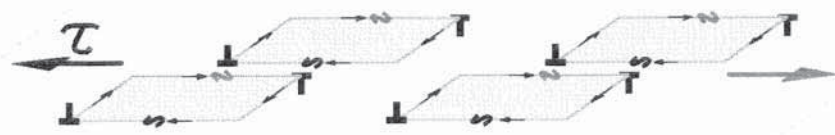
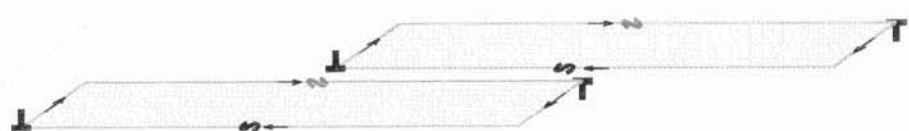


Figure 26 (Continued).



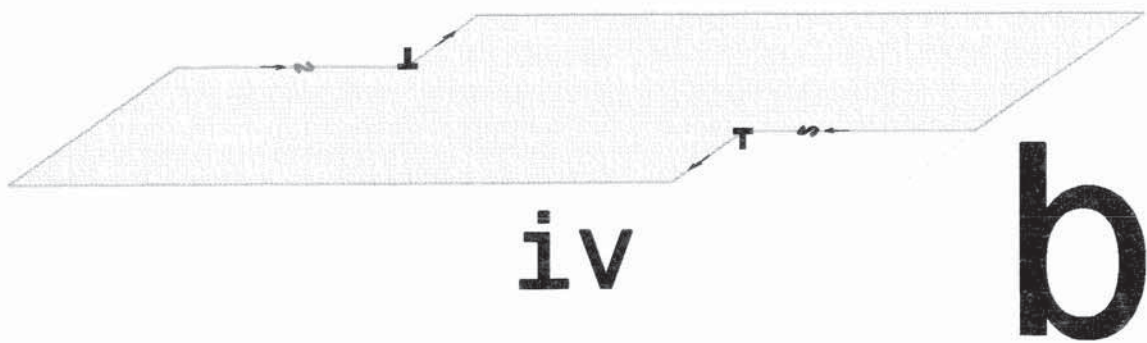
i



ii



iii



iv

b